NPS-67-82-004

NAVAL POSTGRADUATE SCHOOL

Monterey, California

AN INVESTIGATION OF THE EFFECTS OF SMOKE SUPPRESSANT FUEL ADDITIVES ON ENGINE AND TEST CELL EXHAUST GAS OPACITIES

Donald W. Thornburg, Thomas R. Darnell
David W. Netzer

May 1982

Prepared for:

Naval Air Propulsion Center
Trenton, NJ 08600

NAVAL POSTGRADUATE SCHOOL
Monterey, California

Rear Admiral J. J. Ekelund
Superintendent

D. A. Schrady
Acting Provost

The work reported herein was supported by the Naval Air Propulsion Center, Trenton, New Jersey, as part of the Naval Environmental Protection Technology Program.

This report was prepared by:

UNCLASSIFIED
SECURITY CLASSIFICATION OF THIS PAGE *(When Data Entered)*

RMS **REPORT DOCUMENTATION PAGE**

READ INSTRUCTIONS BEFORE COMPLETING FORM

1. REPORT NUMBER: NPS-67-82-004	2. GOVT ACCESSION NO.
3. RECIPIENT'S CATALOG NUMBER	
4. TITLE *(and Subtitle)*: An Investigation of the Effects of Smoke Suppressant Fuel Additives on Engine and Test Cell Exhaust Gas Opacities	5. TYPE OF REPORT & PERIOD COVERED: FINAL 1981
6. PERFORMING ORG. REPORT NUMBER	
7. AUTHOR(s): Donald W. Thornburg, Thomas R. Darnell, David W. Netzer	8. CONTRACT OR GRANT NUMBER(s): N6237681WR00014
9. PERFORMING ORGANIZATION NAME AND ADDRESS: Naval Postgraduate School Monterey, California 93940	10. PROGRAM ELEMENT, PROJECT, TASK AREA & WORK UNIT NUMBERS
11. CONTROLLING OFFICE NAME AND ADDRESS: Naval Air Propulsion Center Trenton, New Jersey 08628	12. REPORT DATE: May 1982
	13. NUMBER OF PAGES: 104
14. MONITORING AGENCY NAME & ADDRESS *(if different from Controlling Office)*: Naval Postgraduate School Monterey, California 93940	15. SECURITY CLASS. *(of this report)*: UNCLASSIFIED
	15a. DECLASSIFICATION/DOWNGRADING SCHEDULE

16. DISTRIBUTION STATEMENT *(of this Report)*

Approved for public release; distribution unlimited.

17. DISTRIBUTION STATEMENT *(of the abstract entered in Block 20, if different from Report)*

18. SUPPLEMENTARY NOTES

19. KEY WORDS *(Continue on reverse side if necessary and identify by block number)*

Turbojet
Test Cell
Pollution
Fuel Additives

20. ABSTRACT *(Continue on reverse side if necessary and identify by block number)*

Tests were conducted in a one-eighth scale turbojet test cell with a ramjet type combustor to investigate the effects of fuel additives on smoke reduction. Particle size and mass concentrations were determined at the engine and stack exhausts using three wavelength optical detector systems. Particulate samples were also collected at the engine exhaust and analyzed with a scanning electron microscope.

DD FORM 1 JAN 73 1473 EDITION OF 1 NOV 65 IS OBSOLETE
S/N 0102-LF-014-6601

UNCLASSIFIED
SECURITY CLASSIFICATION OF THIS PAGE *(When Data Entered)*

Combustor temperature and fuel additives were found to significantly affect particulate mass concentrations emitted from the engine while particle size appeared to be unaffected. No significant changes in the particulate size or mass occured from the engine exhaust to the stack exhaust.

The optical determination of exhaust mean particulate size/mass concentration with three wavelength optical detector systems appears to be reasonably accurate technique for evaluating the effects of engine and test cell operating conditions and fuel composition changes on the emitted particulates.

TABLE OF CONTENTS

LIST OF TABLES

LIST OF FIGURES

TABLE OF SYMBOLS AND ABBREVIATIONS

AUG. RATIO	Augmentation ratio
C_{m_e}	Engine exhaust particulate mass concentration ($\times 10^{-6}$ gm./liter gas)
C_{m_s}	Stack exhaust particulate mass concentration ($\times 10^{-6}$ gm./liter gas)
D_{32}	Volume-to-surface mean particle diameter (microns)
$\left(\frac{f}{a}\right)_p$	Fuel to air ratio (primary air); $\dot{m}_f/\dot{m}_p$
$\left(\frac{f}{a}\right)_{p+s}$	Fuel to air ratio (primary + secondary air); $\dot{m}_f/\dot{m}_e$
m	Complex refractive index
$\dot{m}_{aug.\ T.}$	Augmentor Tube mass flow rate (lbm/sec.)
$\dot{m}_{BP}$	Bypass air mass flow rate (lbm/sec.)
$\dot{m}_{c_e}$	Particulate mass flow rate at the engine exhaust (gm./sec.)
$\dot{m}_{c_s}$	Particulate mass flow rate at the stack exhaust (gm./sec.)
$\dot{m}_e$	Engine air mass flow rate ($\dot{m}_p + \dot{m}_s$) (lbm/sec.)
$\dot{m}_{e_T}$	Total engine air mass flow rate ($\dot{m}_{BP} + \dot{m}_e$) (lbm/sec.)
$\dot{m}_f$	Fuel mass flow rate (lbm/sec.)
$\dot{m}_p$	Combustor primary air mass flow rate (lbm/sec.)
$\dot{m}_s$	Combustor secondary air mass flow rate (lbm/sec.)

NO_x	Nitrogen Oxide concentration; parts per million (PPM), non-calibrated
T_λ	Percent transmittance at wavelength λ
T_2	Combustor gas temperature at the tail pipe (°R)
T_{BP}	Bypass air temperature (°R)
T_c	Combustor exhaust temperature at combustor exit (°R)
T_{MIX}	Bulk temperature of the fuel/air mixture at the engine exhaust (°R)
T_R	Gas stagnation temperature at the stack end of the augmentor tube (°R)
Q_e	Volume flow rate of gas at the engine exhaust ($\times 10^4$ in^3/sec.)
Q_s	Volume flow rate of gas at the stack exhaust ($\times 10^4$ in^3/sec.)
σ	Geometric standard deviation

I. INTRODUCTION

Jet engine test cells are stationary structures which enable the jet engine to be operated under controlled, static conditions. Such facilities are required for engine development, post-maintenance and post-overhaul turn-ups. They permit instrumentation for troubleshooting and qualifying engines in a manner that could not be done were the engine installed in its intended airframe. Thus, test cells are a vital part of the logistics and safety programs for both military and commercial aviation.

Like all fuel-burning devices, jet engines expel emissions. In light of the 1970 amendments to the Clean Air Act and the standards established by the Environmental Protection Agency (EPA), engine manufacturers, commercial aviation and the military establishment have placed emphasis on the reduction and/or elimination of harmful emissions generated by jet engines. There is considerable difficulty in determining what the acceptable levels of emission from the jet engine combustion process should be and whether or not the standards are attainable. The EPA issued emission standards which apply to jet engines installed in commercial and private aircraft in 1973. Military aircraft are not subject to these standards. In addition, standards specifically applicable to jet engine test cells have not been formulated. However, due to the amendment to the Clean Air Act in 1977 [Ref. 1] and recent court decisions [Ref. 2], test cells are currently classified as stationary sources of pollution and subject to regional and community pollution control boards. Hence, regulations might vary significantly from facility to

facility.

The exhaust of the gas turbine engine is made up primarily of large volumes of nitrogen, oxygen, carbon dioxide and water vapor. Within this, in relatively small quantities, are particulates, oxides of nitrogen (NO_x), sulfur oxides (SO_x), unburned hydrocarbons (UHC) and carbon monoxide (CO). The quantities and proportions of these emissions can vary greatly depending on the engine type and the operating level of the engine. This is particularly true for military engines due to the very wide operating ranges required of them. For example, a fighter aircraft requires engines that operate at power settings from idle through afterburner as opposed to a commercial engine which effectively operates at only one or two power settings.

The jet engine per se has not been a major contributor of pollution to any particular region. The emissions from aircraft engines have been estimated to be of the order of less than 3% of the overall urban pollution problem [Ref. 3]. This, along with the fact that controlling jet engine emissions is a very complex problem, has resulted in a relatively slow start toward developing abatement systems and anti-pollution technology for installed engines.

One long-term means of controlling emissions is through major engine redesign. Thus, emission control may be built into new engine technology. The development of smokeless combustors is an example. Such work is costly in time and money but represents strides toward acceptable long-term

solutions. The redesign of certain commercial aircraft engines has resulted in some reduction in the output of hydrocarbons, carbon monoxide and smoke emissions. However, the control of oxides of nitrogen is not considered practicable with current technology [Ref. 1]. Some of the newly developed commercial engine technology is directly transferable to military engines. New technology application may be limited, however, by the degree to which the performance of the engines differs, i.e,. high-performance military engines as opposed to commercial engines [Ref. 1]. Thus, for many current inventory engines in service, technology changes may prove impractical due to performance degradation and economic considerations. Since the emissions expelled by a test cell are a function of the engine being operated, short-term solutions to test cell emission control are needed.

As stated earlier, the purpose of a test cell is to provide a facility in which an engine may be operated throughout its entire operating spectrum so that performance deficiencies may be detected prior to installation in an aircraft. Since the engine operating performance is highly dependent on the inlet conditions of the air, the cell must be carefully designed so as to provide flow and thermal fields free of distortions at the engine face. It must also be designed so that exhaust gases are not reingested. The test cell inlet and exhaust structures are primarily designed for noise abatement. An augmentor tube serves as a jet pump and ensures that air flow occurs from front to aft over the engine and that the pressure differential across

the engine is kept to a minimum. It also pumps relatively cool air down the augmentor to mix with the hot engine exhaust gases in order to limit structural temperatures. The consideration of any modifications to the test cell for the purpose of pollution abatement must be done in such a manner as to not alter the design characteristics of the cell. To do so would not allow an accurate assessment of engine performance and would negate the usefulness of the test cell.

In the public view, the most offensive pollutants discharged by jet engines are noise and smoke since they are so readily observed. Since a test cell absorbs much of the noise generated from within, smoke becomes the focal point of immediate concern. Thus, a significant effort has gone into reducing the opacity of the test cell exhaust plume.

Opacity as defined by the EPA is the degree to which emissions reduce the transmission of light and obscure the view of an object in the background [Ref. 4] . The apparent reduction of light is due to absorption and scattering of light by particulate matter in the exhaust. Opacity is related to the transmittance of light beams through the exhaust gas by:

$$\% \text{ OPACITY} = 100\% - \% \text{ TRANSMITTANCE}.$$

Several techniques have been used as a measure or description of opacity. A method used by some pollution control districts to specify regulations on opacity is to use what is known as Ringelmann Number (RN). RN's range from 0 to 5 with 0 representing 0% opacity and 5 representing 100% opacity. A

typical regulation might specify a maximum opacity of Ringelmann Number 1, i.e., 20% opacity. The RN is determined by a trained human observer. The difficulty with this method is that it is subjective and not continuous. Another method of measuring opacity is with a commercial optical transmissometer. The device is designed to measure the attenuation of a light beam transmitted through the exhaust stream. Its advantages over the human observer are that the readings are objective, consistent, provide a permanent and continuous record, and can be calibrated to read opacity directly.

In the case of a jet engine exhaust, light transmittance is blocked by the presence of particulates which are by weight about 96% carbon [Ref. 3]. The formation of the gaseous emissions and the carbon particulates take place in the combustor of the turbine engine. Figure 1 illustrates a typical jet engine combustor. In the primary burn zone, the fuel-air mixture is often inhomogeneous, with regions of fuel-rich mixtures. In these regions, liquid hydrocarbons can be broken down to produce soot-particulates. As the carbon leaves the primary burn zone and moves downstream, more oxygen becomes available and burning may occur on the surface of the carbon particles. The maximum allowable temperature on the engine structure and turbine blades is limited, so cooler air must be mixed with the hot gases to prevent engine damage. This quenching lowers the gas temperature to the point where carbon will no longer burn and the remaining carbon particles are forced out the exhaust.

The exact process by which particulates are formed in the turbojet combustion process is not entirely understood. McDonald [Ref. 5] suggested that the process begins with the accretion of carbon nuclei in the flame zone followed by aggregation via coagulation creating "carbon particles" due to quenching beyond the flame zone. McDonald went on to suggest that "soot particles" are formed by further aggregation prior to the exhaust gases leaving the tailpipe. When the engine is installed in a test cell, changes may continue to occur in the augmentor tube and/or the stack. This possibility must be considered when examining means of reducing test cell plume opacity.

The size of the particulates in question is not well documented. One study found that particulates ranged in size from 0.01 to 0.5 microns [Ref. 6], while others report particulate diameters of 0.05 to 0.1 microns with occasional increases to 0.125 microns [Ref. 3]. It has also been reported that particulates will agglomerate into clusters having dimensions of 0.6 to 0.8 microns [Ref. 3]. Data from Ref. 6 illustrates that particulate sizes and concentrations will vary depending on engine type, power setting and distance from the exhaust nozzle to where the sample is taken.

One technique used to reduce the plume opacity of jet engine test cells is to use fuel additives. A considerable number of these additives have been evaluated by the Naval Air Propulsion Center for possible use in Navy facilities [Ref. 7]. Some of the more effective additives are metallic based and may

cause engine performance degradation due to deposits building up on the combustor walls and on turbine blades. The exact process by which fuel additives reduce smoke opacity is not well understood. Robson, Kesten, and Lessard [Ref. 3] suggest that additives are probably effective because they may lower the ignition temperature of the soot and limit the growth size of the particles. Pagni and Hughes [Ref. 8] suggest that additives serve as surface catalysts of soot oxidation or act as an inhibitive agent of the carbon particle agglomeration mechanism. However, they also found [Ref. 9] that a manganese based additive could actually increase mass emissions and that the additive only shifted the particle size distribution to smaller sizes, thereby decreasing visibility. Thus, additives can actually reduce total carbon particulate mass emission or simply redistribute particle sizes to reduce their visibility while forming metal oxides. Howard and Kausch [Ref. 10] have suggested three different mechanisms for soot removal depending upon the type of metallic additive: (a) production of ions which either decrease the amount of soot formed or produce smaller sizes which are more readily consumed, (b) production of hydroxyl radicals which remove soot from the flame, and (c) acceleration of the soot oxidation rate in the secondary flame zone. Manganese and iron-based additives are proposed to function by the latter mechanism.

Reference 7 reports that of the eighteen additives evaluated, ferrocene ($FeC_{10}H_{12}$) was found to be the most effective overall additive. By adding ferrocene in proper porportions to the engine fuel, test cell exhaust opacity was reduced from as high as 55% opacity to below 20% opacity

[Ref. 11]. It also appeared that ferrocene did not have any detrimental effects on the environment or short-term adverse effects on the particular engine being used. Tests have also shown it to be relatively non-toxic. Long-term effects are still under investigation.

It is obvious that plume opacity is related to particulate size and concentration, but what is not clear is how these properties are altered by the test cell and by the use of fuel additives. Particulates may be altered within the combustor as discussed above. In addition, when the particulates leave the combustor, they are subjected to the effects of dilution from bypass air in the engine (if present), dilution in the augmentor tube, and mixing and cooling in the stack prior to exiting to the atmosphere.

The overall purpose of this investigation was to study the effects of engine operating conditions (flow rates, fuel/air ratio and temperature), test cell design (augmentation ratio, etc.) and fuel additives on the emmited particles from a turbojet test cell. The fuel additives considered included ferrocene, DGT-2, XRG, CV-100, 12% Rare Earth Hex-Cem and 12% Cerium Hex-Cem. The effects of additives and combustor operating conditions on the concentration and size of particulate matter at the engine and stack exhausts were studied using a one-eighth scale test cell in conjunction with a water cooled dump combustor. Mean particulate size and concentration were measured by means of a multiple frequency light transmission technique at the engine exhaust and at the test cell exit plane. The opacity of

the test cell plume was also measured by the use of a commercial transmissometer in order to relate the readings of this often used device to quantitative particulate data. Particulate samples were collected at both the engine exhaust and test cell exit and examined with the aid of an electron microscope in order to provide additional quantitative data on particulate sizes. In addition, NO_x concentration was monitored at the stack exhaust.

II. EXPERIMENTAL APPARATUS

A. SUB-SCALE TURBOJET TEST CELL

The subscale turbojet test cell described in Ref. 12 was used to carry out this investigation. The test cell, shown in Figs. 2 and 3, is a one-eighth (in linear dimensions) scale model of a Naval Air Station, Alameda test cell. Figure 4 illustrates the basic plumbing arrangement. Air was drawn into the test cell through a horizontal inlet with a square bellmouth and a flow straightening section. The test section was enclosed by hinged plexiglas sides to allow easy access and visual monitoring during operation. The augmentor tube exited the cell through a removable wall. Its downstream end was attached to a deflector-plate-equipped vertical exhaust stack. The stack was mounted on a wheel/rail arrangement which allowed translation of the stack/augmentor assembly.

High-pressure air was provided to the externally mounted combustor from a large-volume positive displacement compressor. The combustor exhaust was mixed with bypass air. The bypass air was supplied from an Allis-Chalmers, twelve-stage axial flow compressor. The engine inlet was simulated with a six-inch pipe drawing air through a six-inch bellmouth. An ejector was employed to provide the suction air flow rate. Pneumatically activated servo control valves were installed in each of the four air lines so that air mass flow could be remotely regulated. The "engine inlet" suction air was adjusted so that it was equal to the total mass flow of the combustor and bypass air.

B. COMBUSTOR

The combustor utilized for the test was a ramjet type dump-combustor. The combustor is illustrated in Figs. 5 and 6 and described in detail in Ref. 13. The combustion chamber was designed to operate at pressures of nine atmospheres or greater. The sudden expansion chamber provided good flame stabilization. It was ignited with an oxygen-ethylene torch which was located in the flame stabilizing recirculation zone. The primary and secondary air flows were supplied by a positive displacement compressor with a line pressure of approximately 150 PSIA. A typical total combustor air mass flow rate was about 0.5 LBM/SEC. By varying the primary fuel/air ratio and secondary air flow, the exhaust temperature and particulate concentration (i.e., opacity) could be altered. A secondary fuel injection location was available but not used. The combustion pressure was decreased to approximately two atmospheres by the use of two sonic nozzles. The combustor was water cooled to protect the chamber walls and lower the total temperature.

C. FUEL SYSTEM

The fuel system consisted of a portable fuel supply, a remote control panel, and two precision metering pumps for fuel additive injection.

The portable fuel supply, shown in figure 7, consisted of two interconnected fuel tanks, a cavitating venturi for flow-rate control, and remotely controlled, electrically actuated solenoid valves. The fuel tanks were pressurized using gaseous nitrogen and a hand operated regulator located

on the control panel (figure 8). Each tank was equipped with an electrically activated vent valve. A single fuel line connected both tanks to the combustor through an electrically operated shut-off valve. Fuel flow rate to the combustor was controlled by means of a cavitating venturi installed in the fuel line. The cavitating venturi allowed fuel flow adjustments by simply regulating the upstream pressure in the fuel tanks. A calibration curve for fuel flow rate versus pressure for the .016 in. venturi is shown in figure 9.

Two Eldex, Model E, precision metering pumps, shown in figure 10, were utilized for fuel additive injection into the fuel line just prior to the combustor. A swirl type mixer was incorporated to ensure that mixing of the fuel and additive occurred prior to the combustor. Each pump was capable of delivering between 0.2 and 5.0 ml./min. of fuel additive. The flow rate versus pump micrometer setting was pre-calibrated and the results are shown in figure 11.

D. TEST CELL INSTRUMENTATION AND DATA COLLECTION

The subscale test cell at the Naval Postgraduate School provides the opportunity for easy measurement of pressures and temperatures anywhere within the system during engine operation. Using standard ASME flow calculations [Ref. 14], mass flow rates anywhere within the test cell could be calculated. The pressure tap and temperature sensor locations used during this investigation are shown on a schematic of the test cell in figure 12.

All pressure lines were connected to an automatic-stepping

Scanivalve with a 500-psi pressure transducer. Thermocouple leads from the temperature sensors and electrical leads from the Scanivalve were connected to HP-3495A scanners.

Automatic data acquisition and data processing were provided on demand by an HP-21 MX computer system. Data was acquired by systematically addressing the scanners and an HP-3455A digital voltmeter. The analog data were passed through an A/D converter and then processed by a computer program which provided flow rates and other pertinent system computations. Temperatures, pressures, flow rates, and other pertinent test cell data were then printed out.

The velocity profile in the augmentor was measured with a pitot rake consisting of seven equally spaced small diameter total pressure tubes. The rake was fixed at approximately four inches from the stack end of the augmentor in a vertical position. From the velocity profile, augmentor mass flow rate was calculated and used to determine the augmentation ratio.

During initial testing, it was noted that small changes in the combustor exhaust temperature significantly affected the opacity of the stack gases. For this reason, it was desirable to have a permanent record of the combustor exhaust temperature for each fuel additive analyzed. To provide this record, a high temperature thermocouple was installed at the combustor exhaust and its output was connected to a strip chart recorder.

E. TRANSMISSOMETER

The transmissometer utilized during this study was a

Leads and Northrop model 6597. The transmissometer consisted of a white light source, a detector unit and a signal conditioner/display unit. The white light source and the detector unit were mounted at the top of the test cell on opposite sides of the stack to provide readouts of exhaust stream opacity. Figure 13 shows the source and detector and figure 8 shows the signal conditioner/display unit.

During this investigation, the transmissometer output was connected directly to a strip chart recorder, thus providing recorded values of exhaust opacity as the fuel additives were evaluated.

F. OPTICAL DETECTOR SYSTEM

The transmission of light through a cloud of uniform particles is derived from Bouguer's Law [Refs. 15 and 16]:

$$T = \exp(-QAnL) = \exp\left[-(3QC_mL/2\rho d)\right] \qquad (1)$$

where (T) is the fraction of light transmitted, (Q) is the dimensionless extinction coefficient, (A) is the cross sectional area of a particle, (n) is the number concentration of particles, (ρ) is the density of an individual particle, (L) is the path length the beam of light traverses, (C_m) is the mass concentration of particles, and (d) is the particle diameter.

From Bouguer's Law it is seen that the transmissivity of a beam of light decreases exponentially as the path length,

particle concentration, and Q/d ratio increase.

Mie light scattering theory allows the extinction coefficient (Q) to be calculated as a function of particle size, wavelength of light and the complex refractive index of the particles.

In a paper presented by Dobbins [Ref. 17], Bouguer's Law was revised to allow for a distribution of particle sizes:

$$T = \exp[-(3\bar{Q}C_m L/2\rho d_{32})] \tag{2}$$

where $\bar{Q}$ represents an average extinction coefficient and d_{32} represents the volume-to-surface mean particle diameter. The average extinction coefficient can be calculated as a function of the particle size distribution, the wavelength of light, and the complex refractive index of the particles. Taking the natural logarithm of equation (2):

$$\ln[T] = \bar{Q}[-3C_m L/2\rho d_{32}] \tag{3}$$

Since the transmittance of a beam of light passing through an aerosol of polydisperse particles is directly related to the wavelength of the light, equation (3) can be written for a specific wavelength of light:

$$\ln[T_\lambda] = \bar{Q}_\lambda[-3C_m L/2\rho d_{32}] \tag{4}$$

For two wavelengths of light, the ratio of the natural logs of the transmittances is then given by:

$$\frac{\ln[T_{\lambda_1}]}{\ln[T_{\lambda_2}]} = \frac{\bar{Q}_{\lambda_1}}{\bar{Q}_{\lambda_2}} \tag{5}$$

where C_m, L, ρ, and d_{32} remain constant for both wavelengths. A Mie scattering computer program provided by K. L. Cashdollar of the Pittsburgh Mining and Safety Research Center, Bureau of Mines allowed calculation of $\bar{Q}_\lambda$ and the $\bar{Q}_\lambda$ ratios as a function of d_{32} based on inputs of the complex refractive index of the particles, the refractive index of the surrounding medium, the standard deviation of the distribution and the wavelengths of light. During this investigation, the surrounding medium was assumed to be air with a refractive index of one. The complex refractive index and the standard deviation of the particle size distribution for the exhaust particulate were unknown. Most of the exhaust particulate can be reasonably assumed to be carbon. Therefore, a number of reasonable values for carbon [Ref. 16] were supplied as inputs to the computer program. Once $\bar{Q}_\lambda$, d_{32}, and T_λ are known, mass concentration can be calculated according to the following rearrangement of equation (4).

$$C_m = -\frac{2}{3}\left[\frac{\rho d_{32}}{\bar{Q}_\lambda L}\right] \ln T_\lambda \tag{6}$$

In order to measure transmissivity, a collimated beam

of white light was directed through the exhaust stream to a detector which split the light into three wavelengths. Light intensity was measured using linear photodiodes. Transmissivity was determined by comparing the percentage of photodiode output without particles present to the percentage of photodiode output with particles present. Only two values (two wavelengths) of transmittance are required to calculate d_{32} and C_m if the index of refraction and standard deviation are known. The third wavelength provides for three ratios which can be used to determine three values of d_{32}. Various refractive indices and standard deviation combinations are tried until all three ratios provide the same d_{32}. This redundant calculation of d_{32} provides reasonable assurance that the correct index of refraction and standard deviation have been used [Ref. 16].

In initial testing only two frequencies were used. These were provided by He-Ne (6328A°) and Argon (4880A°) lasers. The lasers were mounted in a building next to the test cell and the light beams were directed to the detector boxes through protective tubing using beam splitters and mirrors [Fig. 14]. Alignment of the source/detector units using this procedure was awkward and vibrations caused by running the engine made accurate measurements difficult.

In order to compensate for the above problems, the light sources were changed from lasers to collimated white light sources; and they were installed directly across from the detector boxes. This change greatly simplified alignment

and insured measurement of the exhaust streams only.

The light detectors, shown in figure 15, have a single entry point for the beam of collimated light, two beam splitters, three narrow pass filters, and three photodiodes. The entry point for the collimated light was a 0.25 inch I.D. tube fashioned to minimize forward scattered light effects [Ref. 16] . After the light entered the detector box, it was passed through two beam splitters which resulted in three separate beams of light. Each of the three beams of light was directed through a narrow pass filter and onto a photodiode. Neutral density filters were used to decrease the light intensity in order to prevent the photodiodes from being overdriven. Figure 16 is a schematic of the detector box and shows the paths followed by the light inside the detector.

The white light source was provided by a projector with a 750 watt incandescent bulb. By adjusting the lens on the projector, a nearly parallel beam of light was realized. In order to provide light of uniform intensity, a piece of diffuser glass was placed between the projector lamp and the focusing lens. The nearly parallel source was then directed onto a 0.040 inch pinhole to develop a point source of light. The divergent beam of light exiting the pinhole was routed through a 31.5 mm diameter achromatic lens with an 80 mm focal length to provide collimated light. The collimated beam of light was then reduced to 0.50 inch diameter by passing it through a reducer tube. The collimated white light source is shown in figure 17.

Two source/detector systems were utilized during this investigation. One source/detector pair was mounted at the test cell stack exhaust and the other pair was mounted at the motor nozzle exhaust.

Alignment of the source/detector pairs was critical, and they were extremely sensitive to vibration during engine operation. To eliminate vibrational problems and the need for continuous realignment, the source/detector pairs were permanently mounted on free-standing platforms separate from the test cell.

Aluminum covers were fabricated to prevent dust and moisture from entering the circuitry and affecting the optics. To futher preclude moisture from the systems, heaters in the form of 15 watt light bulbs were utilized to keep the inside of the covers dry.

The detector unit mounted at the stack exhaust incorporated narrow pass filters of 10140, 6500, and 4500 angstroms while the combustor exhaust unit incorporated filters of 10000, 6943, and 4000 angstroms. It was necessary to use filters separated by at least 2000 angstroms to insure accurate transmittance ratios.

The output of each detector unit was connected to a strip chart recorder to provide real time visual indications and records of fuel additive effects during engine operation.

G. EXHAUST PARTICLE COLLECTION

In order to verify measurements of particle size using

the three frequency light transmission technique, it was necessary to physically collect exhaust particulate matter and measure the particle sizes with a Scanning Electron Microscope (SEM). Initially, impact particle collectors were inserted directly into the exhaust streams. This technique proved unsatisfactory and made particle size measurement difficult since the particulate matter was distorted upon impacting the collector. In order to eliminate this problem, an improved dry impinger particle collection technique was implemented [Ref. 18].

The sampling train, shown in figure 18, was composed of a sampling tube located at the combustor exhaust, a collection box with six sample holders, and a vacuum pump with in-line filters and control valves. The sampling tube, shown in figure 19, was made of 0.25 inch inner diameter stainless steel and was located in the center of the augmentor tube, aft of the combustor exhaust. In order to minimize flow distortion about the sampling tube, it was necessary to remove samples of exhaust gas and particulate matter iso-kinetically. A sonic choke was used to regulate the flow rate through the sampling train. A vacuum pump supplied the pressure differential necessary for proper operation of the sonic choke.

The sample box was designed so that up to six samples of exhaust particulate could be taken during engine operation. Collection times were manually controlled by opening and closing sliding doors which covered each sample holder at ten to twenty second time intervals. An in-line filter

prevented clogging of the sonic choke and ingestion of exhaust particulate by the vacuum pump.

H. NITROGEN OXIDES ANALYZER

A Monitor Labs, Model 8440 E, Nitrogen Oxides Analyzer shown in figure 20 was used to determine fuel additive effects on NO_x production during engine operations. The analyzer is fully described in Ref. 19.

Test cell exhaust gas was sampled using a stainless steel probe mounted on the stack cover. The gas sample was routed through a twelve inch Mott Inertial Filter which removed particulate matter greater than 0.5 microns in diameter. From the filter, teflon tubing was utilized to route the gas to the analyzer.

III. EXPERIMENTAL PROCEDURE

As indicated by Ref. 10, the concentration of fuel additives required to reduce opacity varies with engine type. To determine the concentration required for the combustor used in this study, it was first experimentally determined what fuel/air ratio would yield an opacity between 30% and 50%. The opacity was measured with the commercial transmissometer. After the high opacity was reached, the fuel additive under study was added to the fuel in increasing proportions until a significant reduction in opacity was achieved. This established a baseline from which the study was conducted.

During initial testing the fuel additives were batch mixed with JP-4 and then pressure fed to the combustion chamber of the engine. This procedure was time-consuming as fuel tanks had to be drained and refilled each time fuel additives or concentrations were changed. In order to overcome this problem, precision metering pumps were added to the fuel system. The pumps allowed accurate fuel additive injection and provided ease in changing fuel additive concentrations while the engine was operating.

Initially, all test equipment was turned on and allowed to warm up. This was done to insure that the measurement and recording devices were functioning properly and also to eliminate condensation which might have formed on the optics of the transmissometer and the optical detector system.

After the initial warm-up period, the optical detector

systems and the transmissometer were checked to insure that the alignment between sources and detectors had not been disturbed. The transmissometer was checked by insuring that a zero and a one hundred percent opacity reading were realizable. The optical detector system was checked by measuring the maximum detector outputs and comparing them to output data taken when the system was first installed and aligned.

Once it was evident that the measurement equipment outputs were reliable and correct, air pressures within the test cell were adjusted. A remote control cart was located near the computer console. Pneumatically actuated valves in the six-inch suction line and the three high-pressure lines were opened. The computer then analyzed test cell conditions and a printout of test cell pressures, temperatures, and flow rates was provided. The pneumatically actuated valves were manipulated until desired test cell conditions and flow rates were set.

The air flowing through the test cell caused the optical detector system outputs to decrease and the opacity reading from the transmissometer to increase slightly. In order to obtain test results due to exhaust particulate only, the transmissometer was rezeroed and the new one hundred percent transmittance point for each output of the optical detector systems was marked on the strip chart recorders.

With final adjustments made, the fuel tank/cavitating venturi pressure was adjusted to provide the desired fuel flow rate. An oxygen/ethylene ignition torch was used to

ignite the JP-air mixture within the combustor.

Once the desired combustor exhaust temperature was achieved through manipulation of the fuel flow rate, and steady state outputs were obtained, a particulate sample and data were taken. In all tests conducted during this investigation values for fuel tank pressure, venturi pressure, NO_x concentration, opacity, and combustor exhaust temperature were manually recorded. The latter two were also recorded by a strip-chart recorder. Once JP-4 data were obtained, the fuel additive pumps were activated. Additive flow rates were adjusted until minimum opacity readings occurred. Data were recorded at each pump setting and a particulate sample was collected when the minimum opacity readings occurred. After data collection was completed, and the engine had been shut down, post-run zeros and one hundred percent points were marked on the strip chart recordings to insure that alignment of the optical measuring equipment had not changed.

In order to standardize the experimental investigation of fuel additive effects on smoke production, the fuel flow rates and air mass flow rates were set to the same values each time a test was conducted. Nominal values for test cell air mass flow rates were:

6 inch suction line ----------	1.031 (lbm/sec)
3 inch bypass line ----------	.939 (lbm/sec)
Combustor primary air --------	.281 (lbm/sec)
Combustor secondary air ------	.198 (lbm/sec)

These settings provided a test cell augmentation ratio of 3.95 and an augmentor tube mass flow rate of 7.03 lbm/sec

with the nominal flow resistance grid installed in the exhaust stack. The cavitating venturi pressure was normally set at 560 psig to insure a fuel flow rate of .017 lbm/sec and a combustor exhaust temperature of 2010°R.

The particulate samples collected during each test were analyzed for particle size using a scanning electron microscope and the results were used to verify data obtained from the outputs of the optical detector systems.

IV. RESULTS AND DISCUSSION

A. INTRODUCTION

Initial data in this investigation were obtained using two laser beams. This was found to be unsatisfactory as discussed above. However, several results provided guidance for the subsequent test program. Combustor exit (tailpipe) temperatures above 1800°R were required for the additives to be effective. Exhaust gas opacity was also found to be very sensitive to the tailpipe temperature, the higher temperatures throughout the combustor apparently provided sufficient residence time for significant consumption of the carbon.

Since the mechanisms by which an additive reduces opacity is of importance, a brief comparison of the ramjet type dump-combustor used in this study to a turbojet combustor is needed. Fuel atomization in the dump-combustor was achieved by radial injection through eight 0.010-inch holes located circumferencially in the pipe wall upstream of the combustion chamber (Fig. 6). This is in contrast to a conventional atomizer used in turbojet combustors. However, the difference should not significantly alter the manner in which the formation of carbon particles is initiated nor the mechanism by which an additive operates within the primary combustion zone. In the dump-combustor there appeared to be good flame stability and a distinct primary combustion zone as is found in a turbojet. Of significant difference is the rapid air quench in the dump-combustor as opposed to the gradual dilution in the turbojet. Additive effects in the dilution zone could be signifi-

cantly different, depending upon the residence time required for the dominant mechanism of the additive. Recall that Howard and Kausch [Ref. 10] have suggested that the mechanism by which manganese and iron-based additives reduce soot is by accelerating the soot oxidation rate in the secondary (dilution) flame zone. Gradual cooling/particle growth should be similar in the dump-combustor tailpipe and sub-scale test cell to that in an actual turbojet and test cell. During the experiments, the exhaust nozzle was operated at high subsonic to just choked conditions.

A combustor operating point had to be found which provided a significant plume opacity when operating without an additive. This would provide a reference from which to compare the effects of an additive. It was found that the primary fuel-to-air ratio $(f/a)_p$ had to be near stoichiometric to achieve a plume opacity of 30 to 50% as measured by the transmissometer.

Before the second test series was initiated, screening tests were conducted to determine the approximate effectiveness (measured by exhaust stack opacity) of each of the additives and the most effective additive concentration. In these tests ferrocene was found to be very effective. DGT-2 was found to be less effective, whereas CV-100 and XRG were found to be ineffective. Based on these results the second test series emphasized ferrocene and two new additives supplied by Mooney Chemicals, Inc., 12% Cerium Hex-Cem and 12% Rare Earth Hex-Cem.

The data collected during this investigation are summarized in tables I and II. Recorded data and data reduced from strip chart recordings are summarized in tables III, IV, and V. A typical set of strip chart recordings is shown in figures 21-24. To supplement the information presented in tables I-V, pertinent data from these tables are presented graphically in figures 25-30. SEM photographs of exhaust particulate collected during the fuel additive tests are shown in figures 31-40.

Except in figure 25, data points are connected with straight lines. Figure 25 implies that significant changes in stack gas opacity and engine exhaust particulate mass concentration (C_{m_e}) resulted from small changes in primary fuel-air ratio $(f/a)_p$. Combustor exhaust temperature (T_c) and combustor fuel/air ratio are directly related and both serve as good indicators of overall engine operating conditions.

In an effort to determine the effects of fuel additives and test cell operating conditions on opacity, and average particle size (D_{32}) and mass concentration; run-to-run variations in combustor exhaust temperature were considered in analysis of the data (presented in figures 25-30). If T_c remained constant, changes in opacity, etc. should be due primarily to varying fuel additive concentrations.

B. ADDITIVE EFFECTS ON STACK GAS OPACITY

Figure 26 summarizes the effects of additive concentration on stack gas opacity for the three fuel additives tested. For additive concentrations of zero, the points plotted actually represent the average value of opacity taken before and after the fuel additive test. Ferrocene and 12% Cerium Hex-Cem produced significant decreases in test cell stack opacity for additive concentrations between twenty and thirty milliliters per gallon of JP-4. The additive 12% Rare Earth Hex-Cem was ineffective, the stack opacity actually increased as the additive concentration was increased.

Ferrocene was tested on two separate days with slightly different test cell operating parameters. The tests on 10 November were conducted at a slightly higher combustor exhaust temperature than the tests on 19 November. Increasing combustor exhaust temperature decreased opacity and this is why one curve is lower than the other on figure 26. The use of Ferrocene resulted in thirty to forty percent reductions in opacity.

The 12% Cerium Hex-Cem additive was also tested on 19 November with essentially the same results as for Ferrocene. The curve in figure 26 is lower than for Ferrocene, partly due to the higher combustor exhaust temperatures during the test.

To summarize, 12% Rare Earth Hex-Cem was ineffective in reducing stack gas opacity. Considering variations in test cell operating conditions, Ferrocene and 12% Cerium Hex-Cem additives both decreased opacity about thirt-five

percent for additive concentrations between twenty and thirty milliliters per gallon of JP-4.

C. ADDITIVE EFFECTS ON D_{32}

Using the three transmittance values derived from the strip chart recordings (Table III), three extinction coefficient ratios were determined for each fuel additive concentration tested. With the use of the Mie Scattering computer program outputs and equation 5, three D_{32} values were determined for each additive concentration for a specific complex refractive index and standard deviation. Sample outputs of the computer program are included as figures 41-56. The refractive indices and standard deviations used in these figures were the only ones which provided consistent D_{32} values (from the three transmittance ratios) throughout this investigation. An average value of $D_{32} \pm .03$ microns was used as the basis for accepting data derived in the above manner. The derived values for engine and stack exhaust mean particle diameter (D_{32}) are shown in Table IV. Stack values are also presented graphically in figures 27-30.

Throughout this investigation D_{32} varied between .18 and .24 microns with an average value of about .21 microns. Considering the inaccuracies in measurements of the transmittance values, .18 to .24 microns was not considered a significant change in average particle diameter. For this reason, it was concluded that the particle diameters remained essentially the same throughout all the tests and that varying

additive concentrations had no significant effect on D_{32}. The data presented in table IV also indicated that no significant variations in particle diameter occurred between the engine exhaust and the stack exhaust.

D. ADDITIVE EFFECTS ON MASS CONCENTRATION

Using the derived D_{32} values from table IV, figures 41-56 were entered to determine a value for the extinction coefficient ($\bar{Q}_\lambda$) at each wavelength of light analyzed. The curve used in determining $\bar{Q}_\lambda$ had the same complex refractive index and standard deviation as the curve used to obtain D_{32}. Equation 6 was then used to calculate a mass concentration value at each wavelength. Soot particle density was assumed to be 1.5 gm/cm^3. The value for L was .762 meters at the stack exhaust and .0498 meters at the engine exhaust. Calculated values of concentration are less accurate than D_{32} values due to the uncertainty in both ρ and $\bar{Q}$. Table IV lists the results for wavelengths of 10000 Angstroms (engine exhaust) and 10140 Angstroms (stack exhaust). The mass concentrations obtained using the other wavelengths were essentially the same and are not included. Engine and stack mass concentration values are also plotted in figures 27-30.

The mass concentrations at the engine and stack exhausts were significantly affected by the fuel additive concentrations and also by variations in the combustor operating conditions. As the combustor exhaust temperature increased,

the mass concentration decreased and vice versa (Figure 25). For approximately constant combustor conditions, Ferrocene and 12% Cerium Hex-Cem tended to decrease the mass concentrations for additive concentrations between twenty and thirty milliliters per gallon of JP-4 while 12% Rare Earth Hex-Cem tended to increase the mass concentration as additive concentration was increased.

Since there was a significant decrease in particulate mass concentration between the engine exhaust and the stack exhaust, mass flow rates of particulate at the engine and stack were calculated to determine if the decrease was due in part to chemical reactions within the test cell or due primarily to the dilution by augmentation air. The particulate mass flow rates can be written as:

$$\dot{m}_{Ce} = C_{m_e} Q_e \tag{7}$$

$$\dot{m}_{Cs} = C_{m_s} Q_s \tag{8}$$

Q is the volume flowrate which can be calculated assuming perfect gases from

$$Q = AV = \frac{\dot{m}RT}{P} \tag{9}$$

at the engine and stack exhausts. The following assumptions were made in these calculations.

$$R = R_{AIR} = 53.3 \text{ ft-lbf/lbm - } ^\circ R$$

$$P = P_{engine} = P_{stack} = 14.7 \text{ PSI}$$

$$\dot{m}_{engine} = \dot{m}_P + \dot{m}_s + \dot{m}_{BP}$$

$$\dot{m}_{st} = \dot{m}_{stack} = \dot{m}_{augmentor\ tube}$$

$$T_{stack} = T_R$$

$$T_{engine} = T_{MIX} = \frac{\dot{m}_{BP}T_{BP} + \dot{m}_e T_2}{\dot{m}_{e_T}}$$

The particulate mass flow rates were then ratioed:

$$\frac{\dot{m}_{ce}}{\dot{m}_{cs}} = \frac{C_{m_e}Q_e}{C_{m_s}Q_s} = \frac{C_{m_e}\dot{m}_e T_{MIX}}{C_{m_s}\dot{m}_{ST}T_R} \qquad (10)$$

Within the limitations of the above approximations, a ratio of 1.0 would indicate that there was no change in the mass flow rates of particulate between the engine and stack exhaust; therefore, any decrease in mass concentration at the stack would be due stricIty to dilution of the exhaust particulate with augmentation air. Table V presents these ratios and the general results indicate (within the limited accuracy of the calculations) that no significant chemical reactions involving the particulates occured within the augmentor tube or exhaust stack.

In summary, fuel additives and increased engine operating temperature decreased the mass concentration of exhaust particulates, and the decrease in mass concentration between the engine exhaust and stack exhaust was due primarily to dilution of the engine exhaust gases within the augmentor tube.

E. ADDITIVE EFFECTS ON NO_x CONCENTRATION

Values for NO_x concentration measured at the stack ex-

haust are included in table III. None of the additives produced any significant change in NO_x concentrations at the stack exhaust.

F. SEM ANALYSIS OF ENGINE EXHAUST PARTICULATE SAMPLES

Scanning electron microscope photographs of engine exhaust particulate collected during tests with JP-4 only are shown in figures 31 and 32. The variation in particle diameters exhibited in these photographs is of particular interest. Figures 31 and 32 show individual particle sizes varying from about .05 microns up to about .40 microns. D_{32} values determined using the light transmission technique represent the volume-to-surface mean particle diameter based on a specific log-normal distribution. As an example, a D_{32} value of .21 microns, derived using a complex refractive index of 1.8 - .60i and a geometric standard deviation of 2.0, is the mean of the distribution. The tails of the distribution for this case were .031 microns and 1.20 microns. Therefore, particle sizes inside the tails of the distribution are to be expected in varying amounts. The predominant particle size should occur around the mean and this appears to be the case for both figures 31 and 32. The optical detector system provided values of .20 and .21 microns for tests conducted using JP-4 only.

Figure 31 also shows large agglomerations of particles but it is not known whether they formed within the combustor/

tailpipe or whether they formed during the sampling process.

Figures 33 and 34 are SEM photographs of particles collected during fuel additive tests with Ferrocene on 10 November 1981. The fuel additive concentration was 32.3 ml./gal. JP-4. A D_{32} value was not calculated from the photographs but the particle sizes in the photographs appear to be very similar to those in figures 31 and 32.

Figures 35 and 36 are photographs of particles collected during tests on 19 November 1981 with a Ferrocene concentration of 19.2 ml./gal. JP-4 and figures 37 and 38 are photographs of particles collected during the same tests with a Ferrocene concentration of 28.8 ml./gal. JP-4. The photographs again indicate no significant change in particle diameters when compared with the photographs with no additives (Figures 31 and 32).

Figures 39 and 40 are photographs of particles collected during tests with 12% Cerium Hex-Cem. The additive concentration was 19.6 ml./gal. JP-4. Although there were fewer particles in these particular photographs, there did not seem to be a significant change in mean particle diameter when compared with the photographs of the other samples.

Particle samples were not taken during the tests using 12% Rare Earth Hex-Cem. This additive did not reduce opacity, and it was felt a sample would provide no useful data.

Overall, the SEM photographs indicate that the values of D_{32} determined using light transmission measurement were

reasonably accurate representations of the actual average particle sizes. No attempt was made to determine D_{32} from the photographs because of the probable effects of the collection method on the sizes collected and on the agglomeration processes.

V. SUMMARY OF RESULTS

An initial test series was completed using the improved subscale test cell (additive pumps, NO_x analyzer, engine exhaust gas sampler, 3-wavelength light transmission devices). Ferrocene, 12% Rare Earth Hex-Cem, and 12% Cerium Hex-Cem were used in varying concentrations to determine their effects on engine and stack exhaust opacities and particulate mean diameter. Major results are summarized below.

(a) Additive concentrations between 0 and 50 ml per gallon of JP-4 were tested. Ferrocene and 12% Cerium Hex-Cem additives both decreased stack exhaust gas opacity between thirty and forty percent for additive concentrations between twenty and thirty milliliters per gallon of JP-4. 12% Rare Earth Hex-Cem was ineffective in tests completed to date.

(b) Exhaust gas opacity was very sensitive to combustor exhaust temperature (primary fuel - air ratio).

(c) Throughout this investigation the particulate volume to surface mean diameter (D_{32}) varied between .18 and .24 microns with an average of about .21 microns. Considering the inaccuracies in measurements of the transmittance values, .18 to .24 microns was not considered a significant change in average particle diameter. For this reason, it was concluded that the particle diameters remained essentially the same throughout all the tests and that varying additive concentrations had no significant effect on D_{32}. The data also

indicated that no variations in particle diameter occurred between the engine exhaust and the stack exhaust. Other investigators (Ref. 9) have found that manganese based additives can reduce particulate size without changing particulate mass. Barium additives have been found not to affect particulate size (Ref. 10). These contrasting results may be due to the type of additive and/or to the different combustor geometries (residence times, quenching rate, etc.) and test conditions employed. The need is apparent for evaluating various additives in one combustor design and at various operating conditions.

(d) Fuel additives and increased engine operating temperature decreased the mass concentration of exhaust particulates, and the decrease in mass concentration between the engine exhaust and stack exhaust was due primarily to dilution of the engine exhaust gases within the augmentor tube. The additives were most effective for combustor exhaust gas temperatures of 1450° F or higher.

(e) None of the additives produced any significant change in NO_x concentrations at the stack exhaust.

(f) The scanning electron microscope photographs of collected engine exhaust particulates indicated that the values of D_{32} determined using light transmission measurements were reasonable accurate representations of the actual average particle sizes. The results obtained in the initial test series with the improved test cell instrumentation indicated that the completed apparatus provided a reasonably

good means for determination of the effects of fuel additives on engine and stack exhaust gas characteristics. For this reason the test series was expanded to re-evaluate all of the additives previously tested. DGT-2, CV-100 and XRG are being tested again together with Ferrocene and the Rare Earth additives.

TABLE I

TEST CELL FLOW RATES DURING ADDITIVE TESTS

ADDITIVE/ CONCENTRATION (ml./gal. JP-4)	$\dot{m}_{BP}$	$\dot{m}_P$	$\dot{m}_s$	$\dot{m}_e$	$\dot{m}_{e_T}$	$\dot{m}_f$	$\left(\frac{f}{a}\right)_P$	$\left(\frac{f}{a}\right)_{p+s}$
*FERROCENE/ 0.0	.830	.268	.186	.454	1.284	.0168	.0627	.0370
*FERROCENE/22.70	.830	.268	.186	.454	1.284	.0168	.0627	.0370
*FERROCENE/25.90	.830	.268	.186	.454	1.284	.0168	.0627	.0370
*FERROCENE/29.10	.830	.268	.186	.454	1.284	.0168	.0627	.0370
*FERROCENE/32.30	.830	.268	.186	.454	1.284	.0168	.0627	.0370
FERROCENE/ 0.0	.810	.254	.154	.408	1.218	.0170	.0671	.0418
FERROCENE/19.20	.829	.248	.169	.417	1.246	.0170	.0687	.0409
FERROCENE/28.80	.850	.255	.190	.445	1.294	.0170	.0668	.0383
FERROCENE/ 0.0	.842	.247	.178	.425	1.267	.0170	.0690	.0401
12% CERIUM HEX- CEM/ 0.0	.834	.249	.175	.424	1.258	.0168	.0673	.0395
12% CERIUM HEX- CEM/19.60	.822	.250	.183	.433	1.254	.0168	.0670	.0387
12% CERIUM HEX- CEM/29.30	.831	.255	.185	.444	1.275	.0168	.0657	.0377
12% CERIUM HEX- CEM/48.90	.831	.255	.189	.444	1.275	.0168	.0657	.0377
12% RARE EARTH HEX- CEM/ 0.0	.886	.244	.194	.438	1.324	.0172	.0705	.0393
12% RARE EARTH HEX- CEM/19.10	.871	.270	.185	.455	1.326	.0172	.0637	.0378
12% RARE EARTH HEX- CEM/47.60	.899	.252	.155	.407	1.306	.0172	.0682	.0422
12% RARE EARTH HEX- CEM/ 0.0	.899	.252	.155	.407	1.306	.0172	.0682	.0422

*Data taken on 10 November 1981; all other data collected on 19 November 1981. See table of symbols and abbreviations for explanation of column headings/units.

TABLE II

TEST CELL FLOW RATES/TEMPERATURES DURING ADDITIVE TESTS

ADDITIVE CONCENTRATION (ml./gal. JP-4)	$\dot{m}_{aug.\ T.}$	AUG. RATIO	T_{BP}	T_2	T_R	T_{MIX}	T_C
*FERROCENE/ 0.0	7.406	4.77	608	1910	642	1068	2048
*FERROCENE/22.70	7.406	4.77	608	1910	642	1068	2058
*FERROCENE/25.90	7.406	4.77	608	1910	642	1068	2013
*FERROCENE/29.10	7.406	4.77	608	1910	642	1068	2067
*FERROCENE/32.30	7.406	4.77	608	1910	642	1068	2008
FERROCENE/ 0.0	7.453	5.12	610	1900	649	1042	2017
FERROCENE/19.20	7.484	5.01	608	1890	641	1037	2012
FERROCENE/28.80	7.416	4.73	609	1890	639	1049	1997
FERROCENE/ 0.0	7.274	4.74	571	1855	616	1002	1972
12% CERIUM HEX- CEM/ 0.0	7.239	4.76	609	1900	643	1044	2026
12% CERIUM HEX- CEM/19.60	7.266	4.79	609	1920	644	1061	2035
12% CERIUM HEX- CEM/29.30	7.252	4.69	610	1920	643	1066	2035
12% CERIUM HEX- CEM/48.90	7.252	4.69	610	1920	643	1066	2040
12% RARE EARTH HEX- CEM/ 0.0	7.464	4.64	607	1885	642	1030	2022
12% RARE EARTH HEX- CEM/19.10	7.469	4.63	607	1880	640	1044	2022
12% RARE EARTH HEX- CEM/47.60	7.521	4.76	607	1885	640	1005	2022
12% RARE EARTH HEX- CEM/ 0.0	7.521	4.76	607	1880	640	1004	2022

*Data collected on 10 November 1981; all other data collected on 19 November 1981. See table of symbols and abbreviations for explanation of column headings/units.

TABLE III

STACK GAS OPACITY, NO_x CONCENTRATIONS, AND TRANSMITTANCE VALUES

ADDITIVE/ CONCENTRATION (ml./gal. JP-4)	PERCENT OPACITY	NO_x	T_λ 10140	T_λ 6500	T_λ 4500	T_λ 10000	T_λ 6943	T_λ 4000
*FERROCENE/ 0.0	39.00	-	86.20	79.00	73.80	95.00	93.10	88.50
*FERROCENE/22.70	28.80	-	90.70	85.40	81.20	96.10	96.90	92.30
*FERROCENE/25.90	28.80	-	93.80	89.10	85.40	97.50	96.40	94.60
*FERROCENE/29.10	23.70	-	93.80	89.50	86.40	99.10	98.10	96.40
*FERROCENE/32.30	42.00	-	89.20	83.50	78.60	97.80	97.70	94.80
FERROCENE/ 0.0	41.20	2.0	84.10	76.40	69.40	94.90	93.60	90.40
FERROCENE/19.20	33.00	2.0	83.10	75.70	68.60	95.40	93.60	90.40
FERROCENE/28.80	34.90	2.0	86.30	80.10	74.20	95.70	94.20	91.70
FERROCENE/ 0.0	50.30	2.0	78.40	69.90	61.80	93.90	91.70	88.40
12% CERIUM HEX- CEM/ 0.0	44.70	1.7	84.20	76.40	64.90	96.40	94.70	92.40
12% CERIUM HEX- CEM/19.60	28.10	1.9	88.00	81.60	76.10	96.70	95.00	92.40
12% CERIUM HEX- CEM/29.30	33.60	1.9	88.30	82.30	77.00	97.20	95.60	93.10
12% CERIUM HEX- CEM/48.90	33.90	2.0	87.20	80.90	75.80	97.20	95.40	92.30
12% RARE EARTH HEX- CEM/ 0.0	48.10	2.0	80.30	71.20	63.30	94.70	92.40	88.20
12% RARE EARTH HEX- CEM/19.10	56.90	1.6	76.40	66.30	58.00	93.40	90.90	86.50
12% RARE EARTH HEX- CEM/47.60	53.60	1.7	78.20	68.80	61.30	93.40	91.50	87.20
12% RARE EARTH HEX- CEM/ 0.0	49.50	1.9	79.70	71.50	65.00	94.40	92.40	88.70

*Data collected on 10 November 1981; all other data collected on 19 November 1981.
-Data not available
See table of symbols and abbreviations for explanation of column headings/units.

TABLE IV

MEAN PARTICLE DIAMETERS (D_{32}) AND MASS CONCENTRATIONS (C_m) FOR EACH TEST

ADDITIVE/ CONCENTRATION (ml./gal. JP-4)	D_{32} STACK EXHAUST (10140/6500/4500)	D_{32} ENGINE EXHAUST (10000/6943/4000)	C_{ms} STACK (10140)	C_{me} ENGINE (10000)
*FERROCENE/ 0.0	.21 ± .01 ; b,d	----------	40.30	-----
*FERROCENE/22.70	.20 ± .005; d	----------	26.90	-----
*FERROCENE/25.90	.20 ± .004; c	.21 ± .01; b,d	17.50	103.3
*FERROCENE/29.10	.22 ± .003; a,c	----------	16.60	-----
*FERROCENE/32.30	.20 ± .003; b	----------	33.50	-----
FERROCENE/ 0.0	.20 ± .02 ; b	----------	51.10	-----
FERROCENE/19.20	.21 ± .03 ; b,d	.21 ± .02; b,d	54.20	205.0
FERROCENE/28.80	.22 ± .03 ; b,d	.24 ± .02; d	40.00	178.0
FERROCENE/ 0.0	.23 ± .03 ; b	.24 ± .01; d	70.40	254.1
12% CERIUM HEX-CEM / 0.0	----------	.21 ± .01; d	-----	149.8
12% CERIUM HEX-CEM /19.60	.19 ± .001; b	.18 ± .01; b,d	37.80	152.7
12% CERIUM HEX-CEM /29.30	.20 ± .01 ; b,d	.21 ± .01; a,c	34.10	122.6
12% CERIUM HEX-CEM /48.90	.22 ± .003; b	.19 ± .01; a,c	39.90	128.2
12% RARE EARTH HEX-CEM / 0.0	.20 ± .01 ; b	.20 ± .02; b,d	64.40	242.9
12% RARE EARTH HEX-CEM /19.10	.22 ± .01 ; b	.22 ± .03; b,d	78.10	299.9
12% RARE EARTH HEX-CEM /47.60	.22 ± .01 ; b,d	----------	66.70	-----
12% RARE EARTH HEX-CEM / 0.0	.24 ± .02 ; b,d	.23 ± .03; b,d	65.40	251.6

Key to complex refractive index/standard deviation:

a) m = 1.80-.60i/1.5 b) m = 1.80-.60i/2.0

c) m = 1.95-.66i/1.5 d) m = 1.95-.66i/2.0

*Data collected on 10 November 1981; all other data collected on 19 November 1981.

-Data not available.

See table of symbols and abbreviations for explanation of column headings/units.

TABLE V

TEST CELL VOLUME FLOW RATES AND PARTICULATE MASS FLOW RATES/RATIOS FOR EACH ADDITIVE TEST

ADDITIVE/ CONCENTRATION (ml./gal. JP-4)	Q_e	Q_s	$\dot{m}_{c_e}$	$\dot{m}_{c_s}$	$\left[\frac{\dot{m}_{c_e}}{\dot{m}_{c_s}}\right]$
*FERROCENE/ 0.0	5.97	20.69	-----	8.35	----
*FERROCENE/22.70	5.97	20.69	-----	5.56	----
*FERROCENE/25.90	5.97	20.69	6.16	3.61	1.70
*FERROCENE/29.10	5.97	20.69	-----	3.43	----
*FERROCENE/32.30	5.97	20.69	-----	6.94	----
FERROCENE/ 0.0	5.52	21.04	-----	10.75	----
FERROCENE/19.20	5.62	20.88	11.53	11.31	1.02
FERROCENE/28.80	5.91	20.63	10.51	8.25	1.27
FERROCENE/ 0.0	5.52	19.51	14.04	13.73	1.02
12% CERIUM HEX- CEM/ 0.0	----	-----	-----	-----	----
12% CERIUM HEX- CEM/19.60	5.79	20.35	8.84	7.70	1.15
12% CERIUM HEX- CEM/29.30	5.91	20.28	7.25	6.90	1.05
12% CERIUM HEX- CEM/48.90	5.91	20.28	7.58	8.09	0.94
12% RARE EARTH HEX- CEM/ 0.0	5.93	20.86	14.41	13.44	1.07
12% RARE EARTH HEX- CEM/19.10	6.02	20.81	18.06	16.24	1.11
12% RARE EARTH HEX- CEM/47.60	----	-----	-----	-----	----
12% RARE EARTH HEX- CEM/ 0.0	5.71	20.95	14.35	13.70	1.05

*Data collected on 10 November 1981; all other data collected on 19 November 1981.
-Data not available.
See table of symbols and abbreviations for explanation of column headings/units.

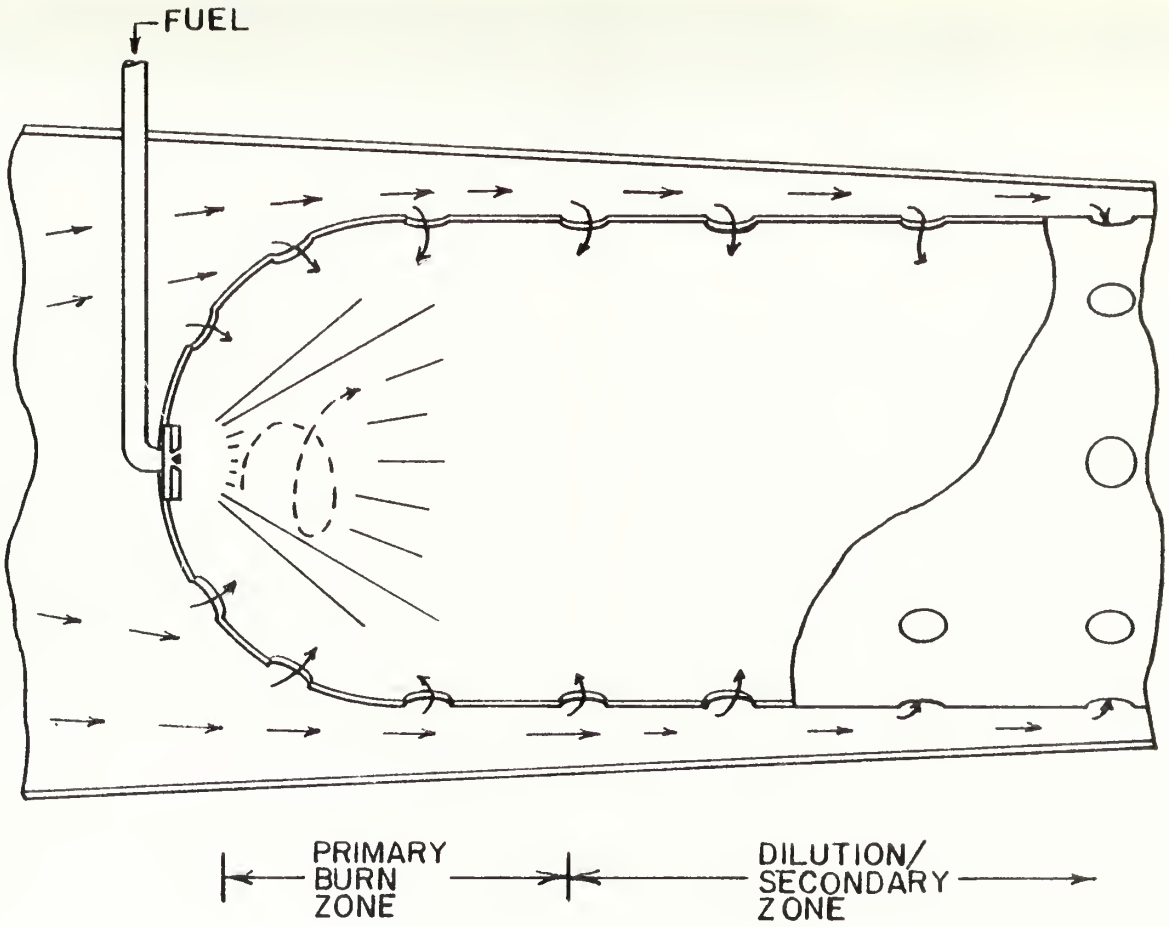

Figure 1. Typical Jet Engine Combustor

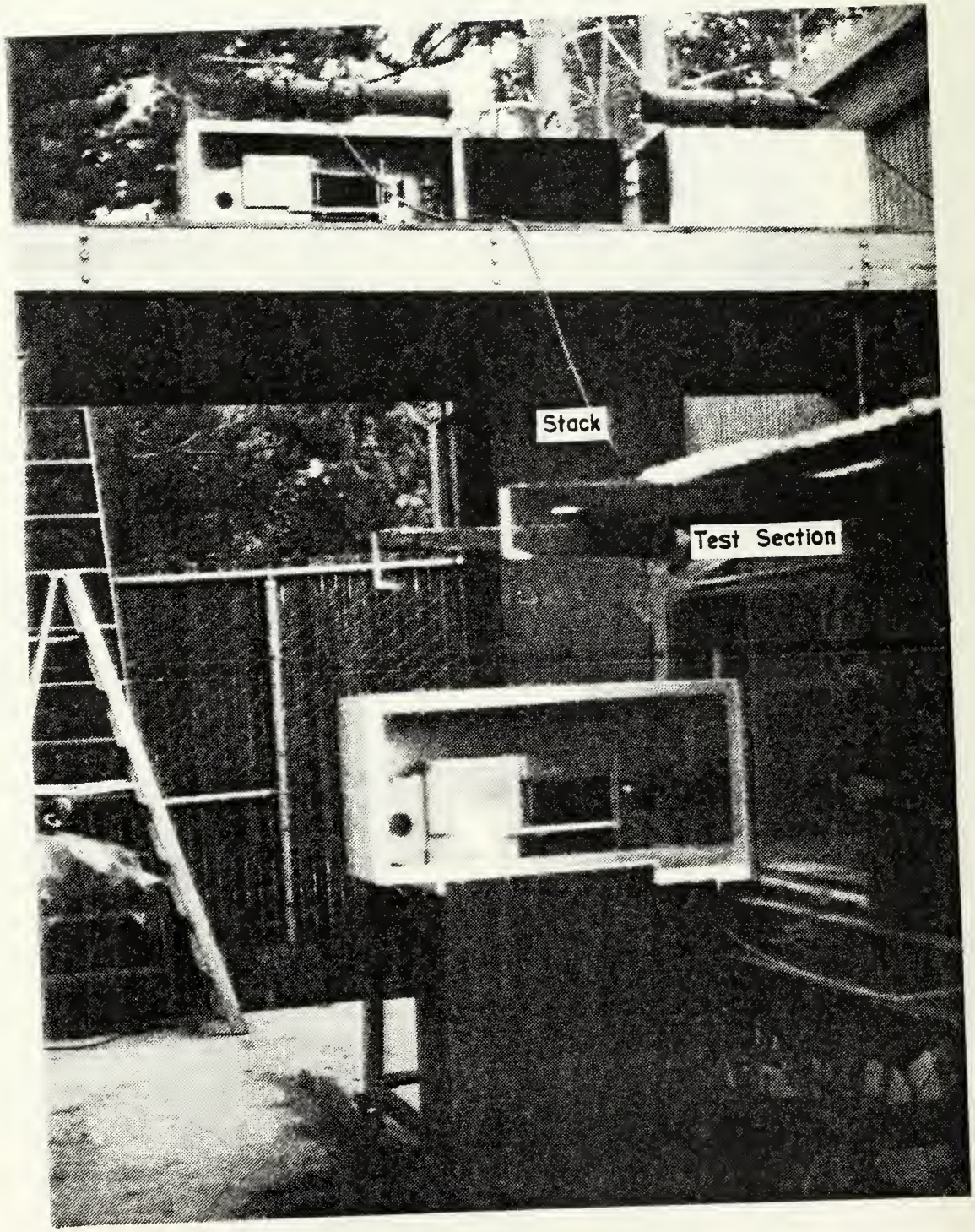

Figure 2. Sub-Scale Turbojet Test Cell

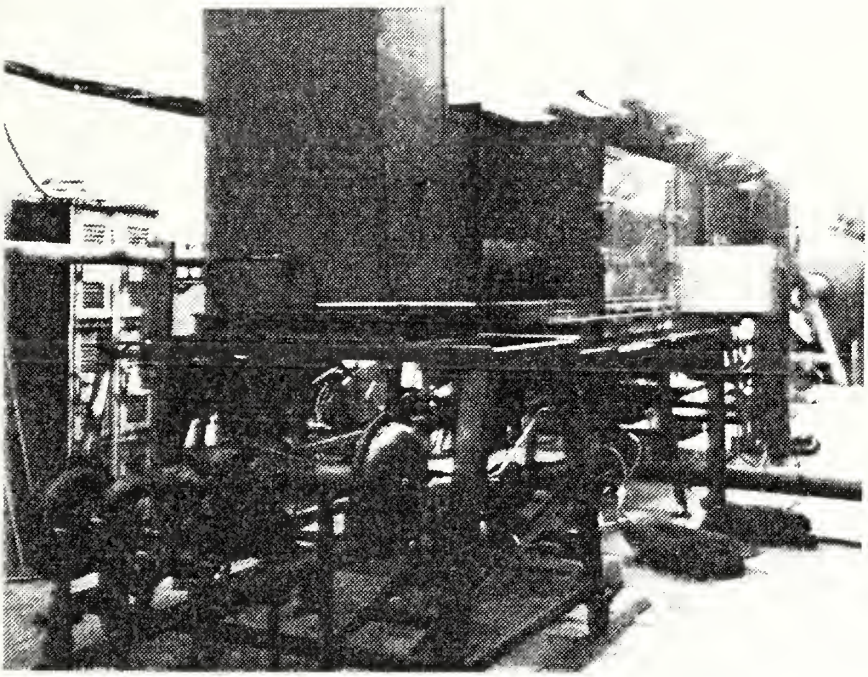

Figure 3

Photograph of Sub-Scale Test Cell

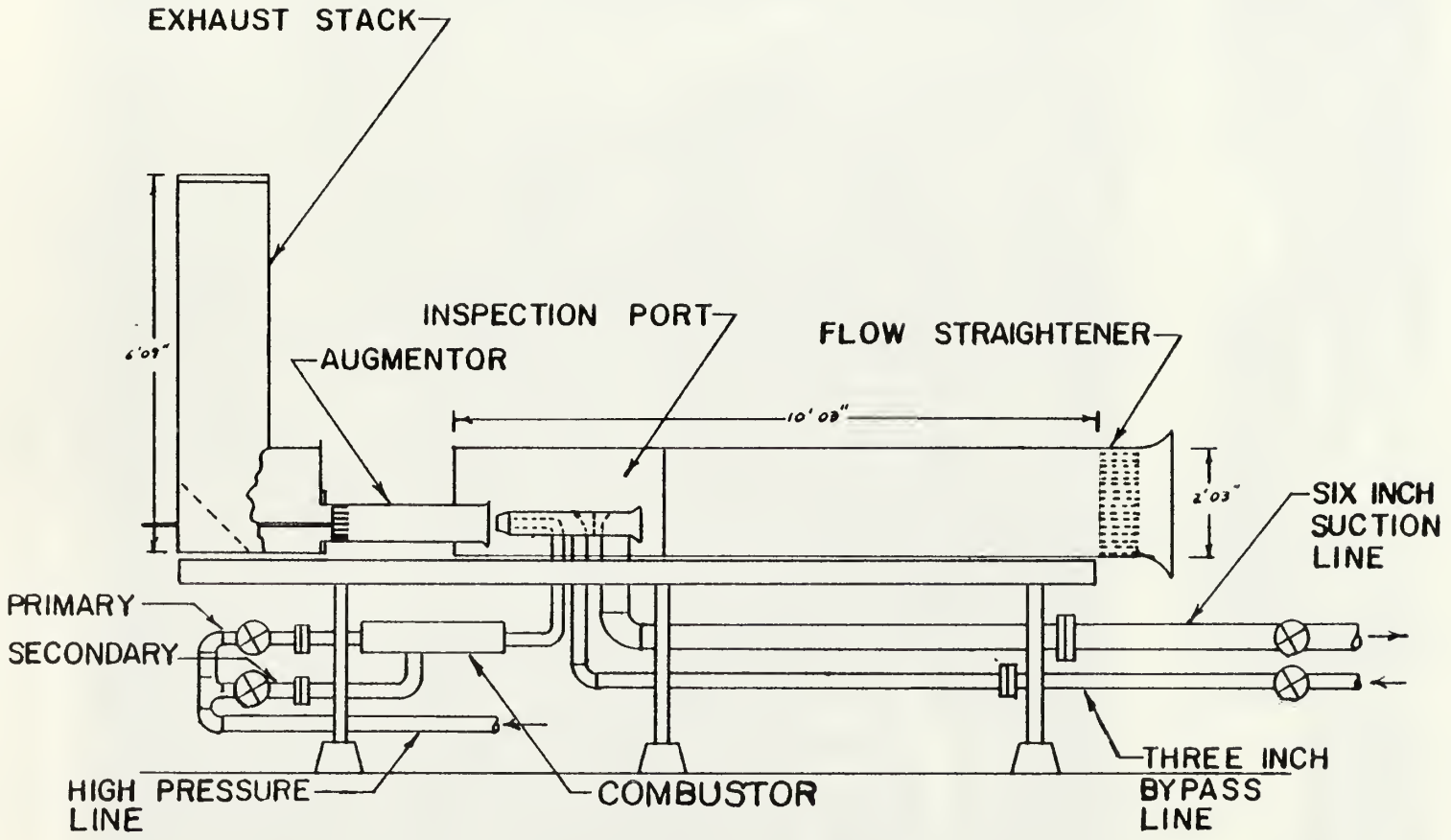

Figure 4. Sub-Scale Test Cell Plumbing

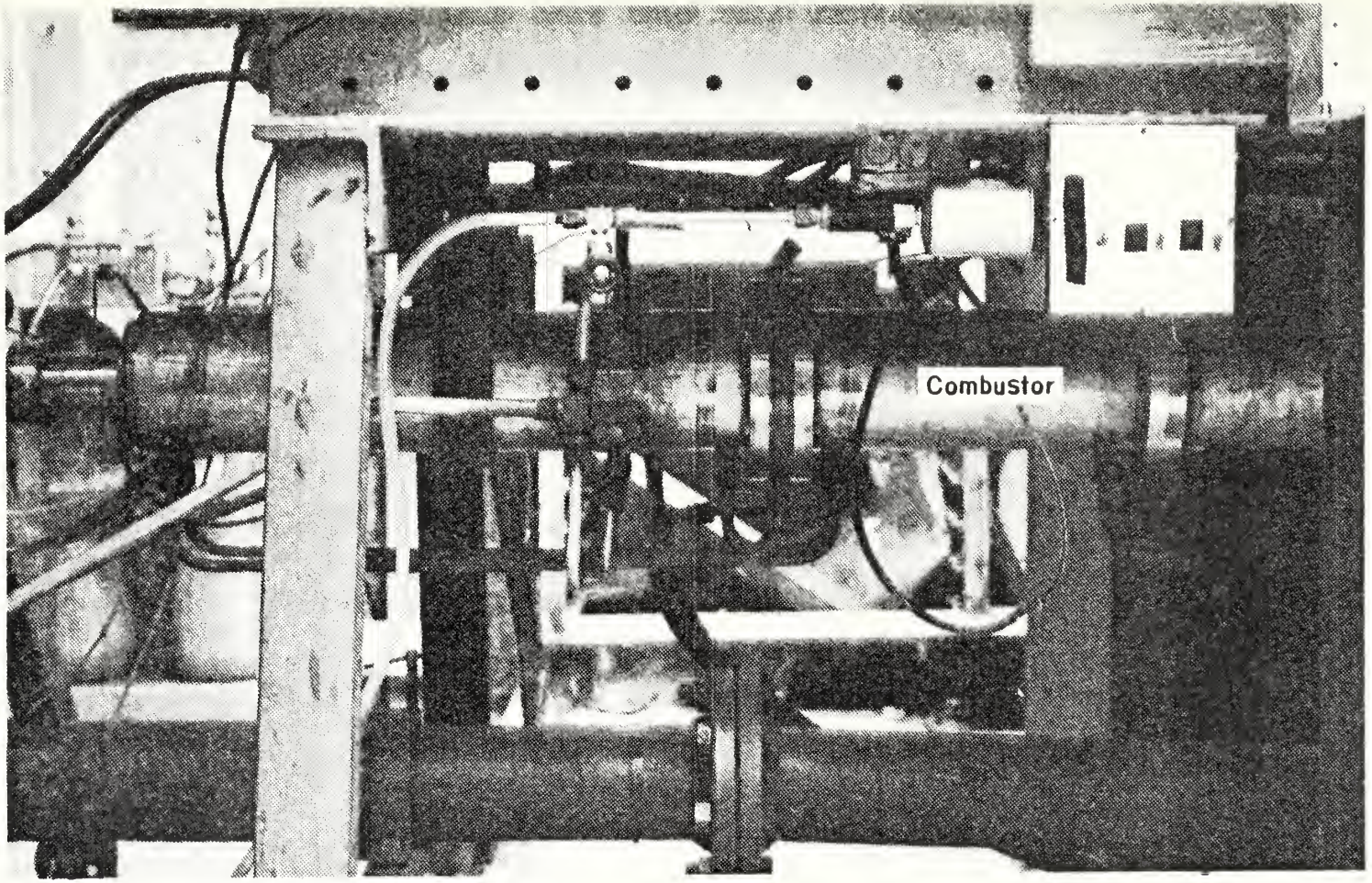

Figure 5. Sub-Scale Turbojet Test Cell Combustor

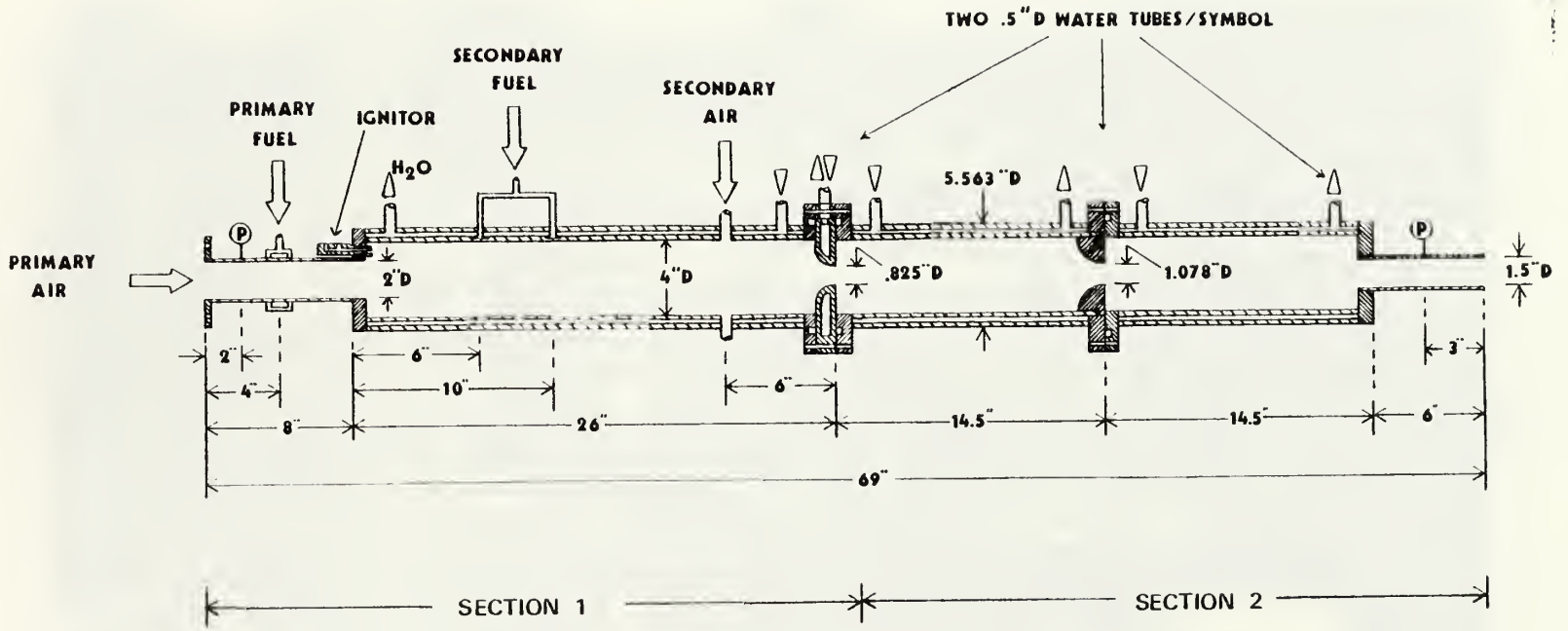

Figure 6. Schematic of Water-Cooled Ramjet Type Dump-Combustor
(Figure 3 of Reference 13)

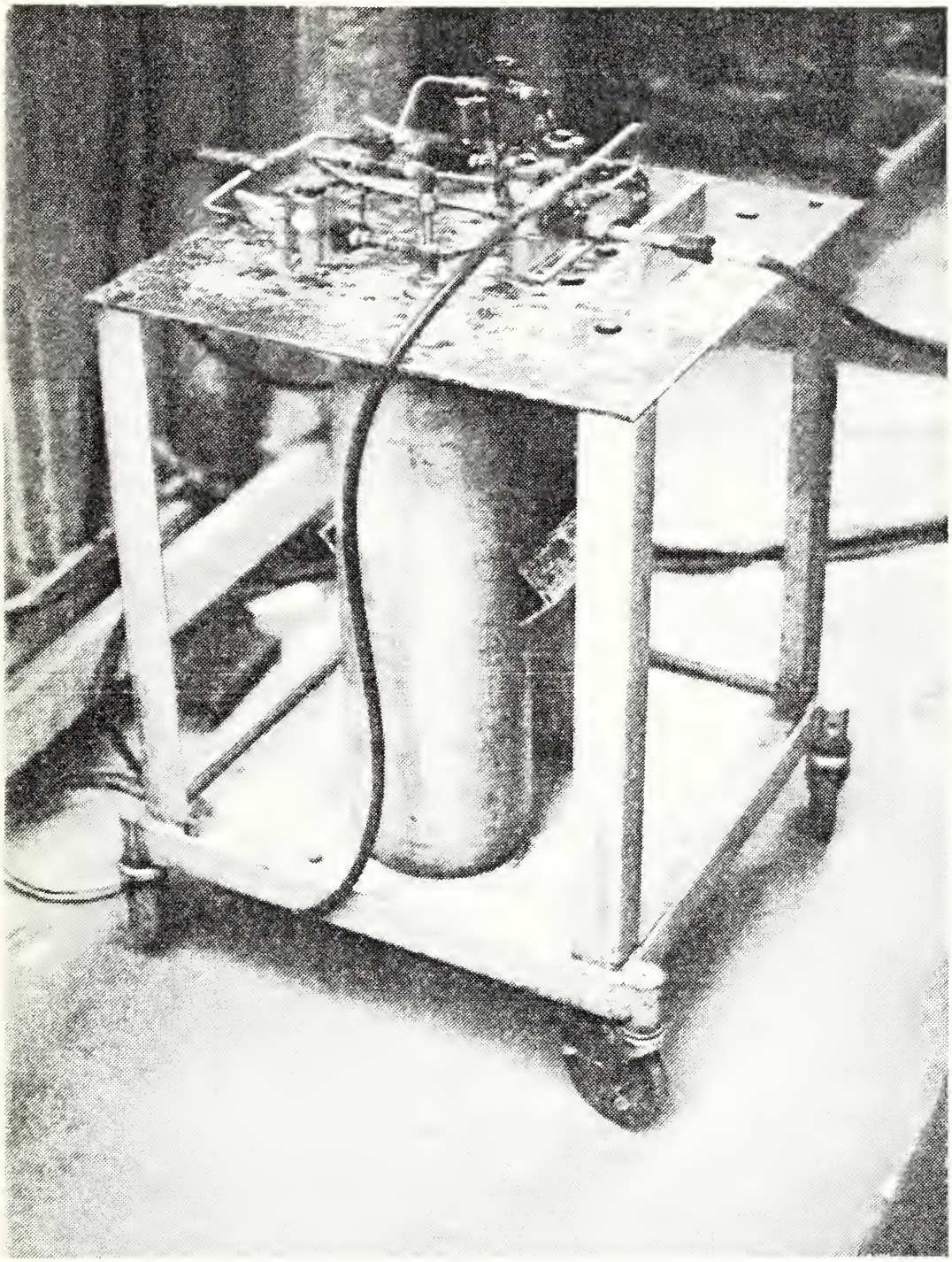

Figure 7. Portable Fuel Supply System

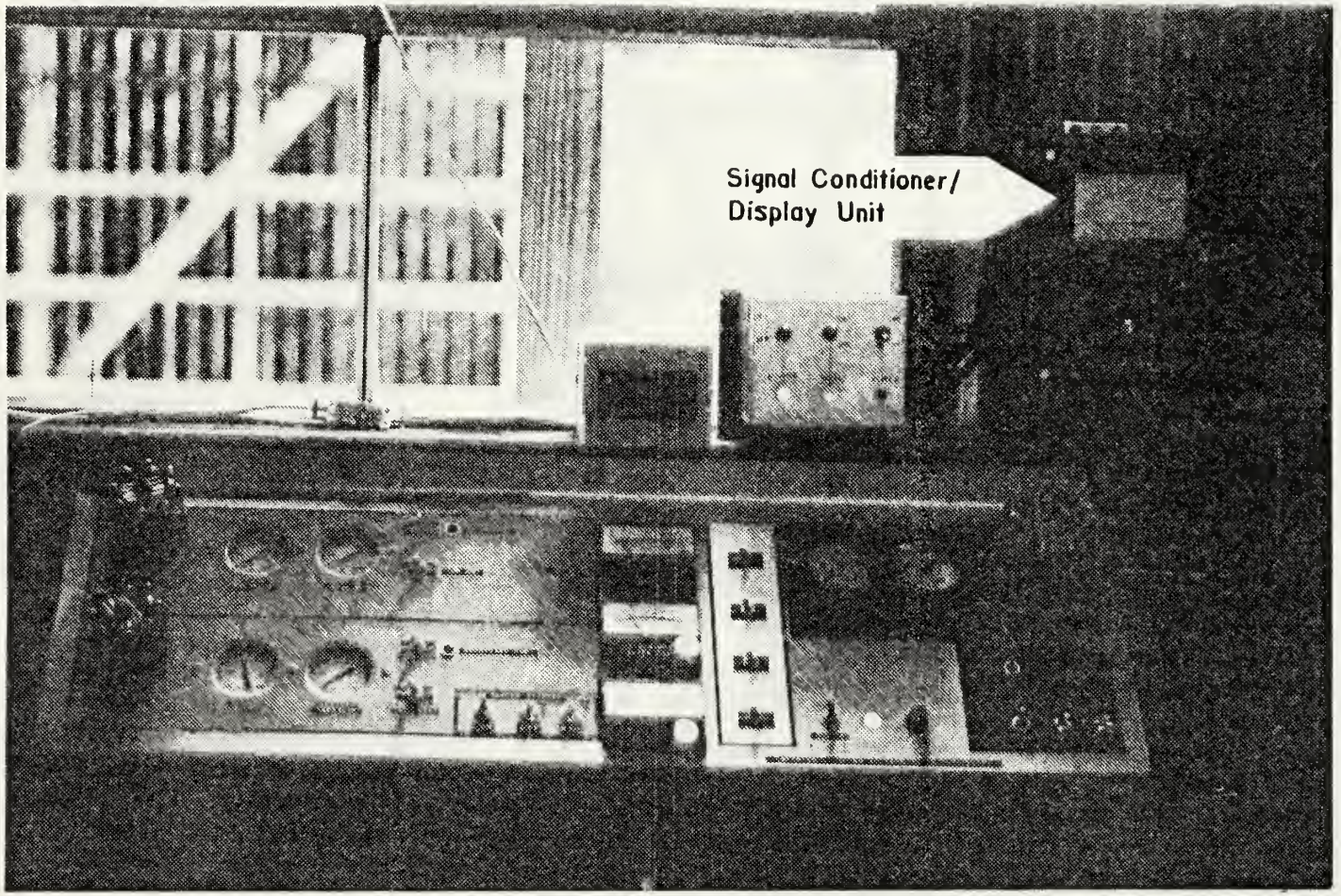

Figure 8. Remote Control Panel and Signal Conditioner/Display Unit

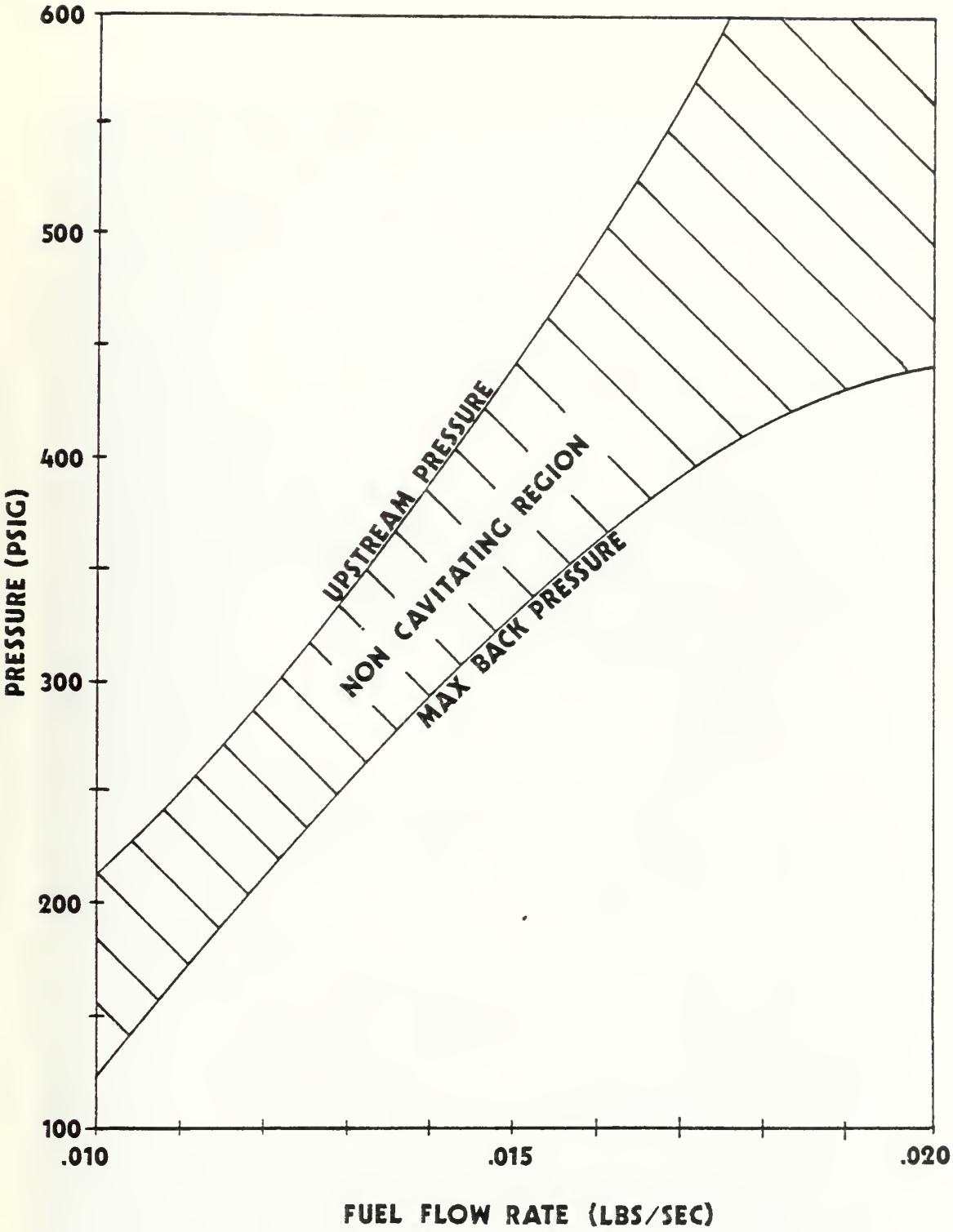

Figure 9. Cavitating Venturi Pressure vs. Flow Rate for .016-Inch Diameter Venturi (Figure 7 of Reference 13)

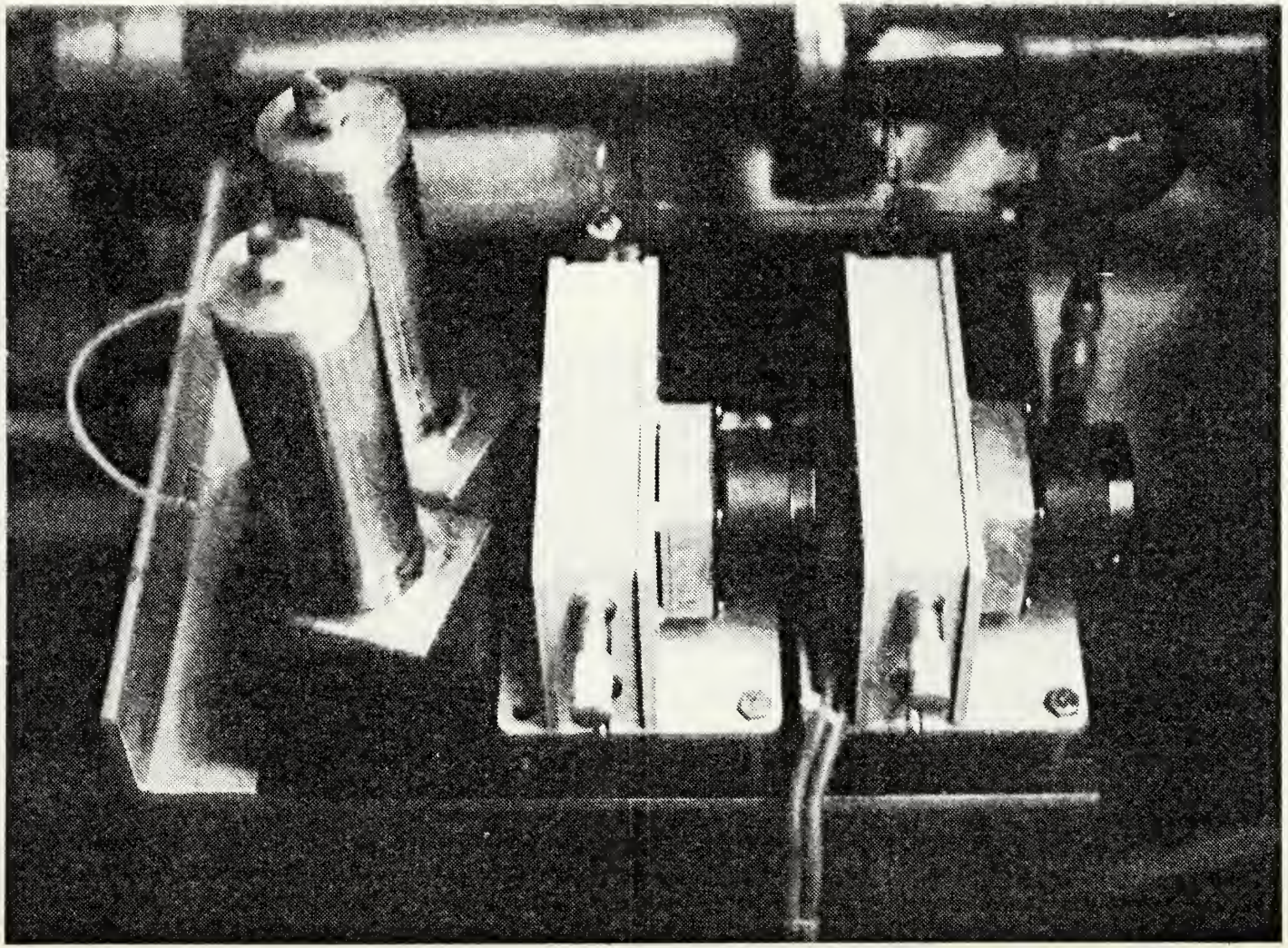

Figure 10. Precision Metering Pumps

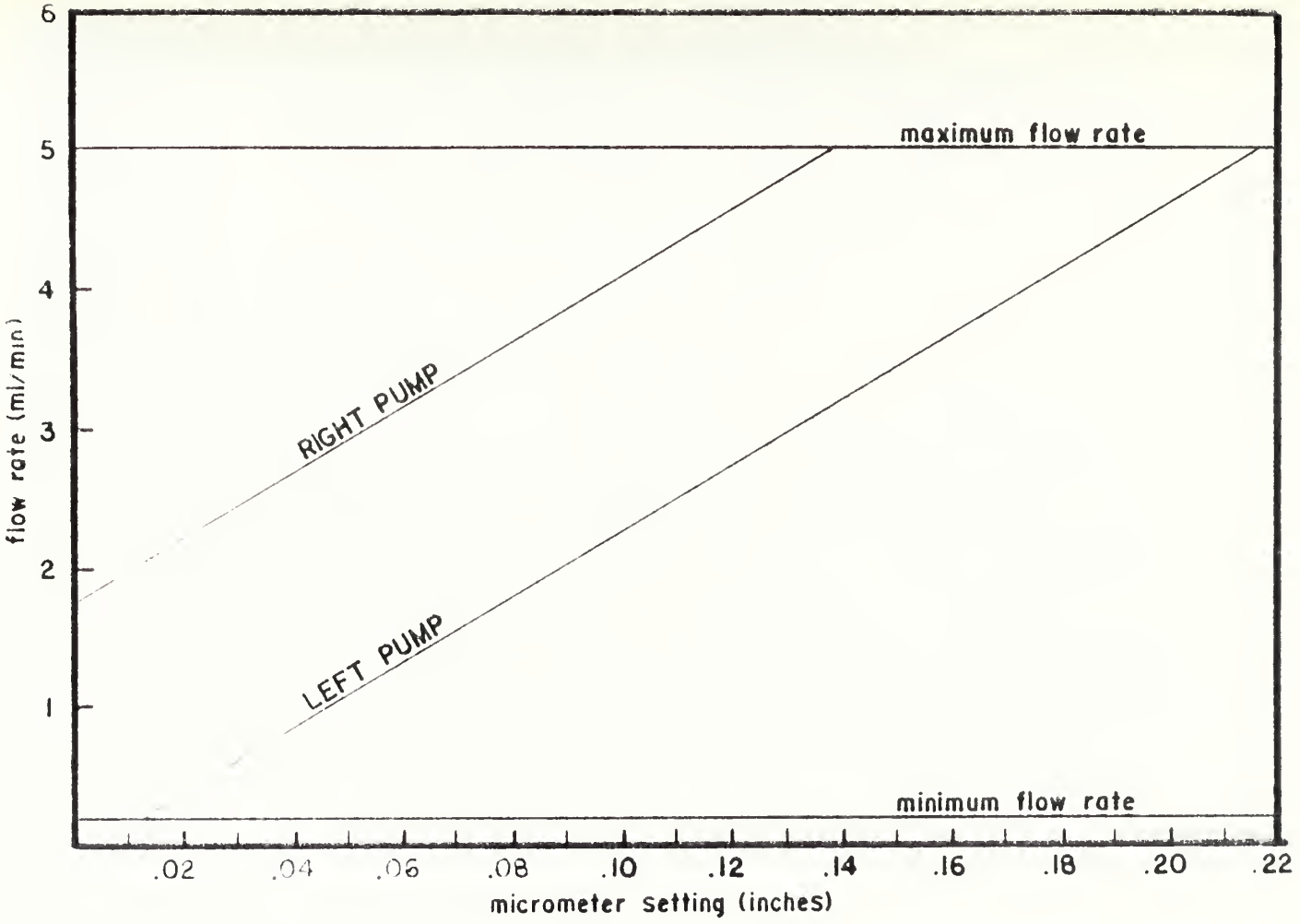

Figure 11. Precision Metering Pump Calibration Curves

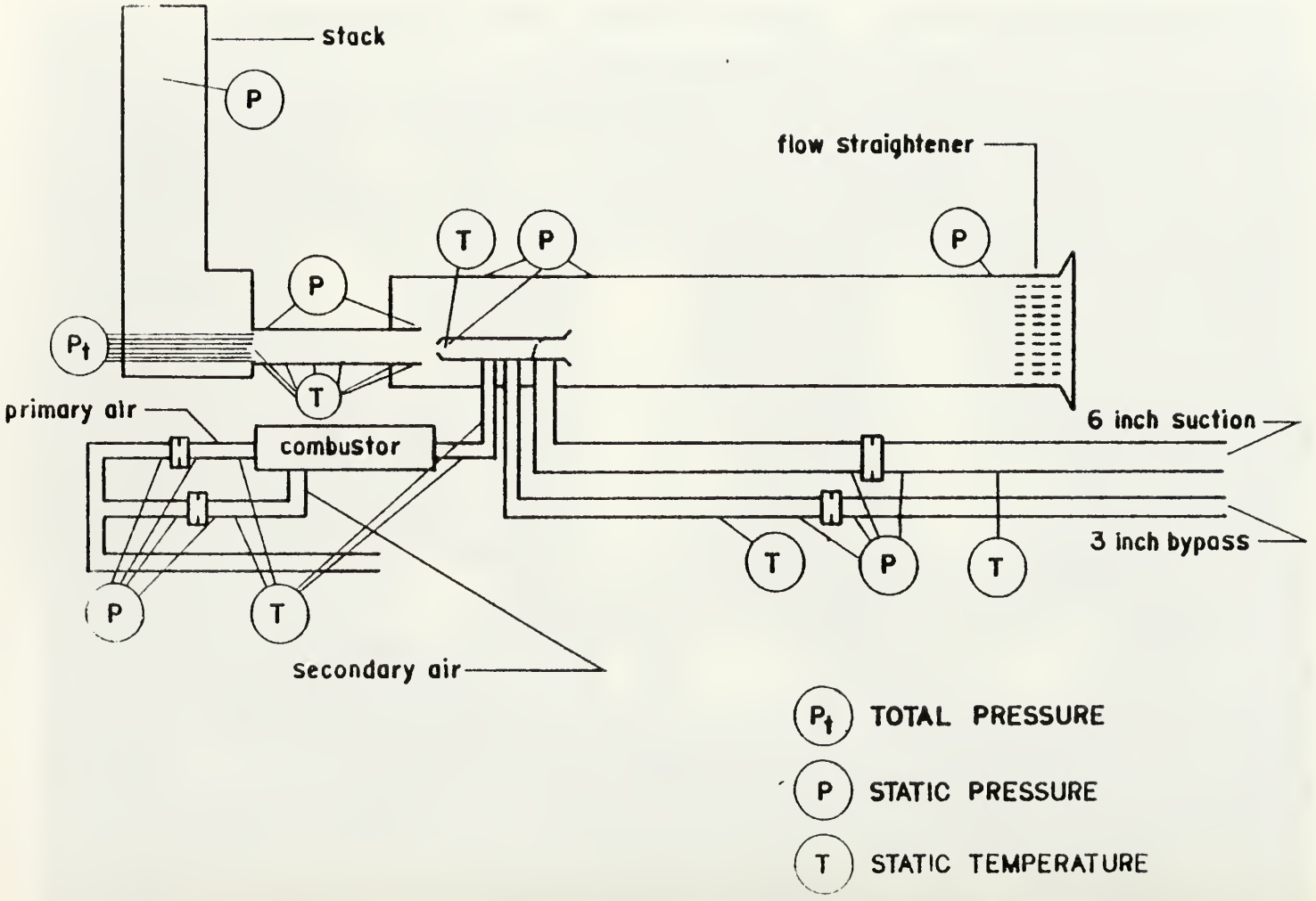

Figure 12. Pressure Tap and Temperature Sensor Locations

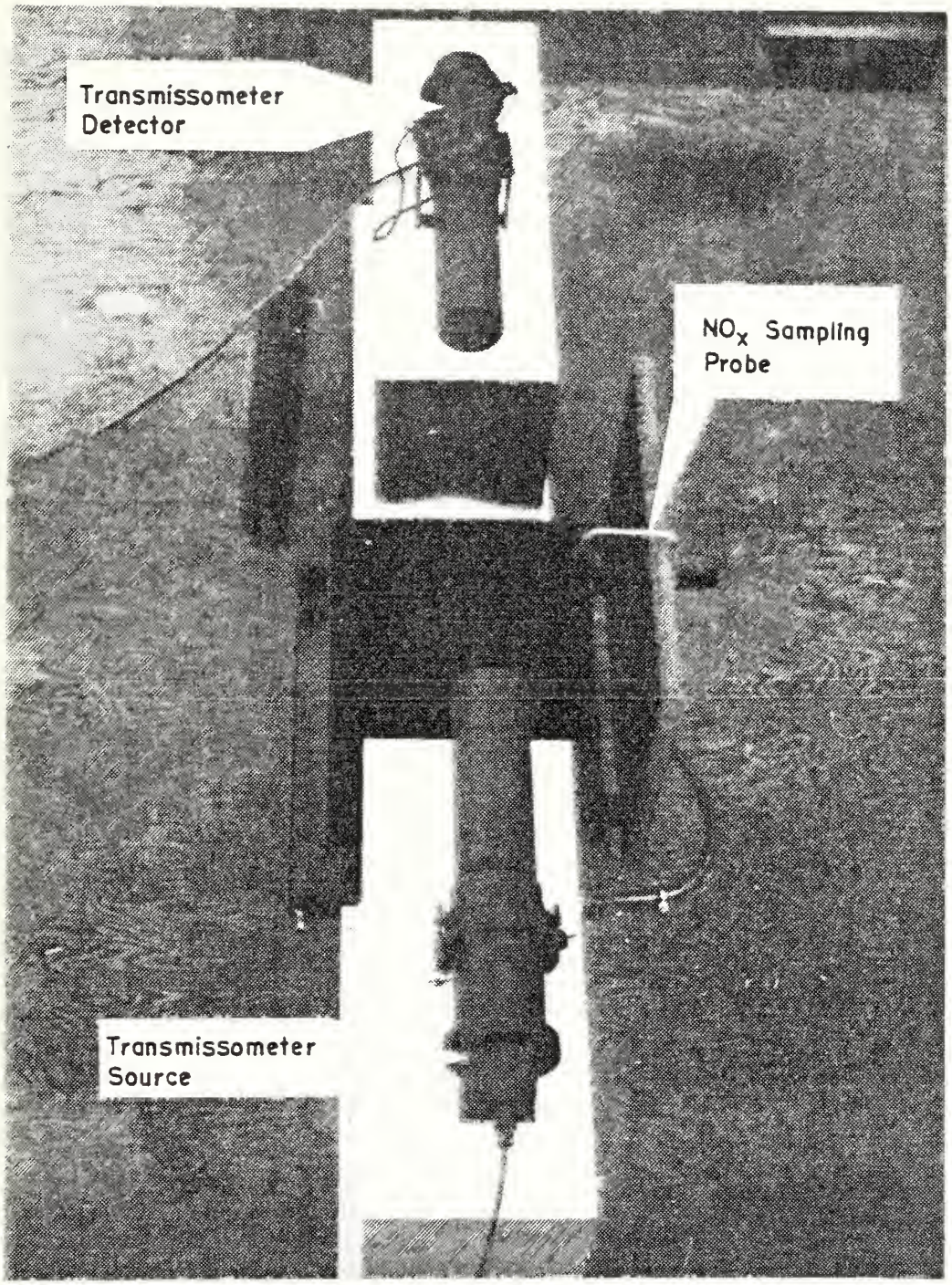

Figure 13. Transmissometer Source/Detector Unit

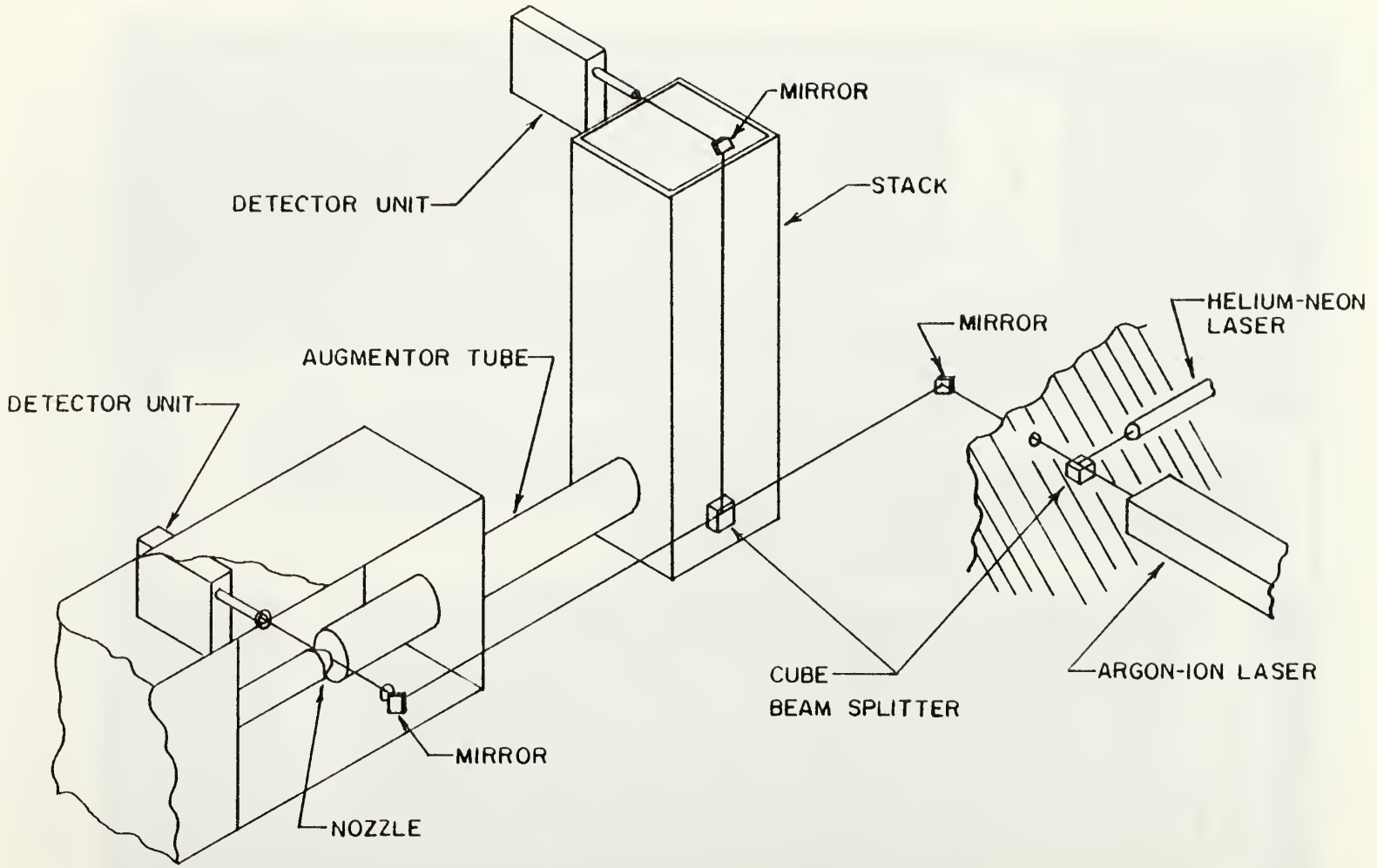

Figure 14. Optical Path of Laser Beams

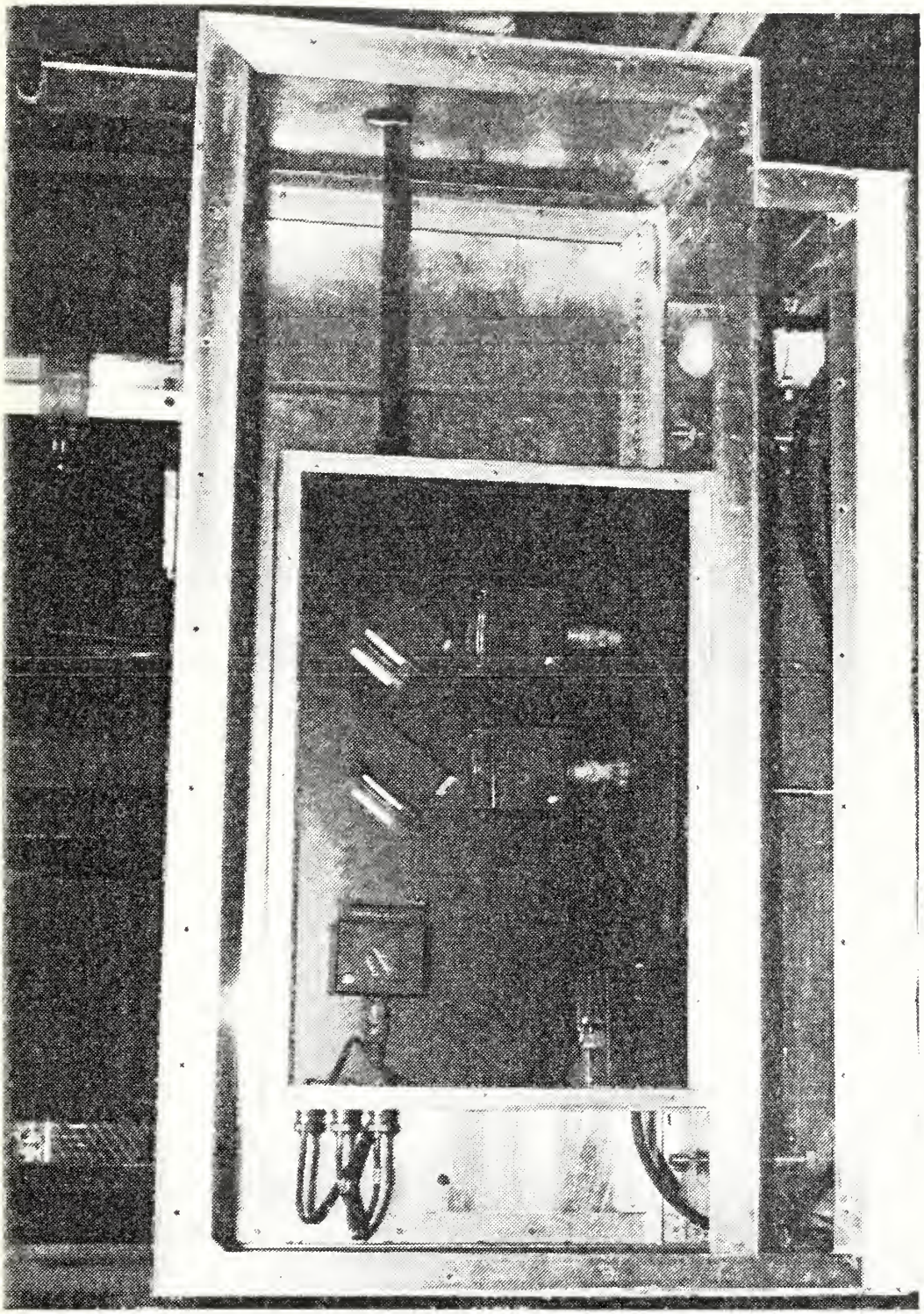

Figure 15. Light Detector

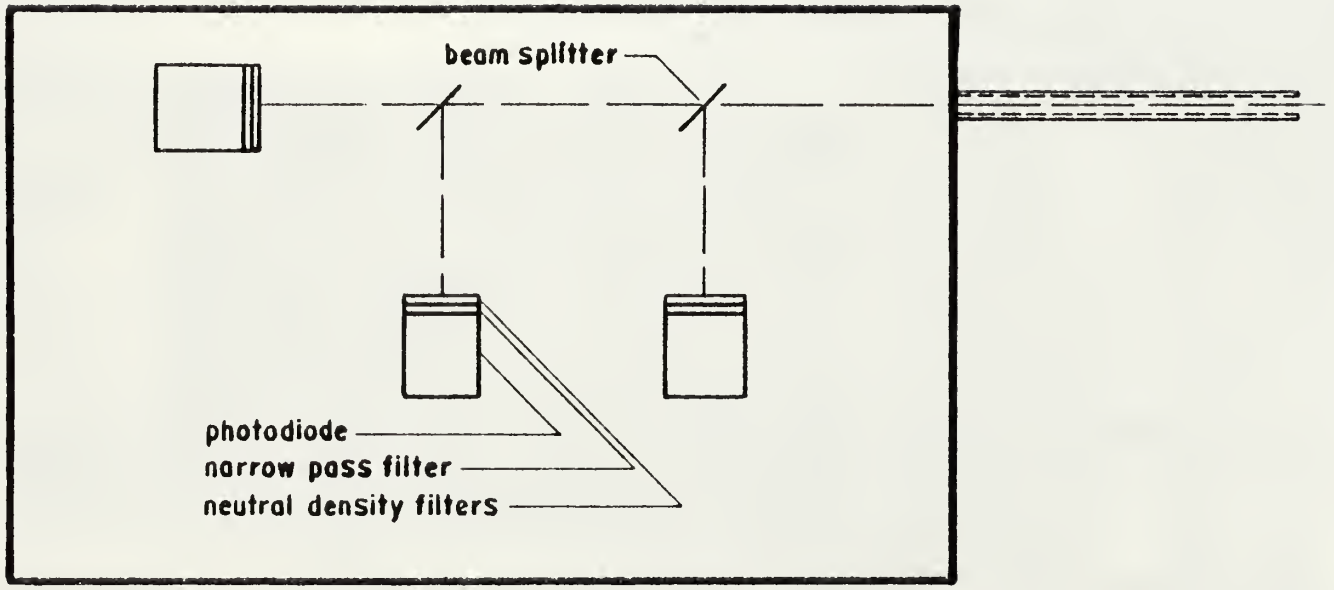

Figure 16. Schematic of Light Path Through the Optical Detector

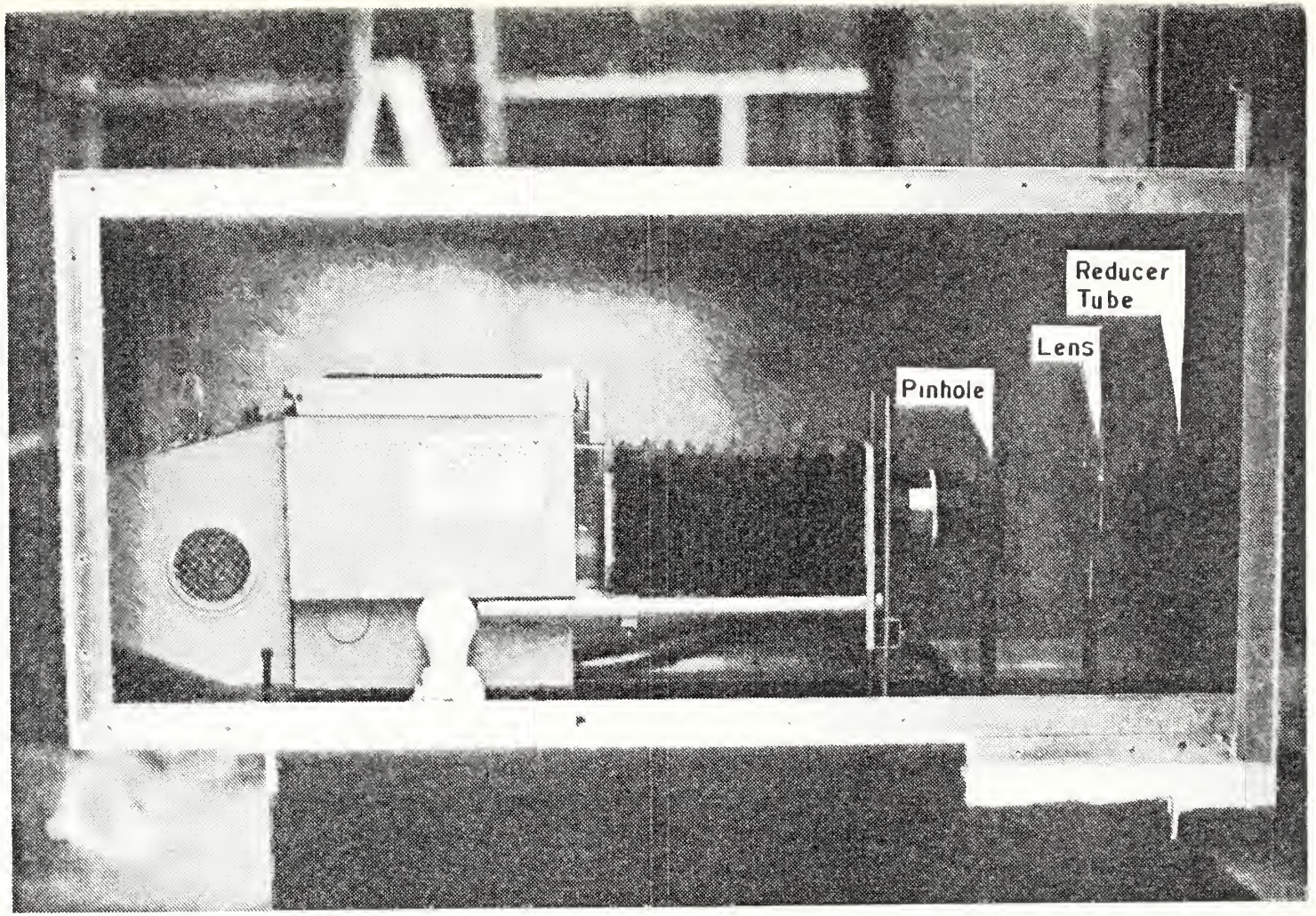

Figure 17. Collimated White Light Source

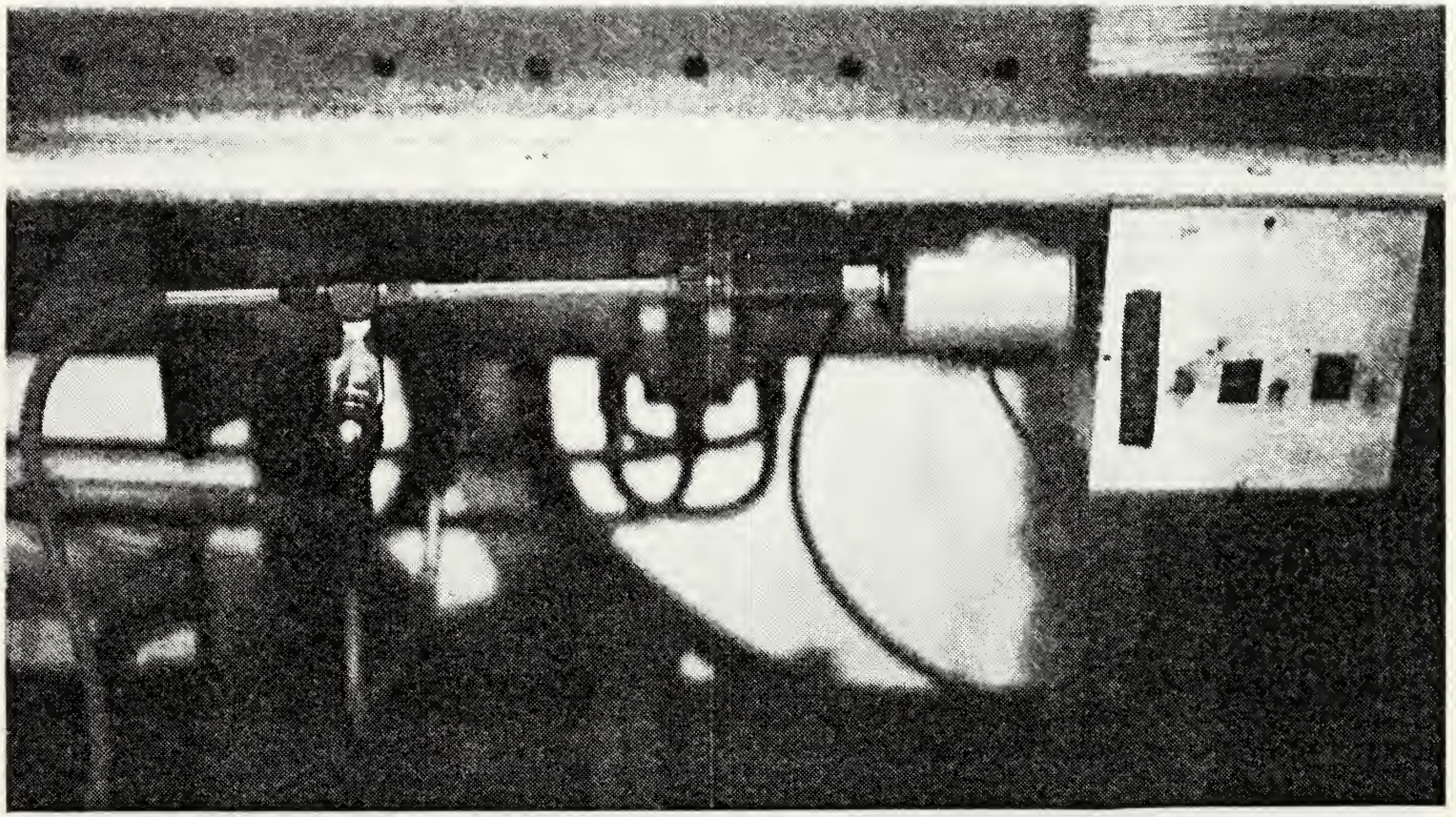

Figure 18. Sampling Train

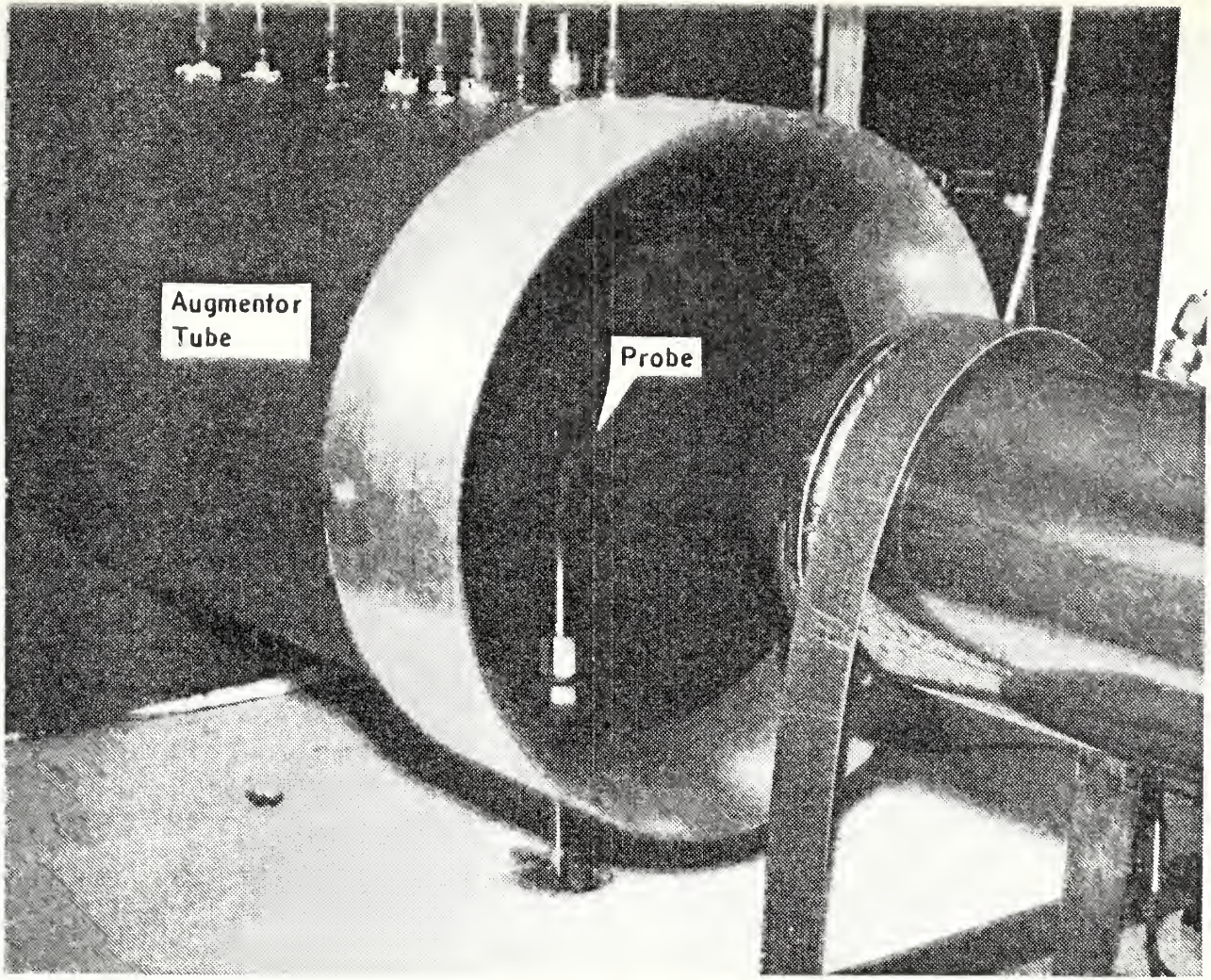

Figure 19. Sampling Probe

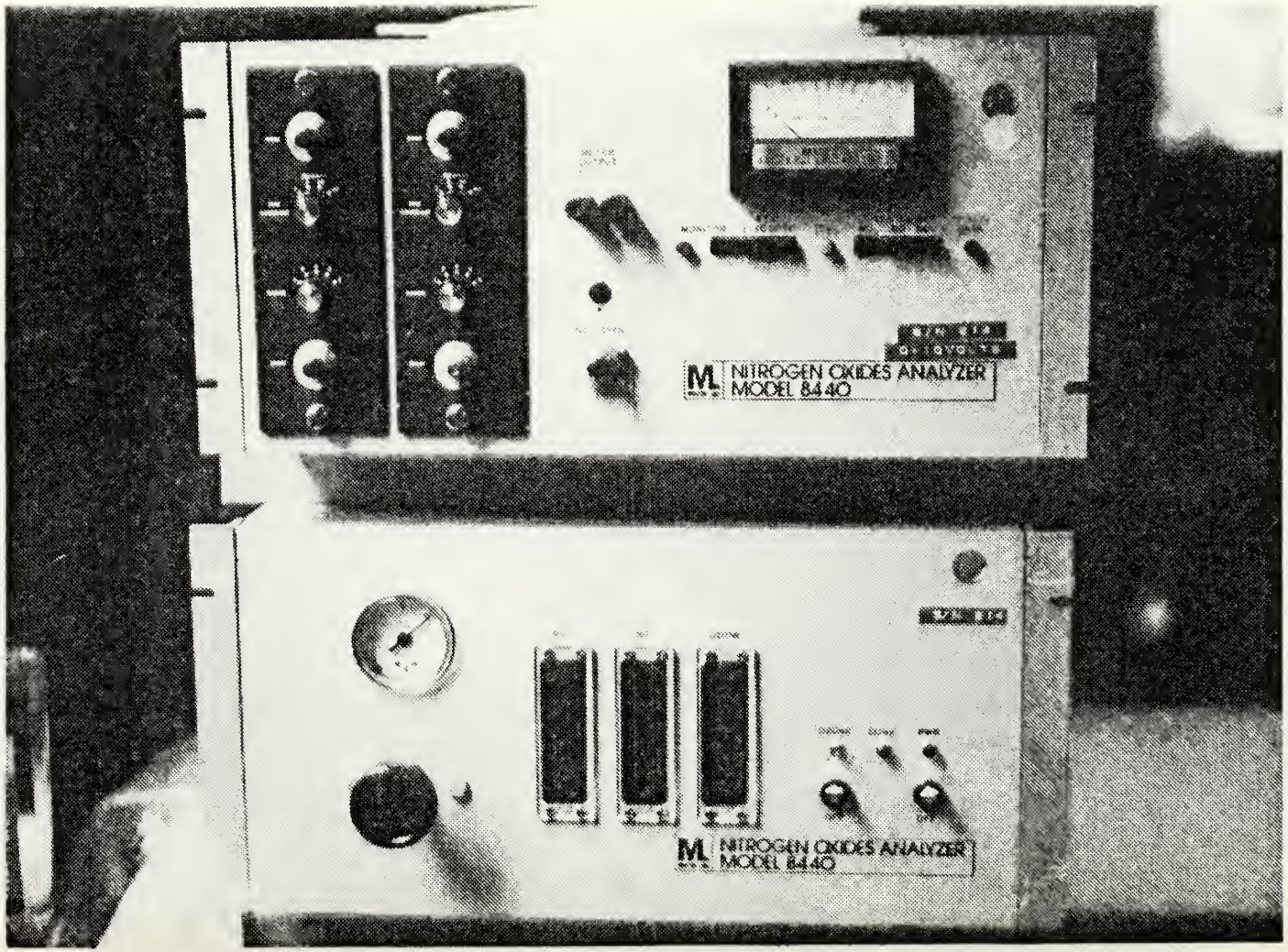

Figure 20. Nitrogen Oxides Analyzer

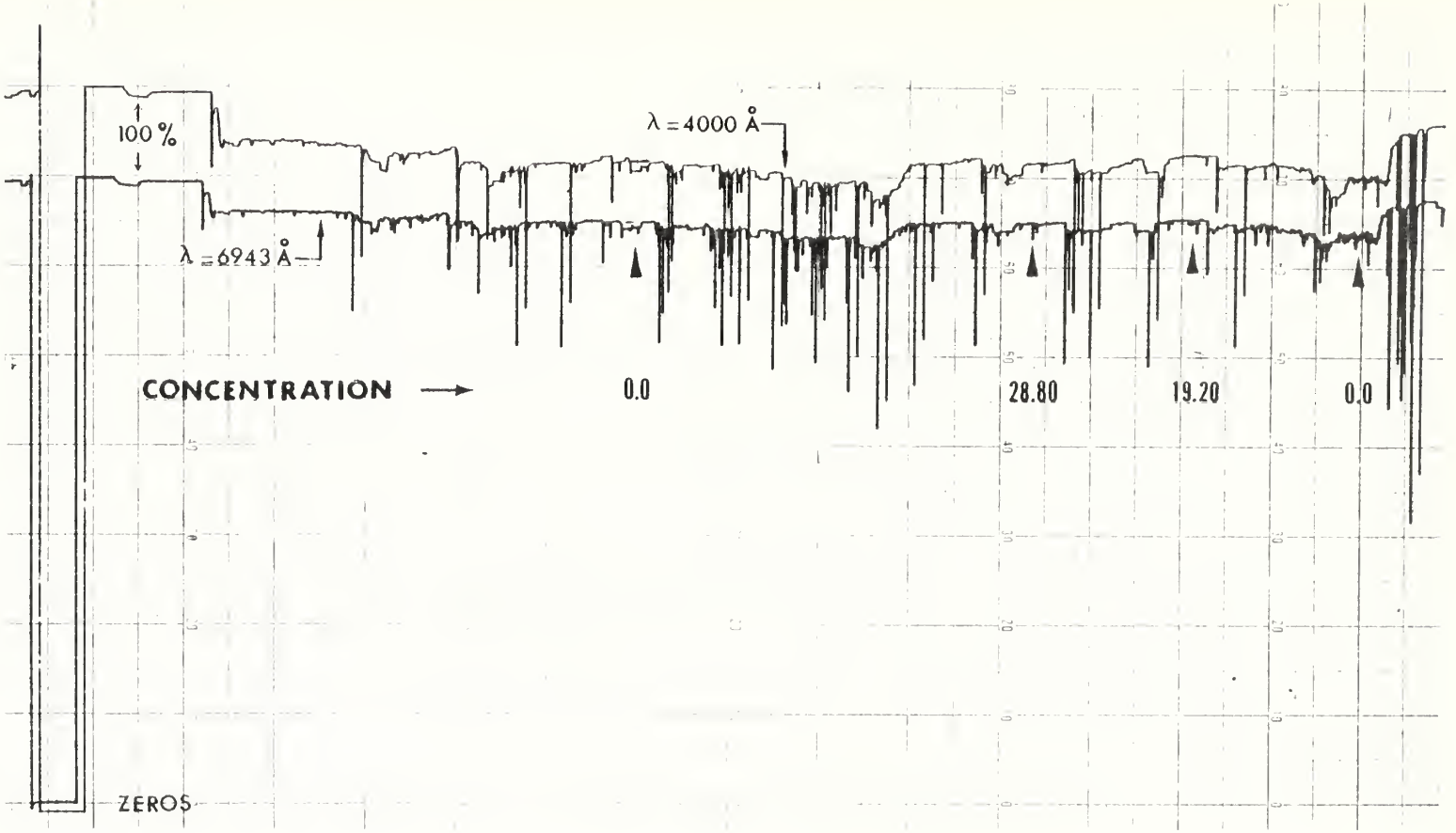

Figure 21. Strip Chart Recording of Ferrocene Test Conducted on 19 November 1981 (λ = 4000 Å; λ = 6943 Å)

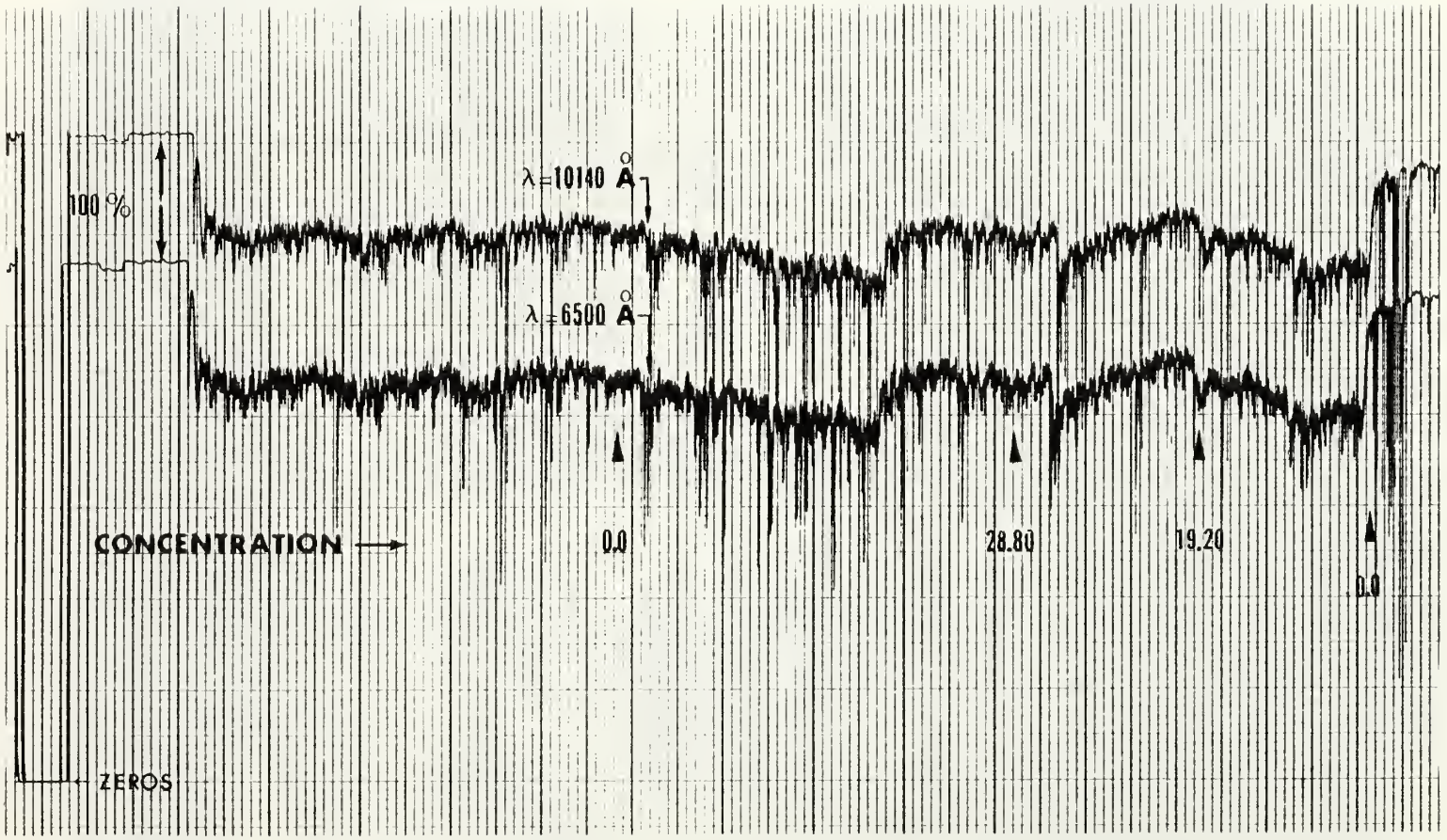

Figure 22. Strip Chart Recording of Ferrocene Test Conducted on 19 November 1981 (λ = 6500 Å; λ = 10140 Å)

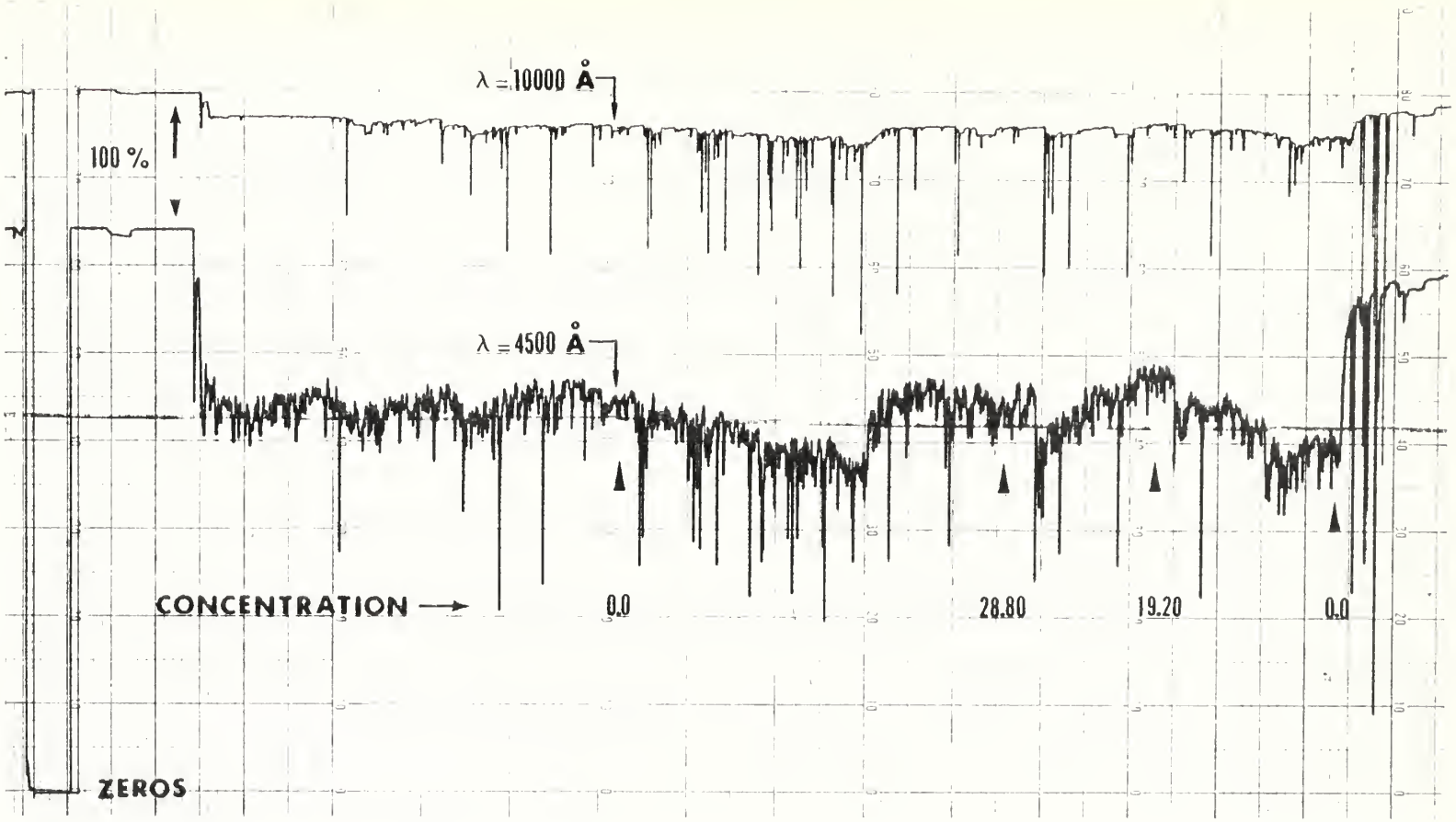

Figure 23. Strip Chart Recording of Ferrocene Test Conducted on 19 November 1981 (λ = 4500 Å; λ = 10000 Å)

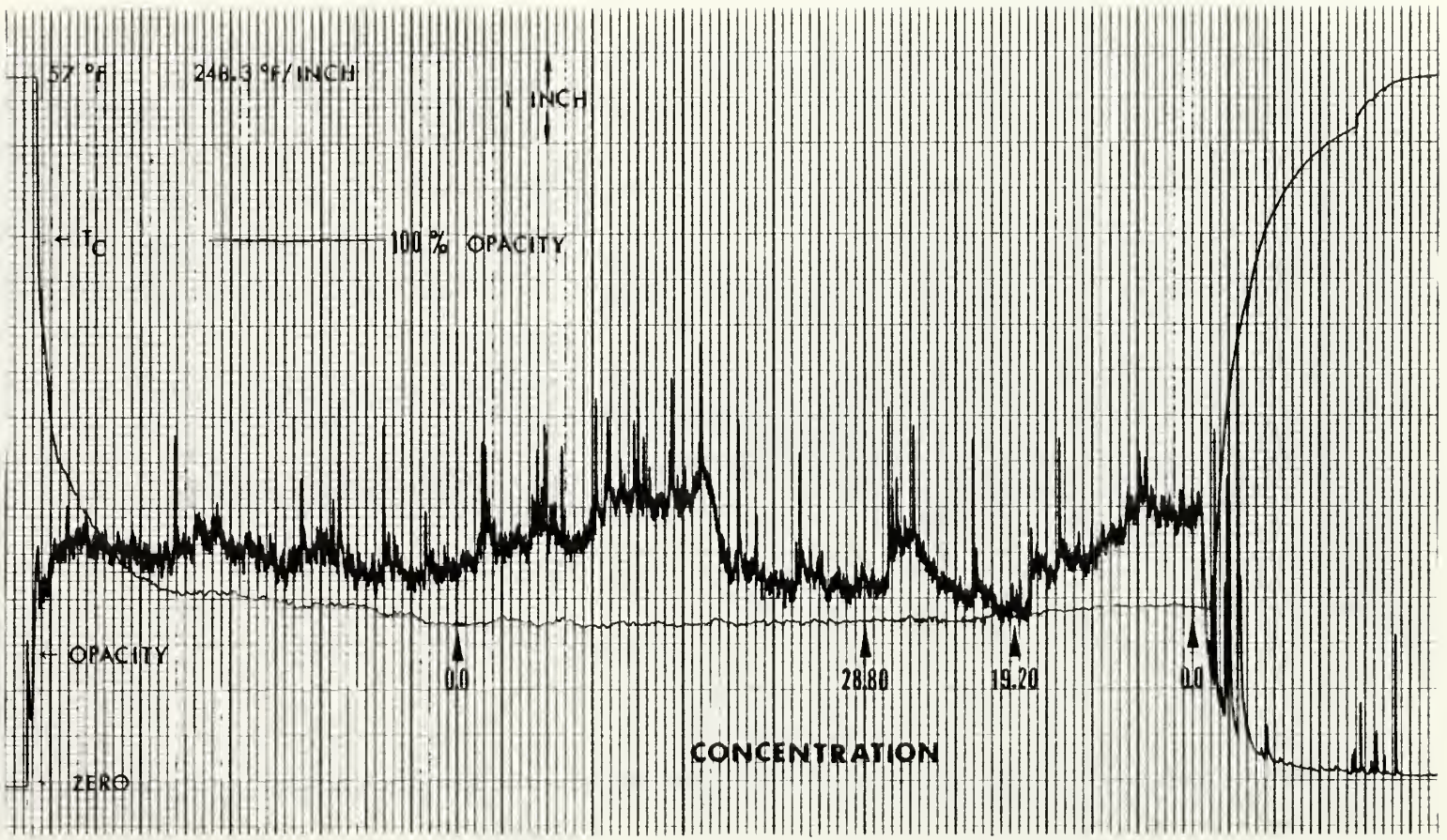

Figure 24. Strip Chart Recording of Ferrocene Test Conducted on 19 November 1981 (Combustor Exhaust Temperature (T_C) and Exhaust Gas Opacity)

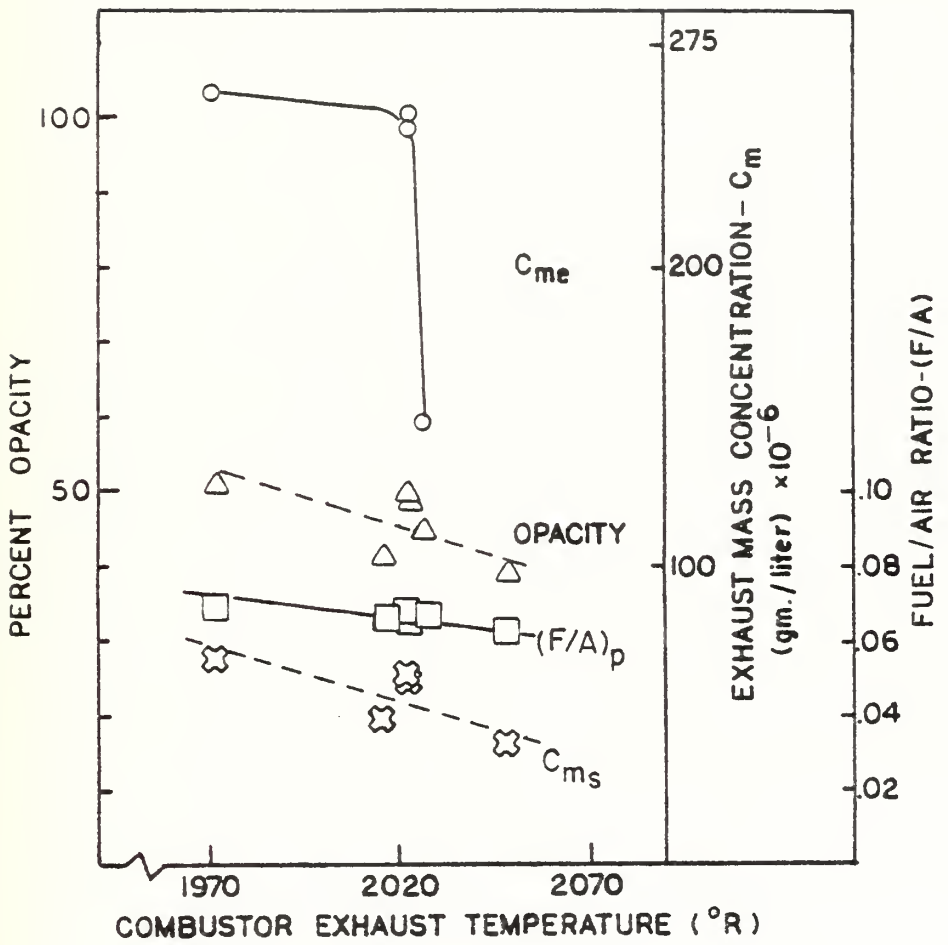

Figure 25. Graph of Exhaust Mass Concentrations, Stack Gas Opacity, and Primary Fuel/Air Ratio vs. Combustor Exhaust Temperature for JP-4

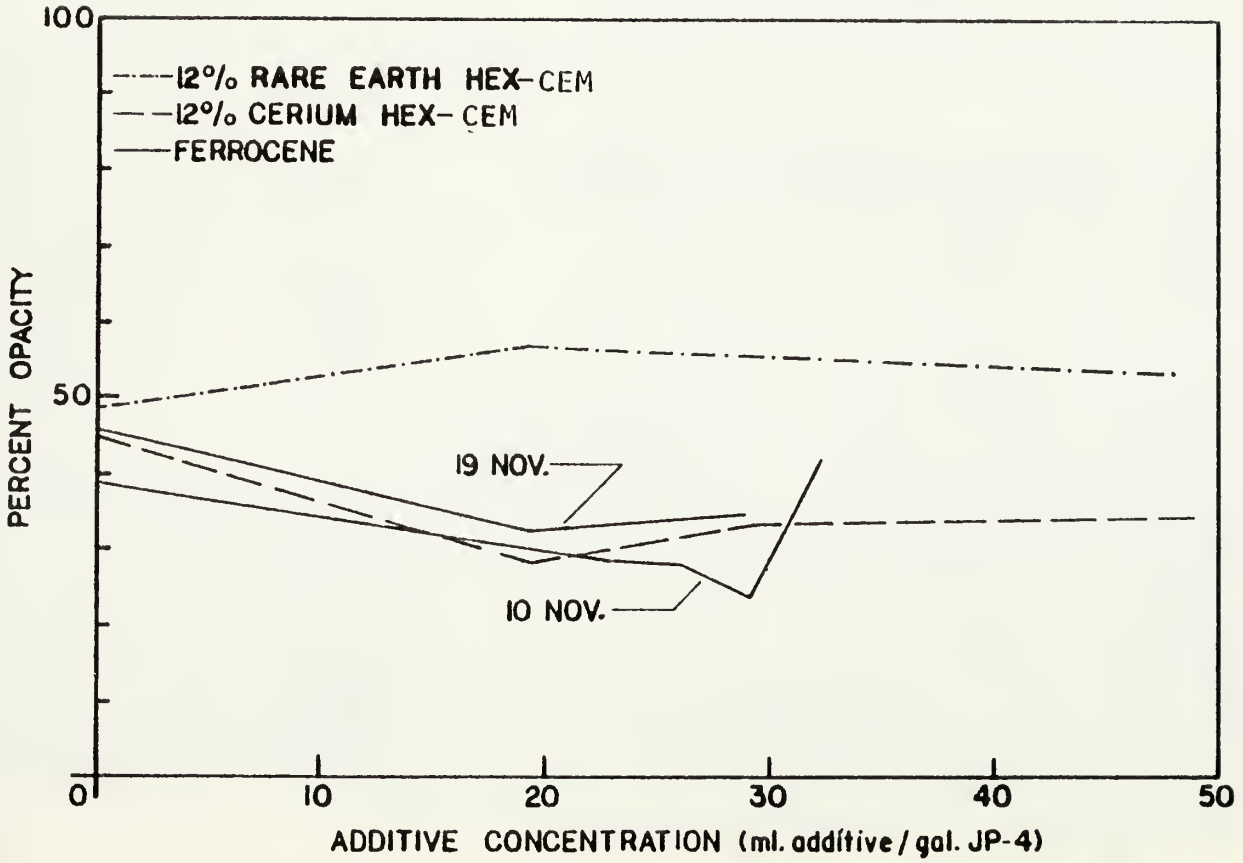

Figure 26. Effects of Additive Concentration on Stack Gas Opacity

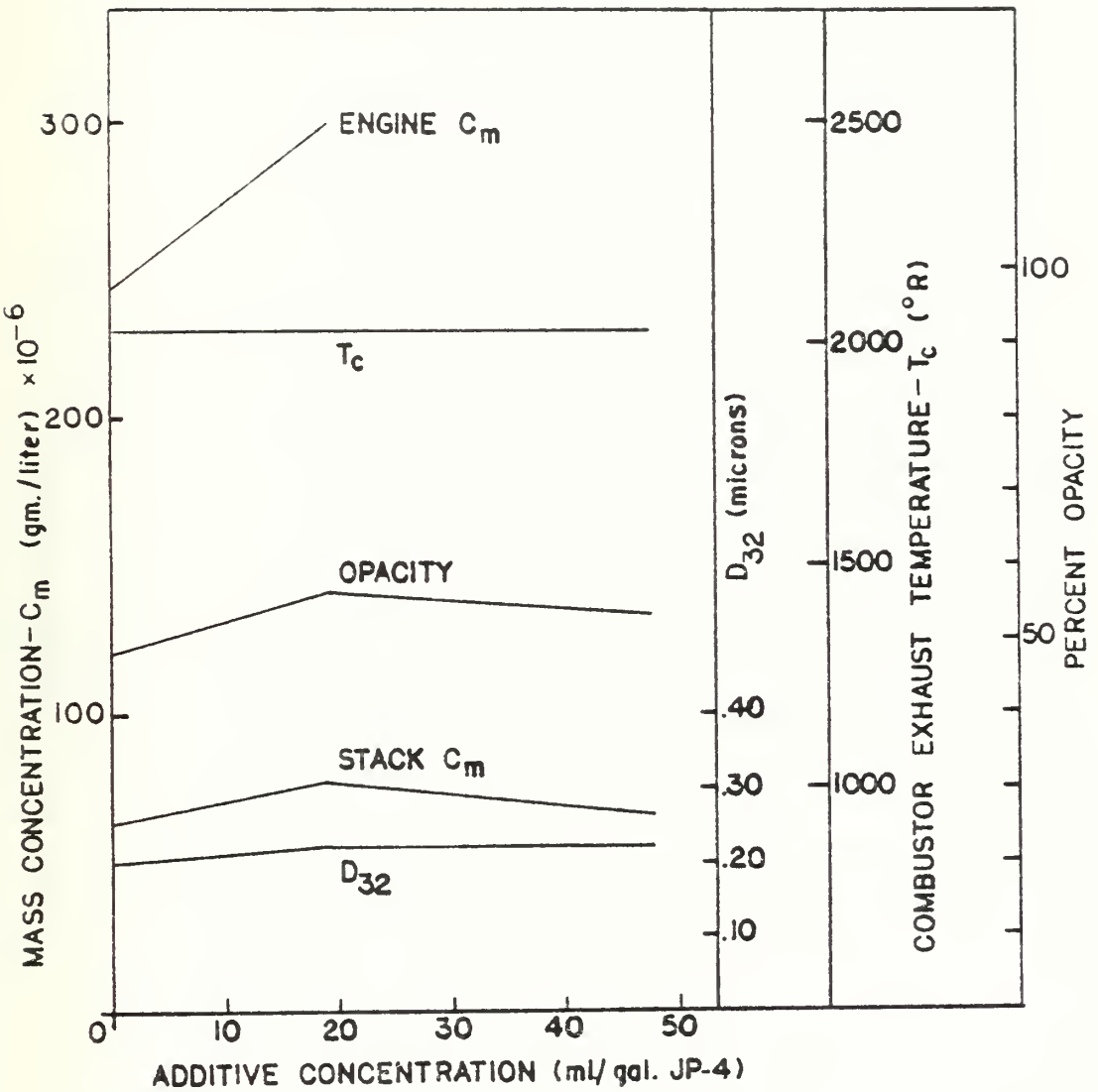

Figure 27. 12% Rare Earth Hex-Cem Concentration vs. Engine/Stack C_m, Stack Gas Opacity, D_{32}, and Combustor Exhaust Temperature

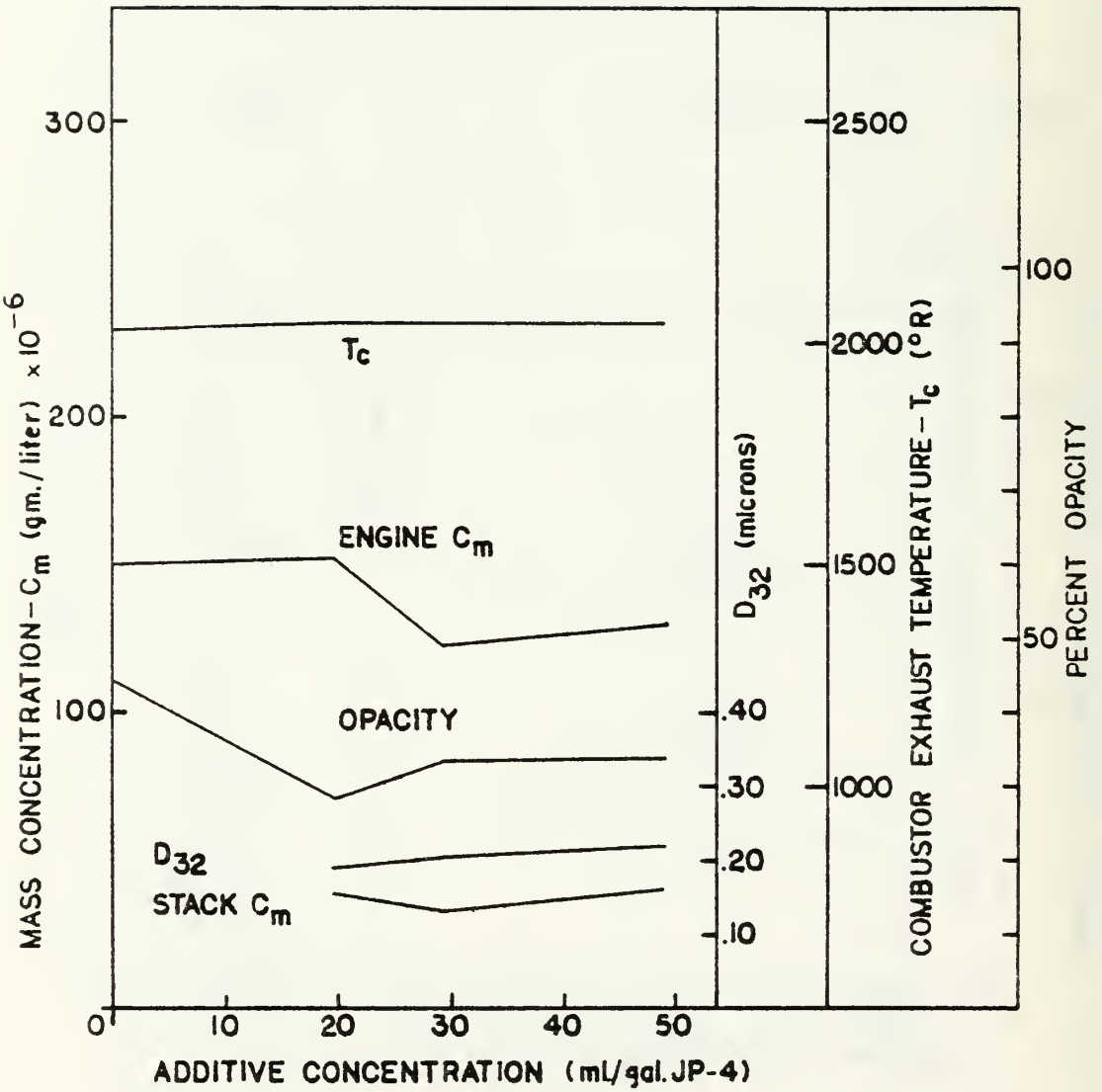

Figure 28. 12% Cerium Hex-Cem Concentration vs. Combustor Exhaust Temperature, Engine/Stack C_m, Stack Gas Opacity, and D_{32}

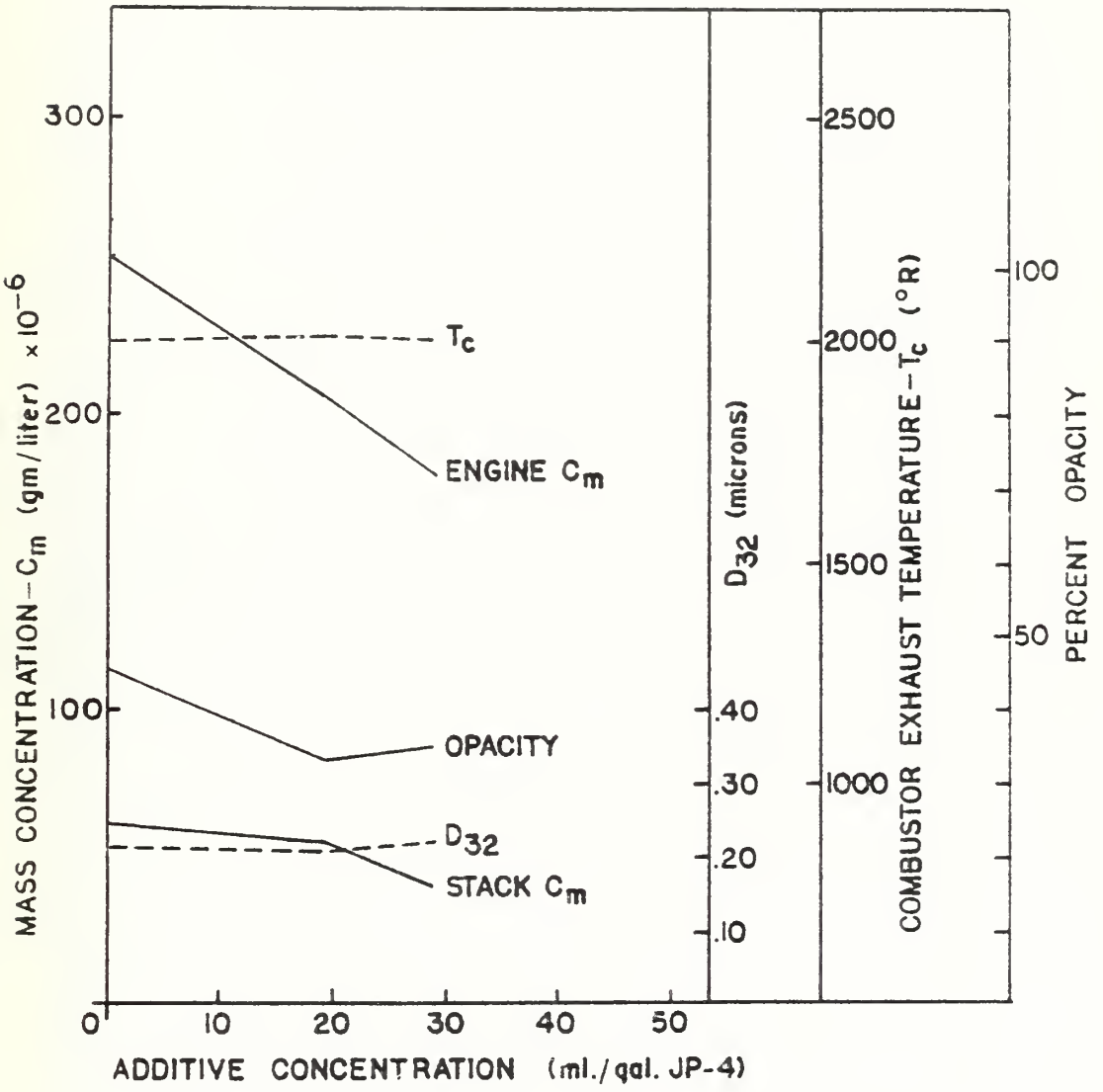

Figure 29. Ferrocene Concentration vs. Combustor Exhaust Temperature, Engine/Stack C_m, Stack Gas Opacity, and D_{32}. 19 November 1981

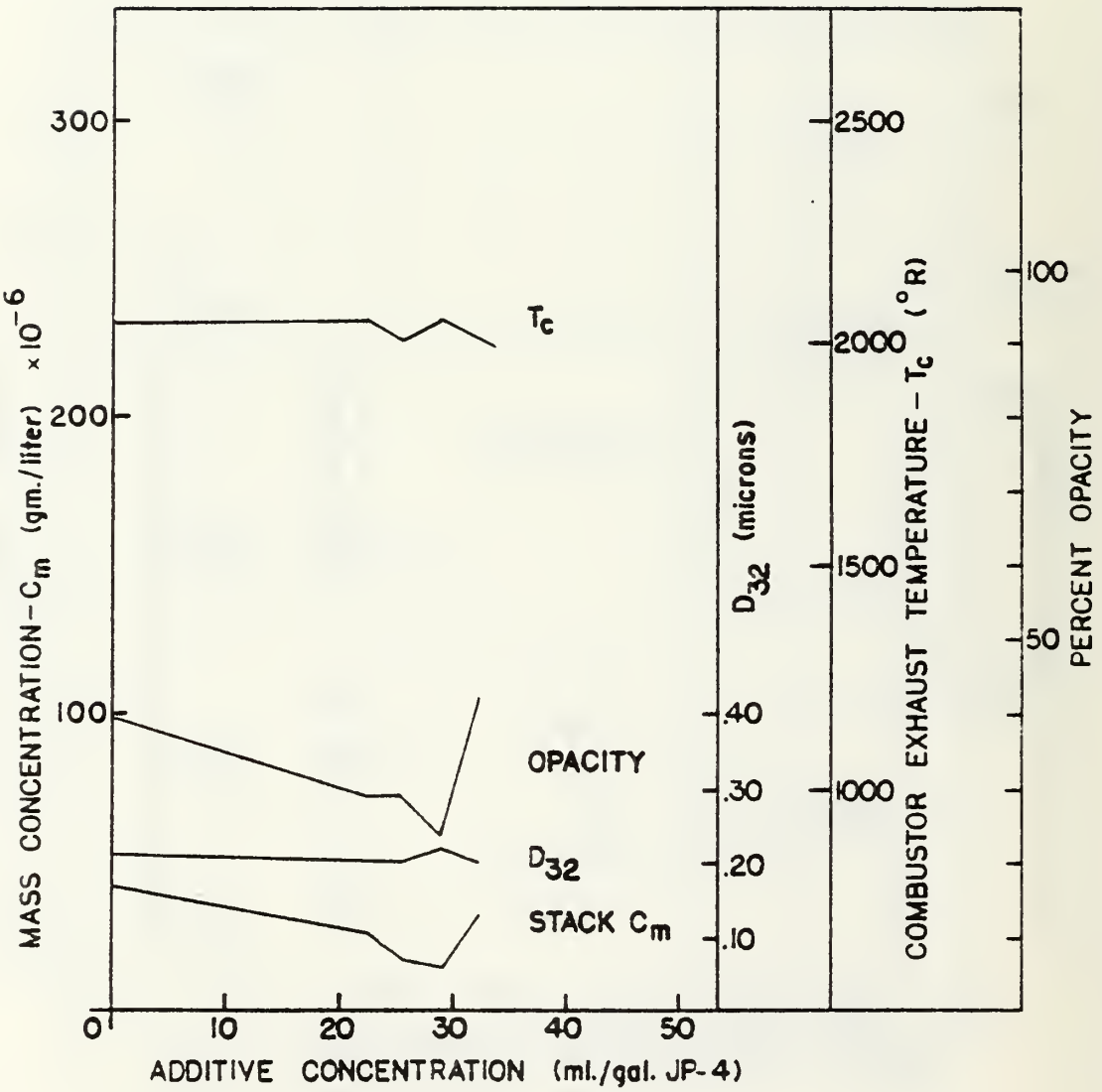

Figure 30. Ferrocene Concentration vs. Combustor Exhaust Temperature, Stack C_m, Stack Gas Opacity, and D_{32}. 10 November 1981

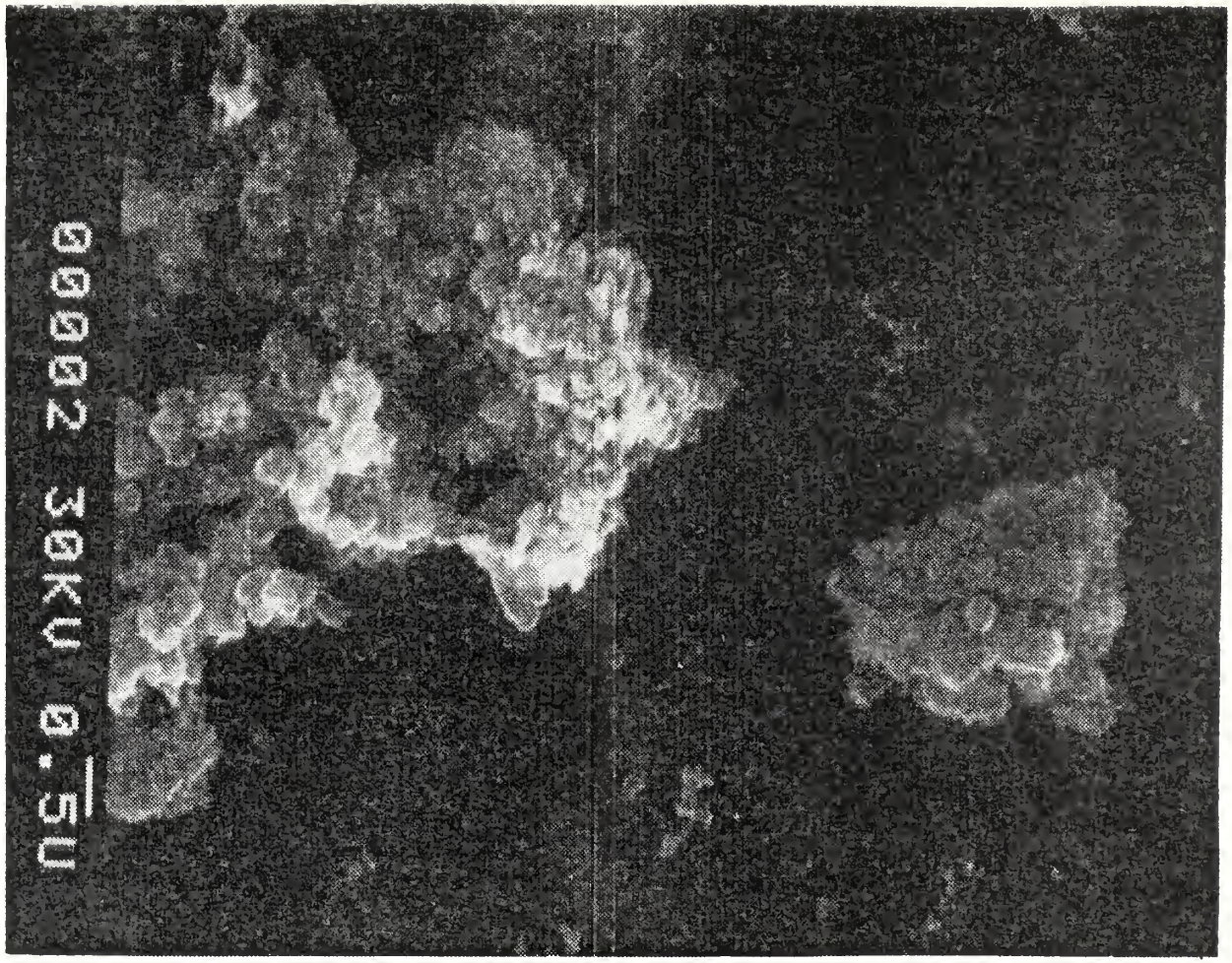

Figure 31. SEM Photograph of Engine Exhaust Particulate Sample Collected During Tests with JP-4 only on 10 November 1981 (10Kx Magnification)

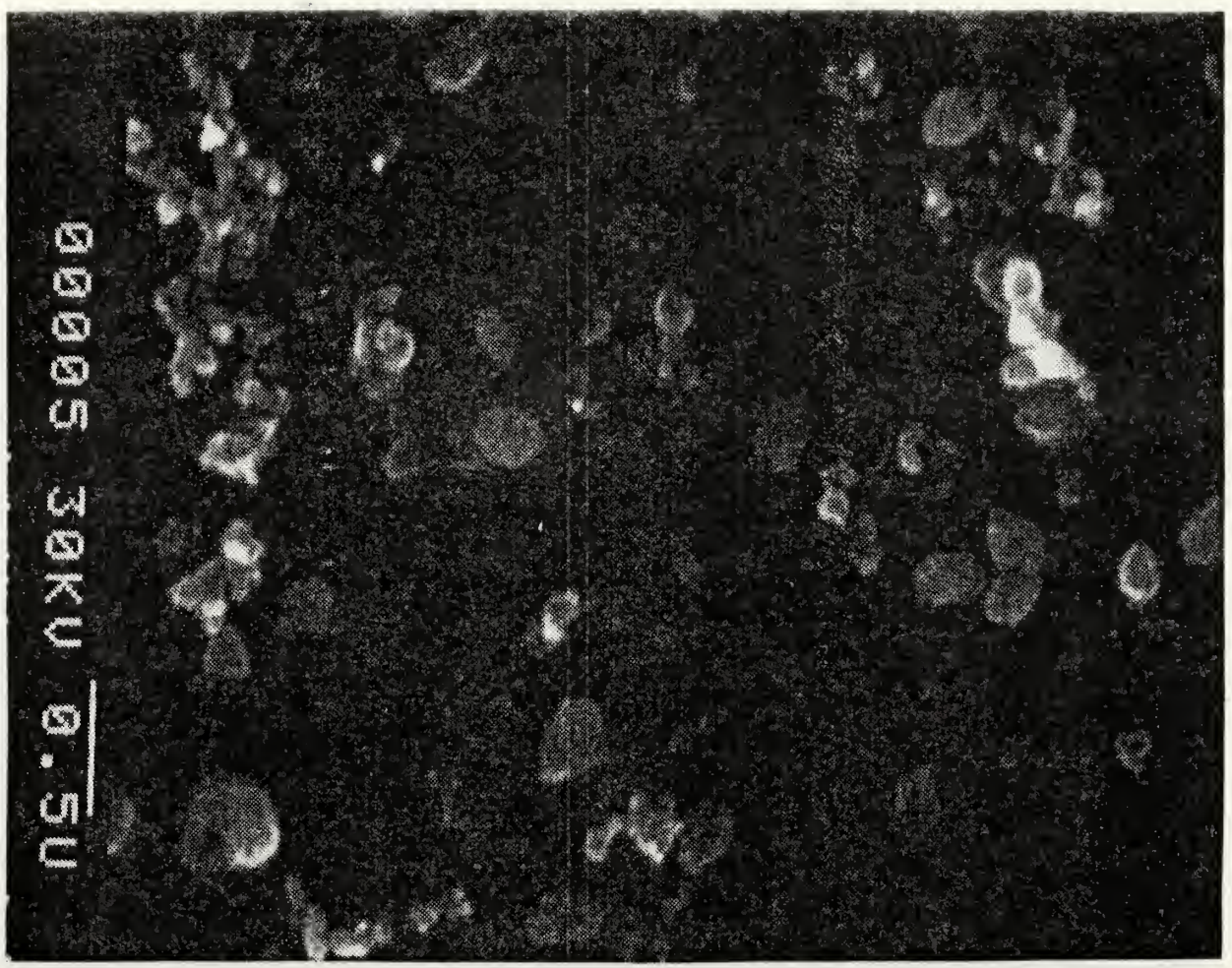

Figure 32. SEM Photograph of Engine Exhaust Particulate Sample Collected During Tests with JP-4 only on 10 November 1981 (25Kx Magnification)

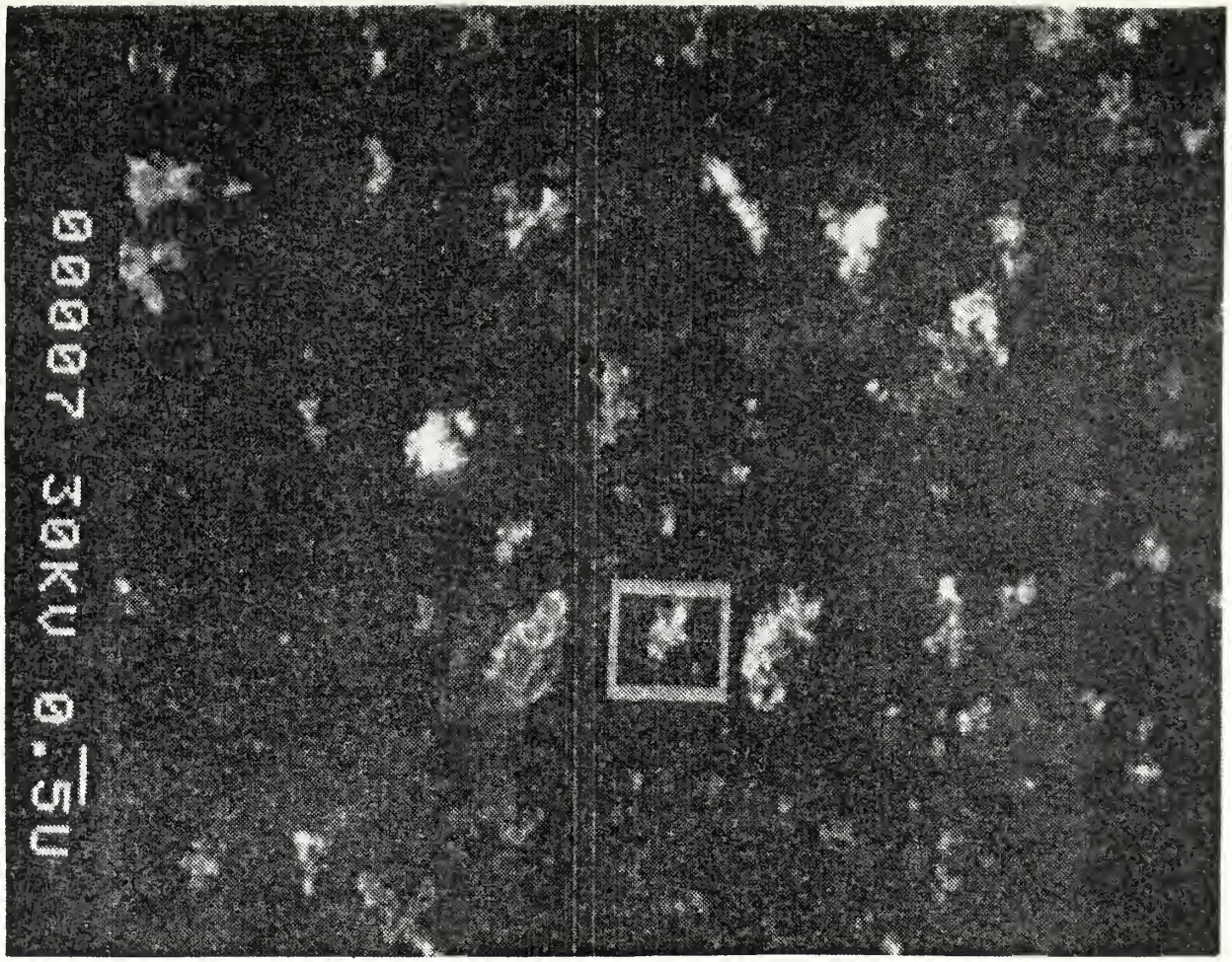

Figure 33. SEM Photograph of Engine Exhaust Particulate Sample Collected on 10 November 1981 During Tests with Ferrocene Concentrations of 32.30 ml. additive/gal. JP-4 (10Kx Magnification)

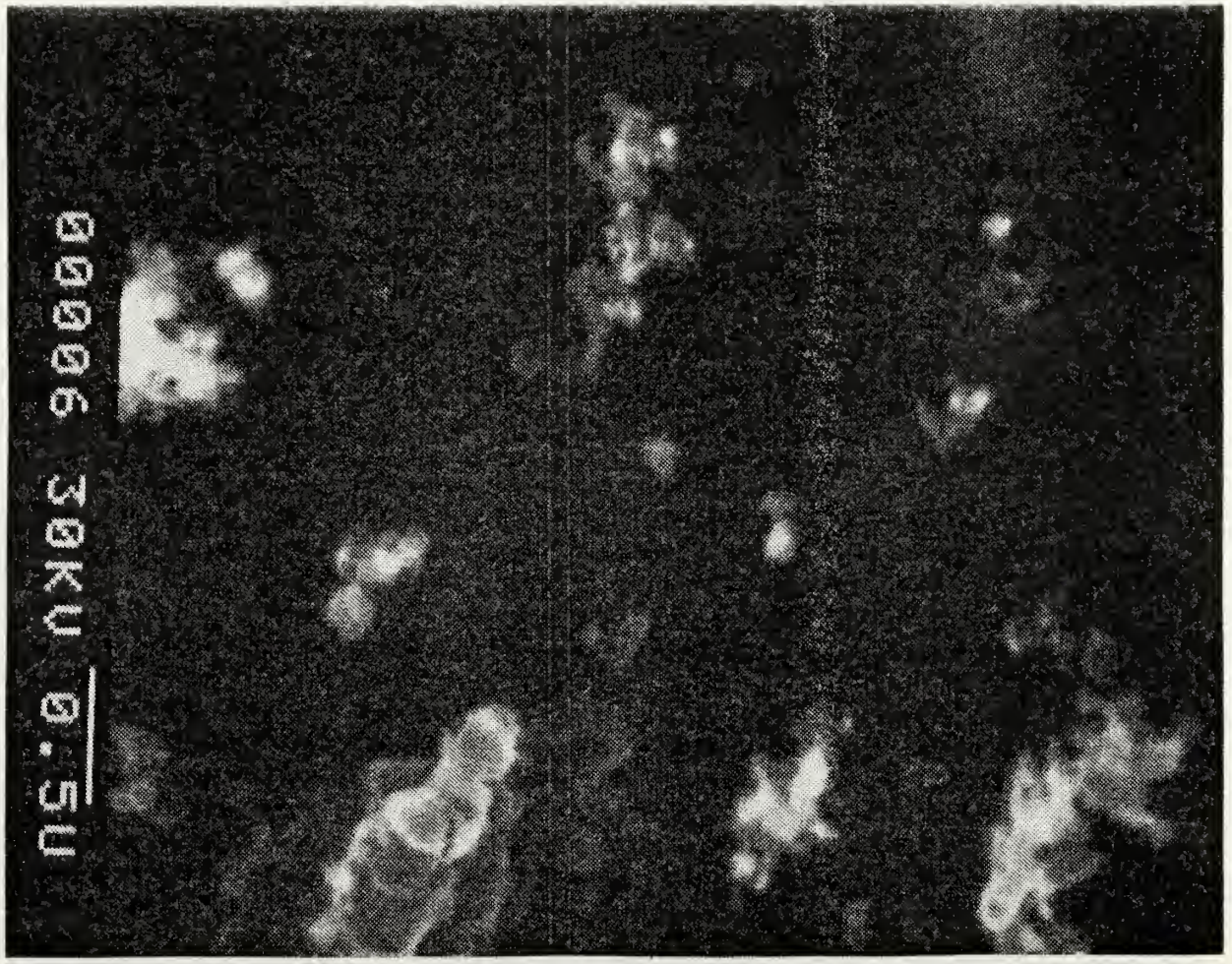

Figure 34. SEM Photograph of Engine Exhaust Particulate Sample Collected on 10 November 1981 During Tests with Ferrocene Concentrations of 32.30 ml. additive/gal. JP-4 (25Kx Magnification)

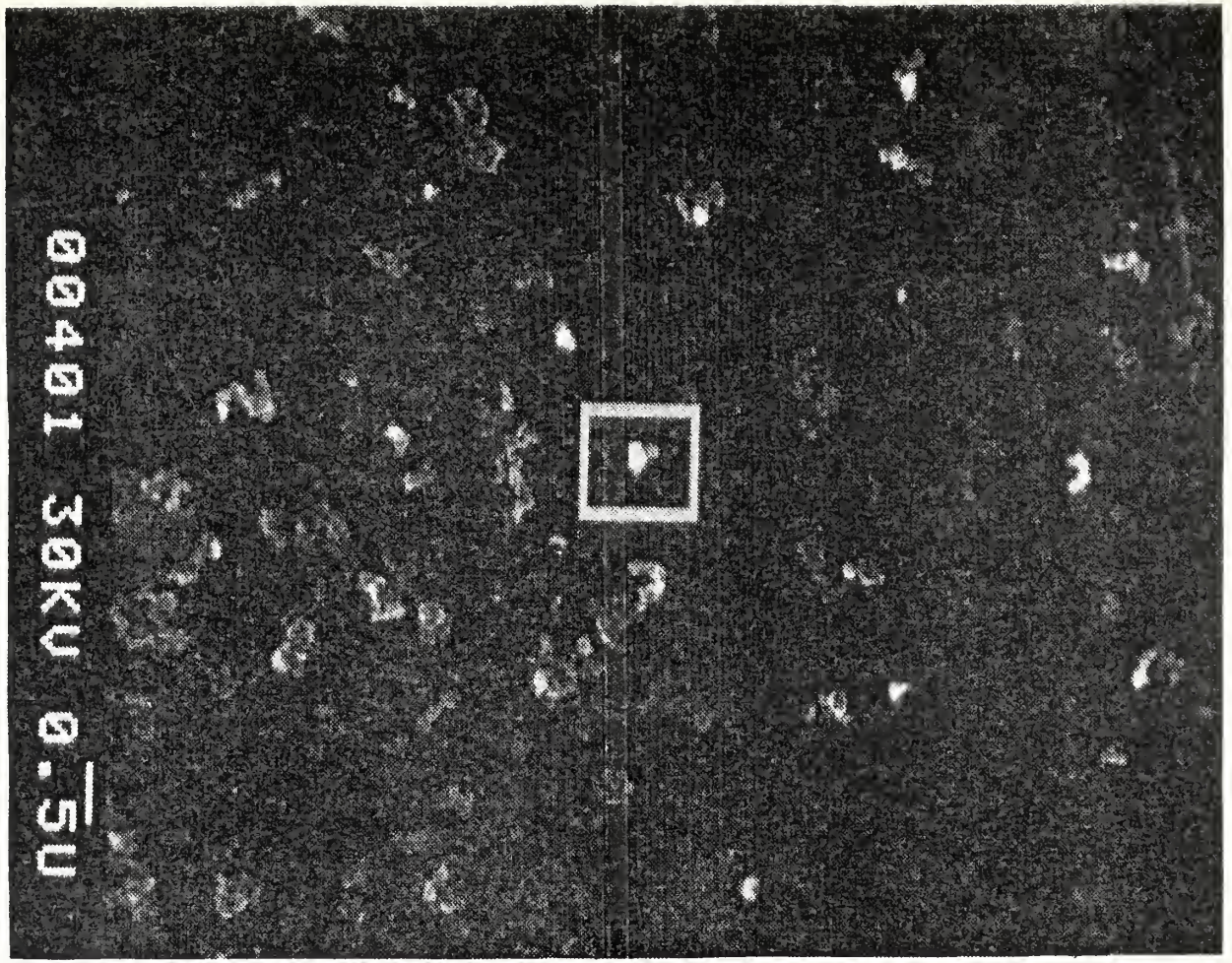

Figure 35. SEM Photograph of Engine Exhaust Particulate Sample Collected on 19 November 1981 During Tests with Ferrocene Concentrations of 19.20 ml. additive/gal. JP-4 (10Kx Magnification)

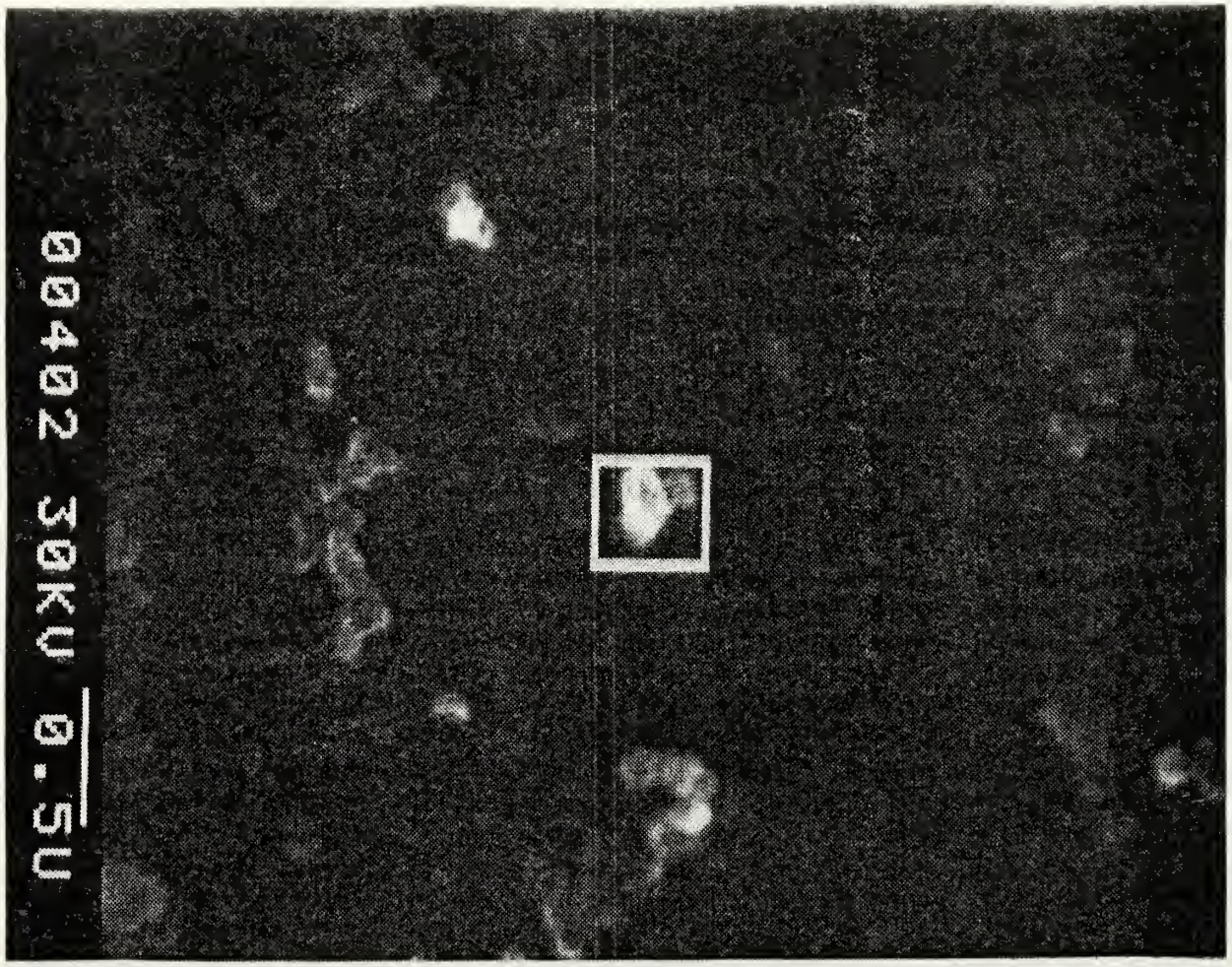

Figure 36. SEM Photograph of Engine Exhaust Particulate Sample Collected on 19 November 1981 During Tests with Ferrocene Concentrations of 19.20 ml. additive/gal. JP-4 (25Kx Magnification)

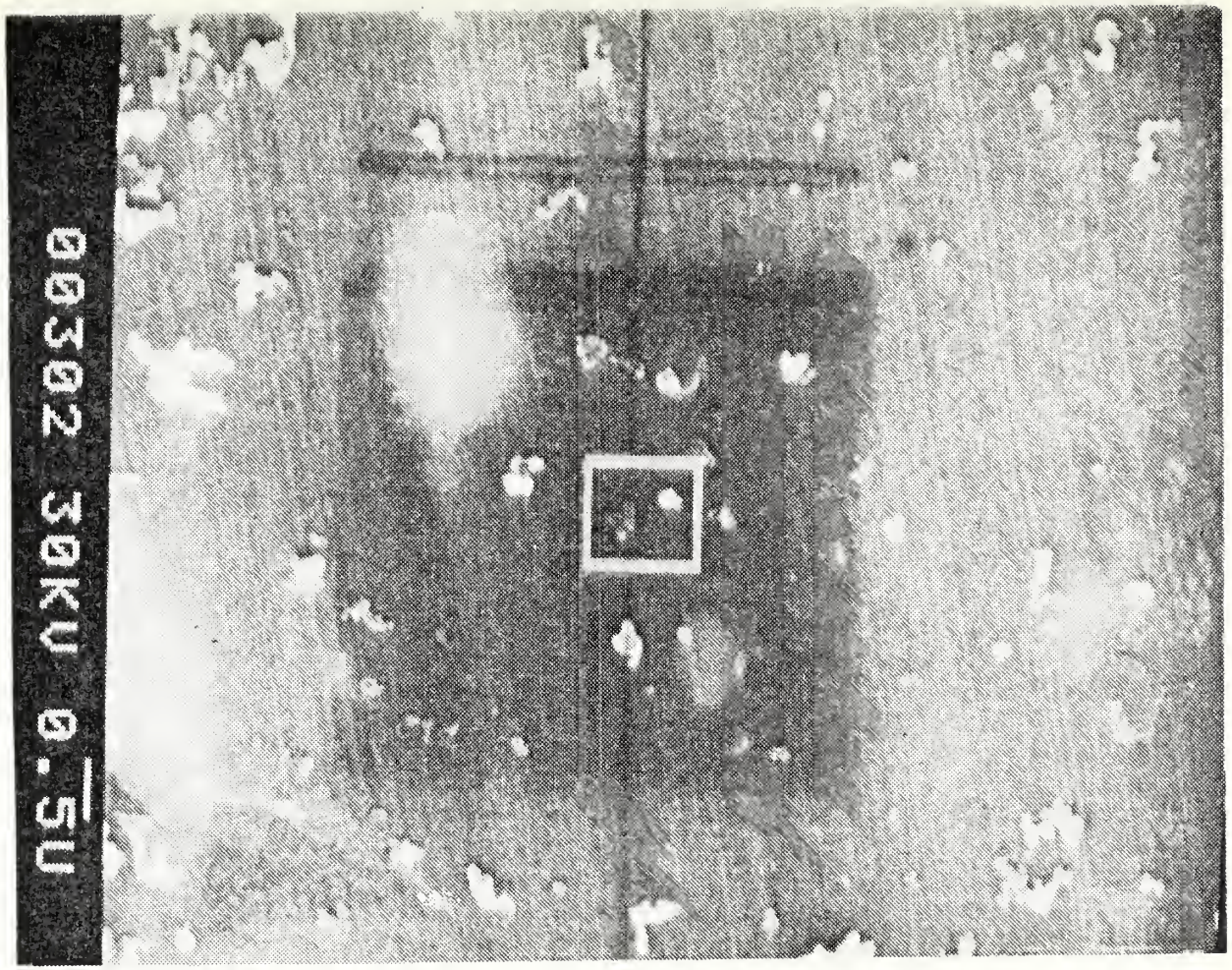

Figure 37. SEM Photograph of Engine Exhaust Particulate Sample Collected on 19 November 1981 During Tests with Ferrocene Concentrations of 28.80 ml. additive/gal. JP-4 (10Kx Magnification)

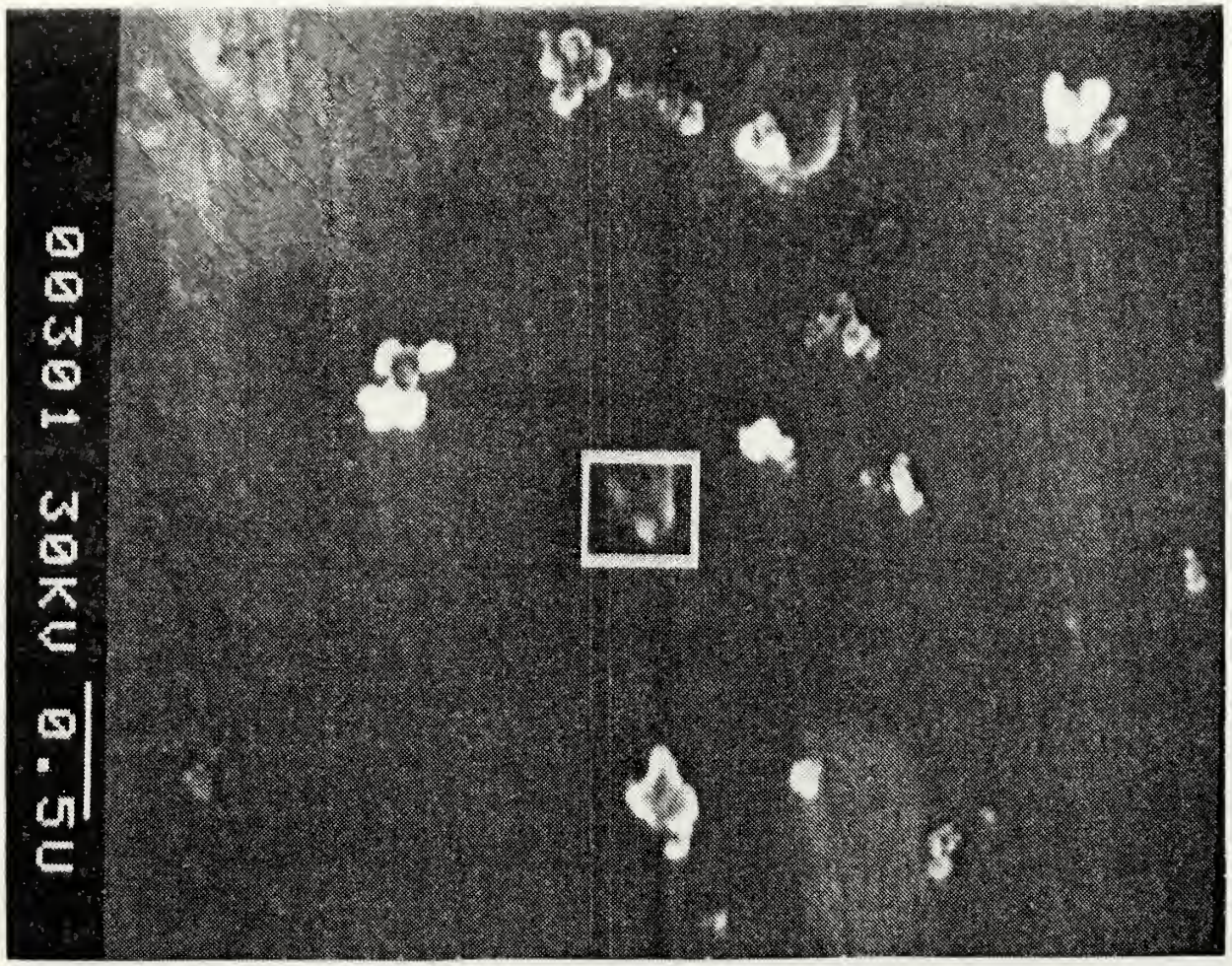

Figure 38. SEM Photograph of Engine Exhaust Particulate Sample Collected on 19 November 1981 During Tests with Ferrocene Concentrations of 28.80 ml. additive/gal. JP-4 (25Kx Magnification)

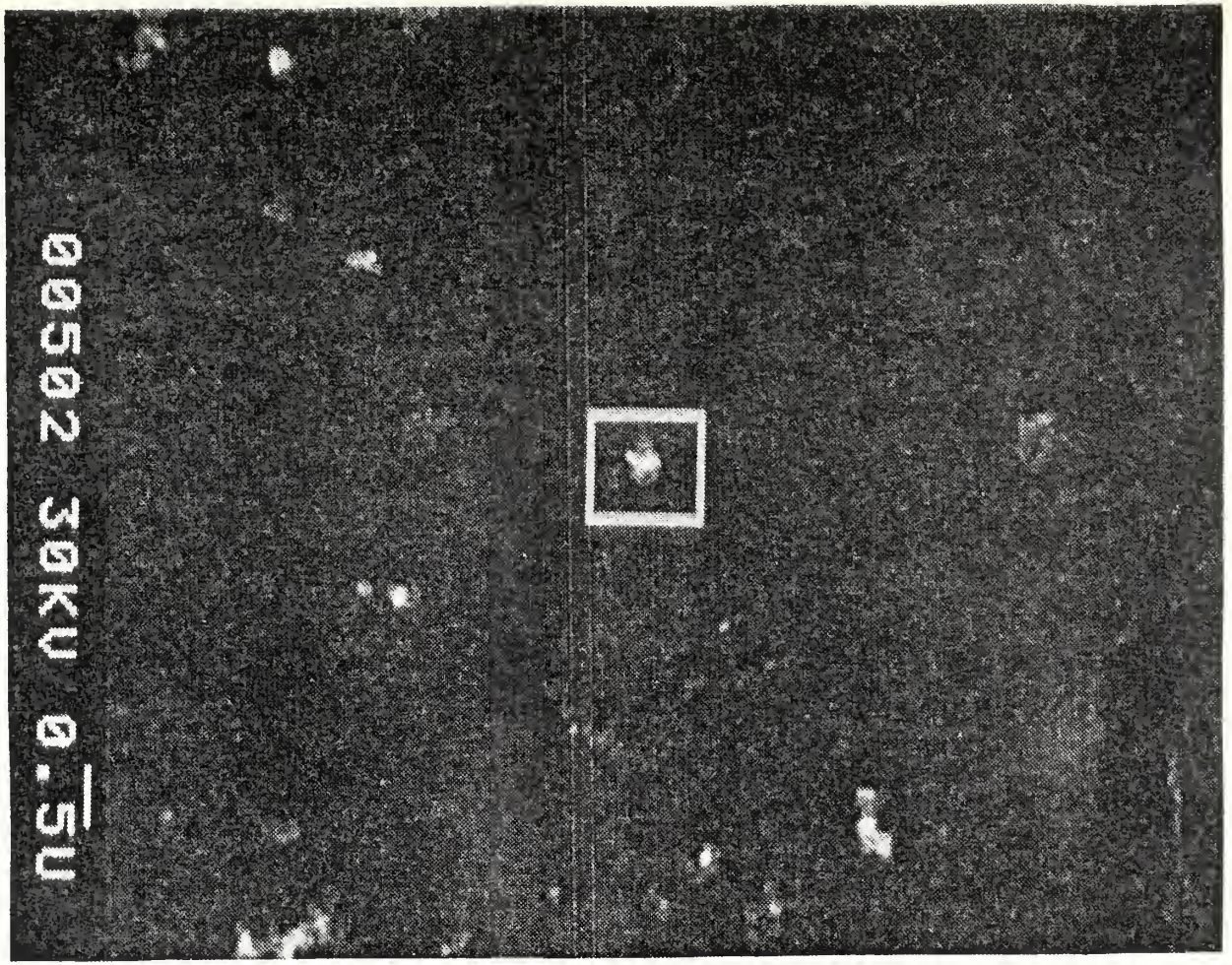

Figure 39. SEM Photograph of Engine Exhaust Particulate Sample Collected on 19 November 1981 During Tests with 12% Cerium Hex-Chem Concentrations of 19.10 ml. additive/gal. JP-4 (10Kx Magnification)

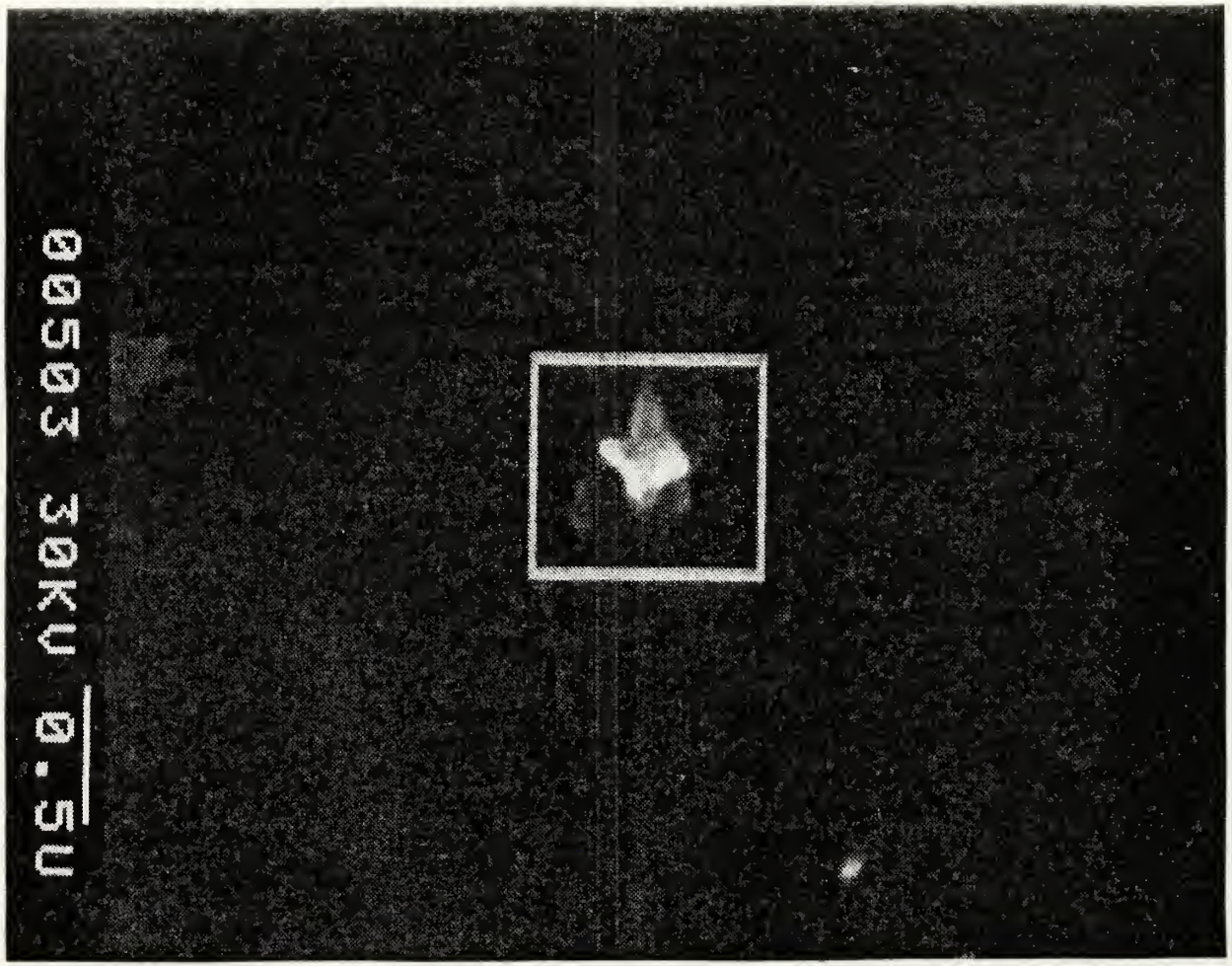

Figure 40. SEM Photograph of Engine Exhaust Particulate Sample Collected on 19 November 1981 During Tests with 12% Cerium Hex-Chem Concentrations of 19.10 ml. additive/gal. JP-4 (25Kx Magnification)

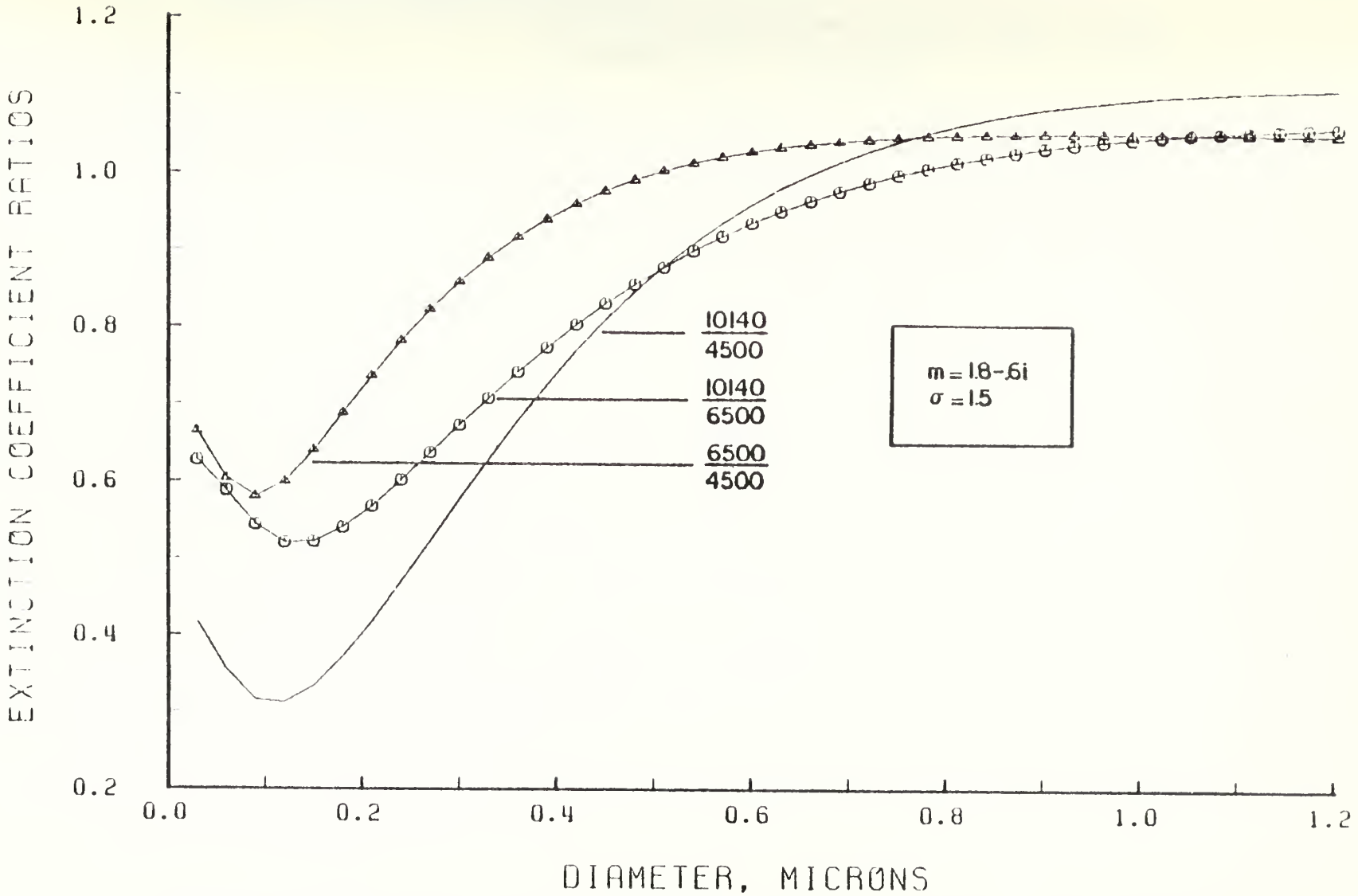

Figure 41. D_{32} vs. Extinction Coefficient Ratios (10140, 6500, 4500)
m = 1.8-.60i/1.5

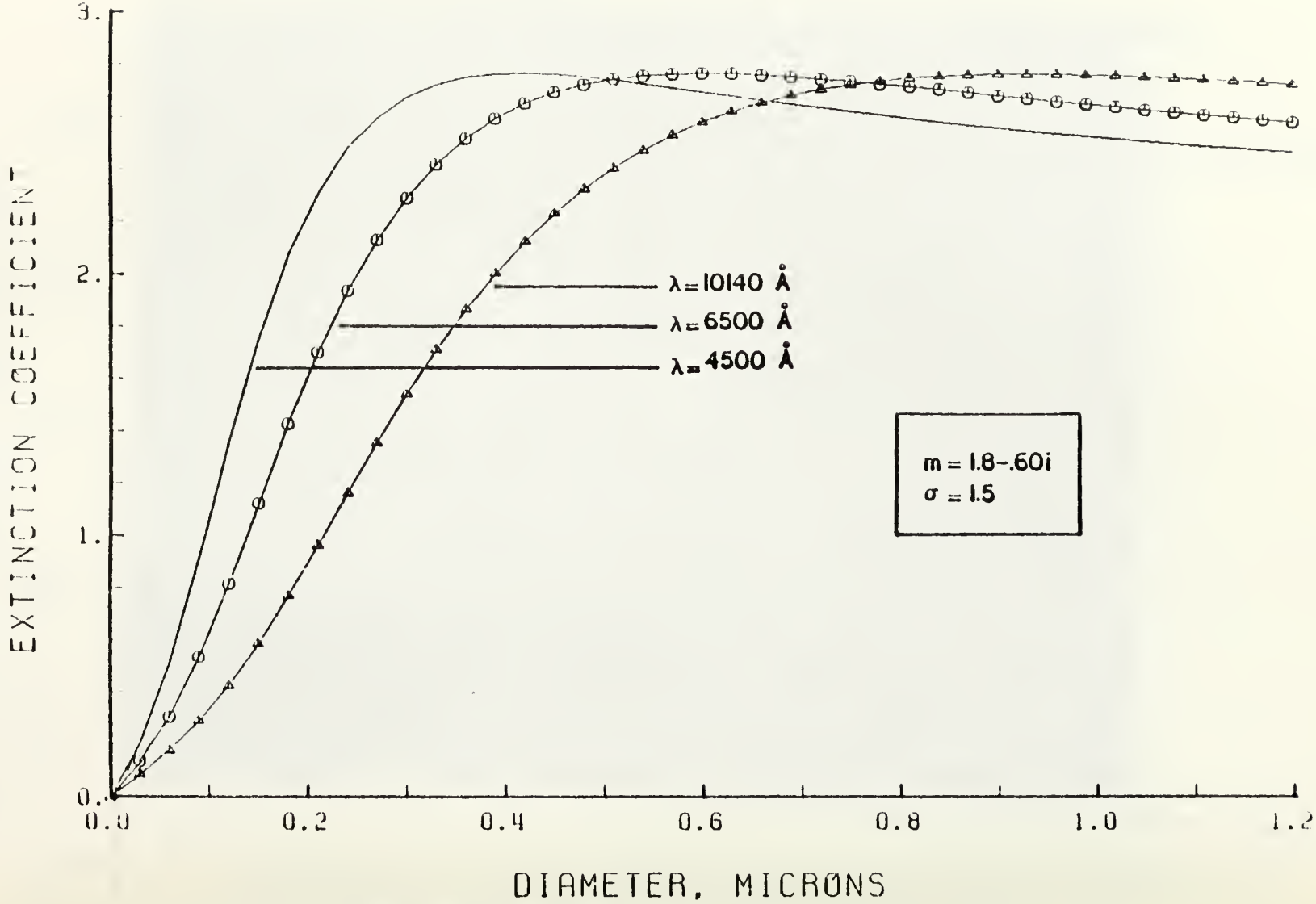

Figure 42. D_{32} vs. Extinction Coefficient (10140, 6500, 4500)
m = 1.80-.60i/1.5

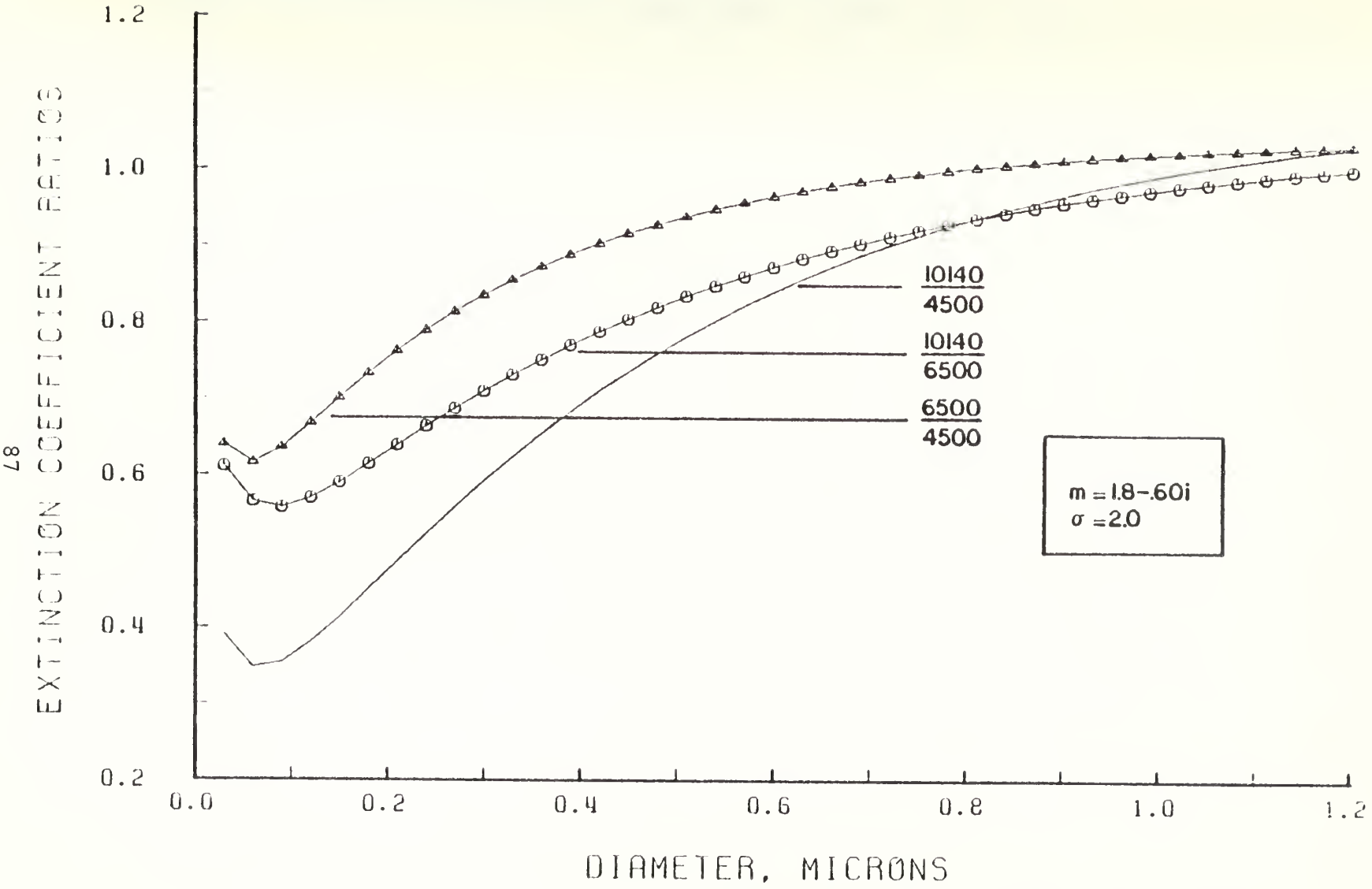

Figure 43. D_{32} vs. Extinction Coefficient Ratios (10140, 6500, 4500)
m = 1.80-.60i/2.0

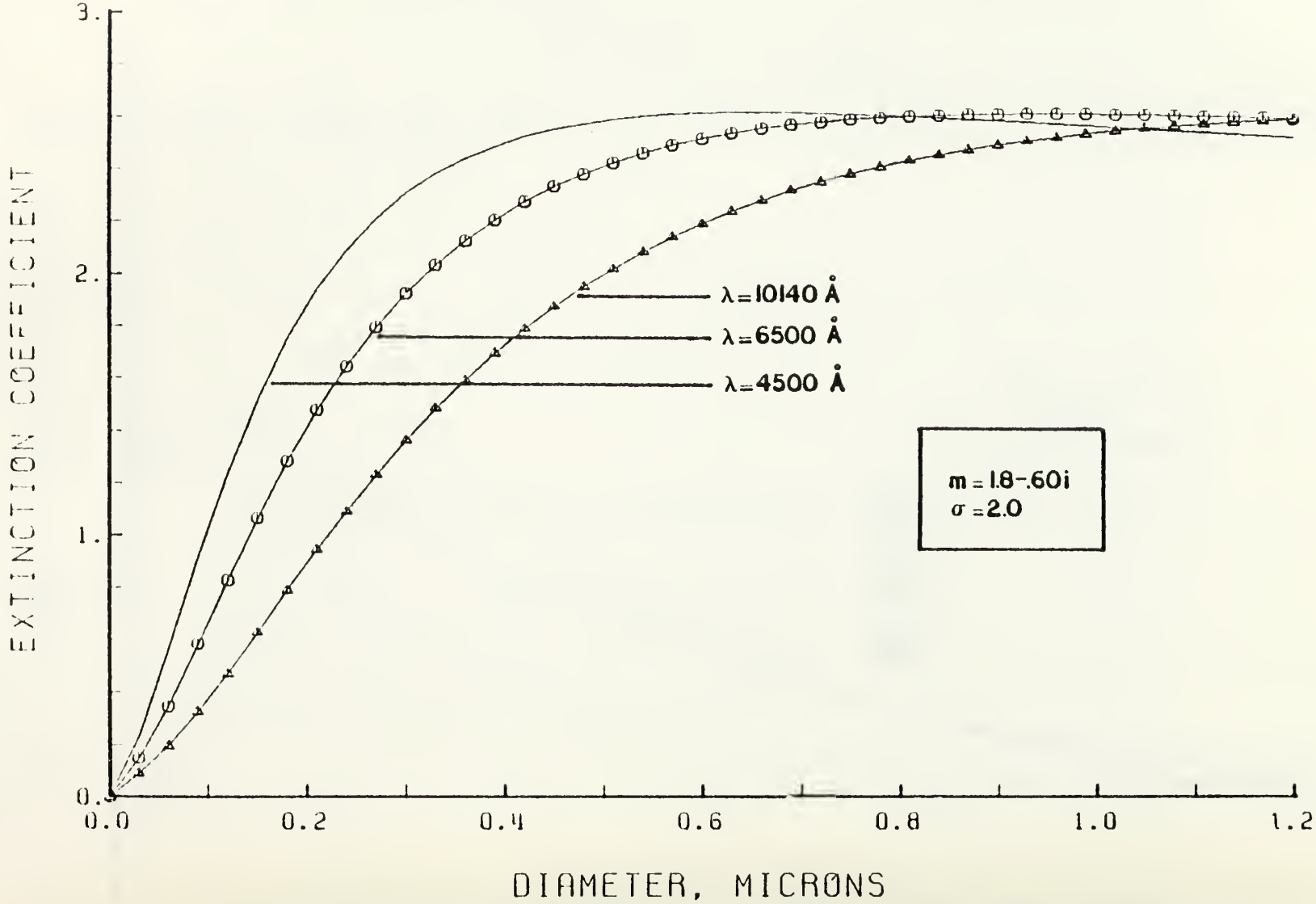

Figure 44. D_{32} vs. Extinction Coefficient (10140, 6500, 4500); m = 1.8-.6i/2.0

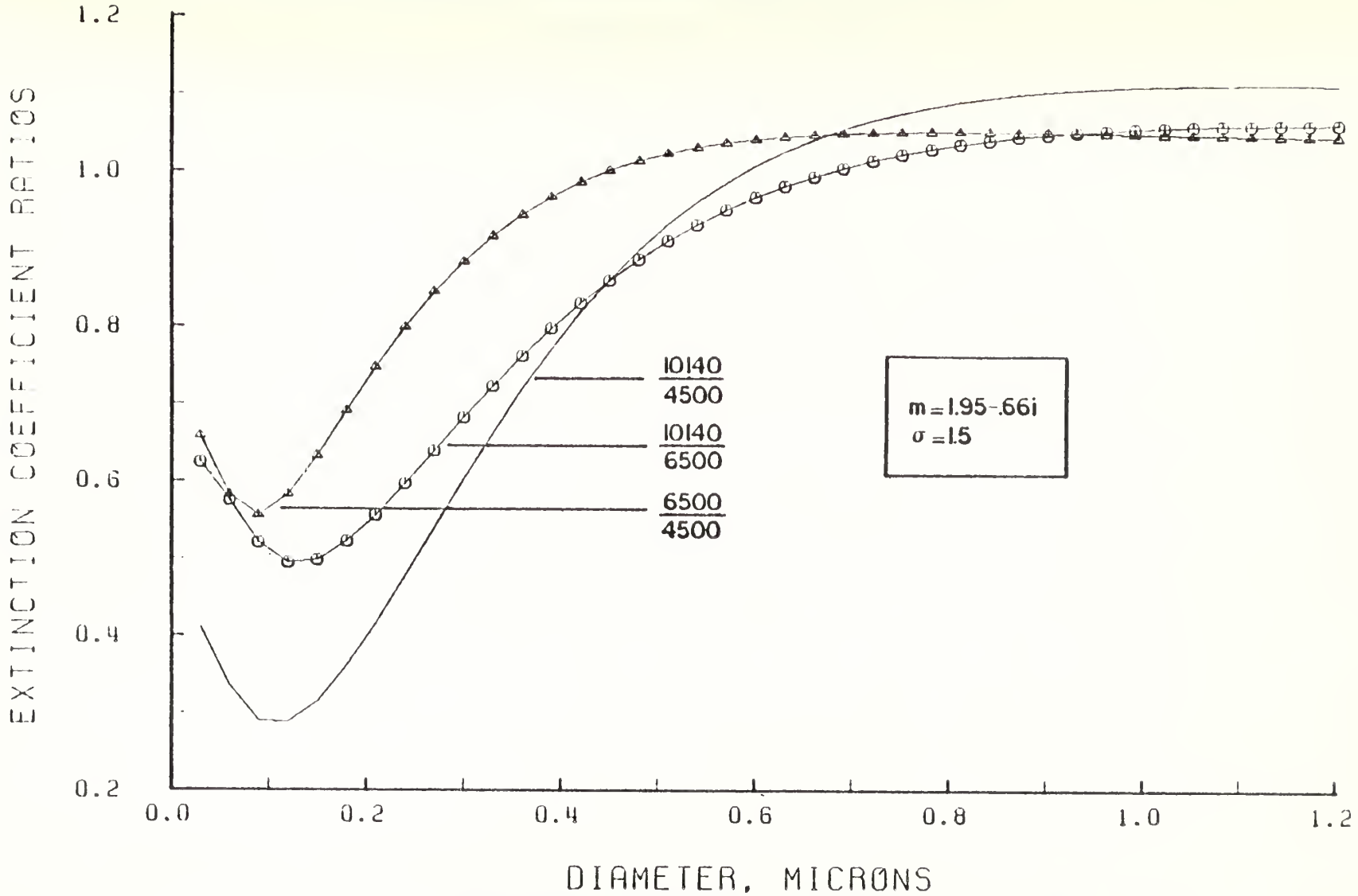

Figure 45. D_{32} vs. Extinction Coefficient Ratios (10140, 6500, 4500)
m = 1.95-.66i/1.5

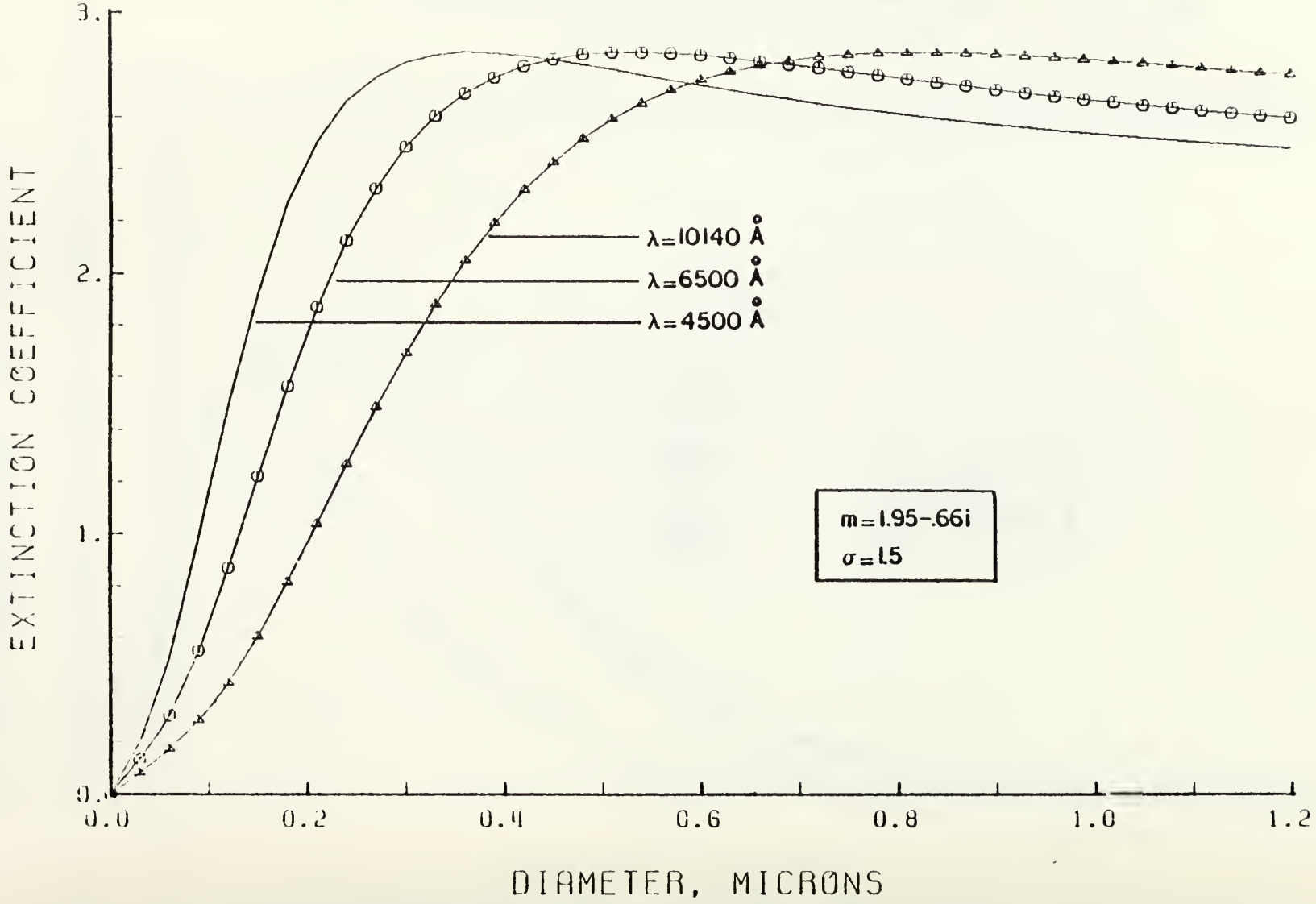

Figure 46. D_{32} vs. Extinction Coefficient (10140, 6500, 4500); m = 1.95-.66i/1.5

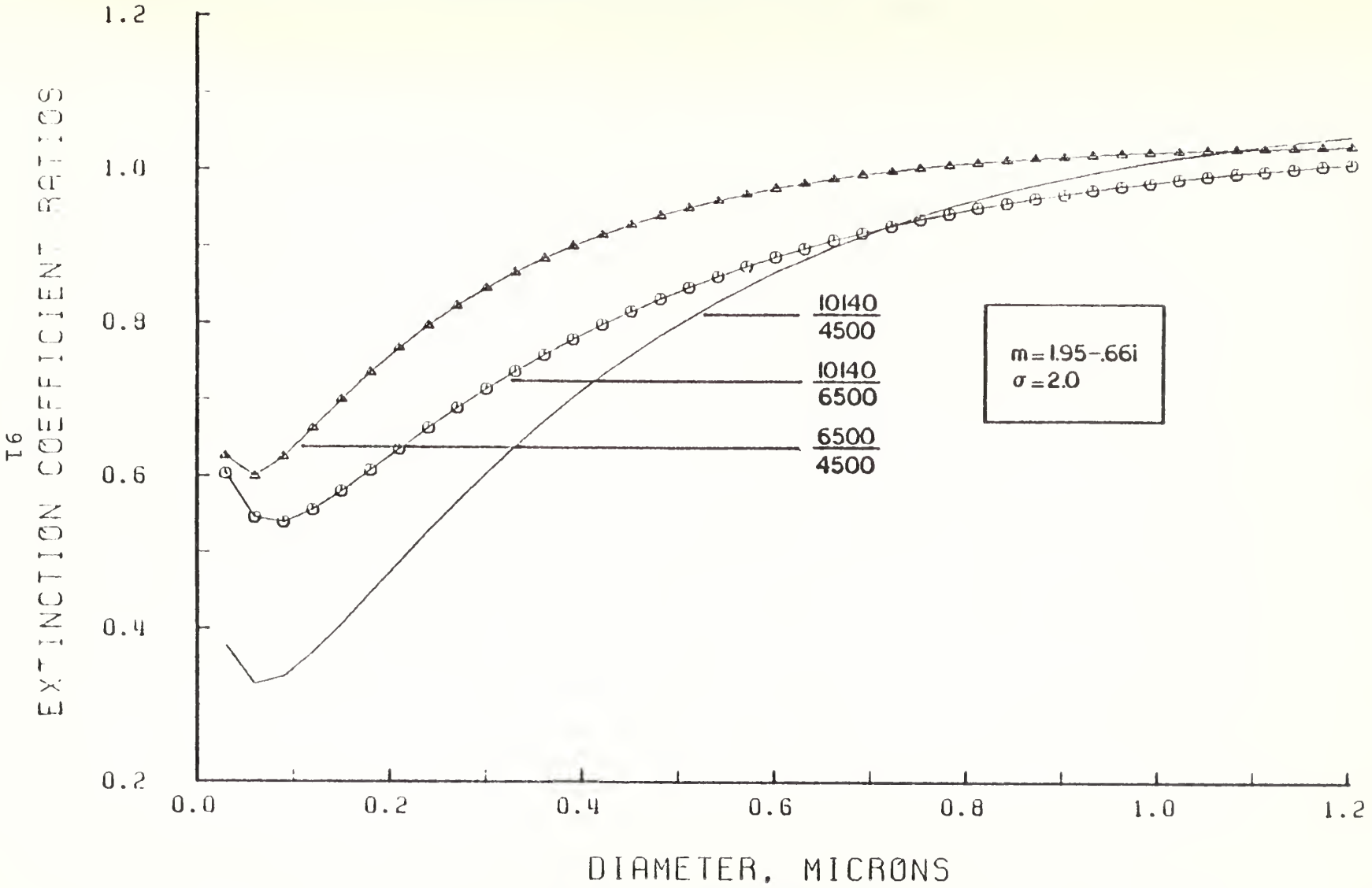

Figure 47. D_{32} vs. Extinction Coefficient Ratios (10140, 6500, 4500)
m = 1.95-.66i/2.0

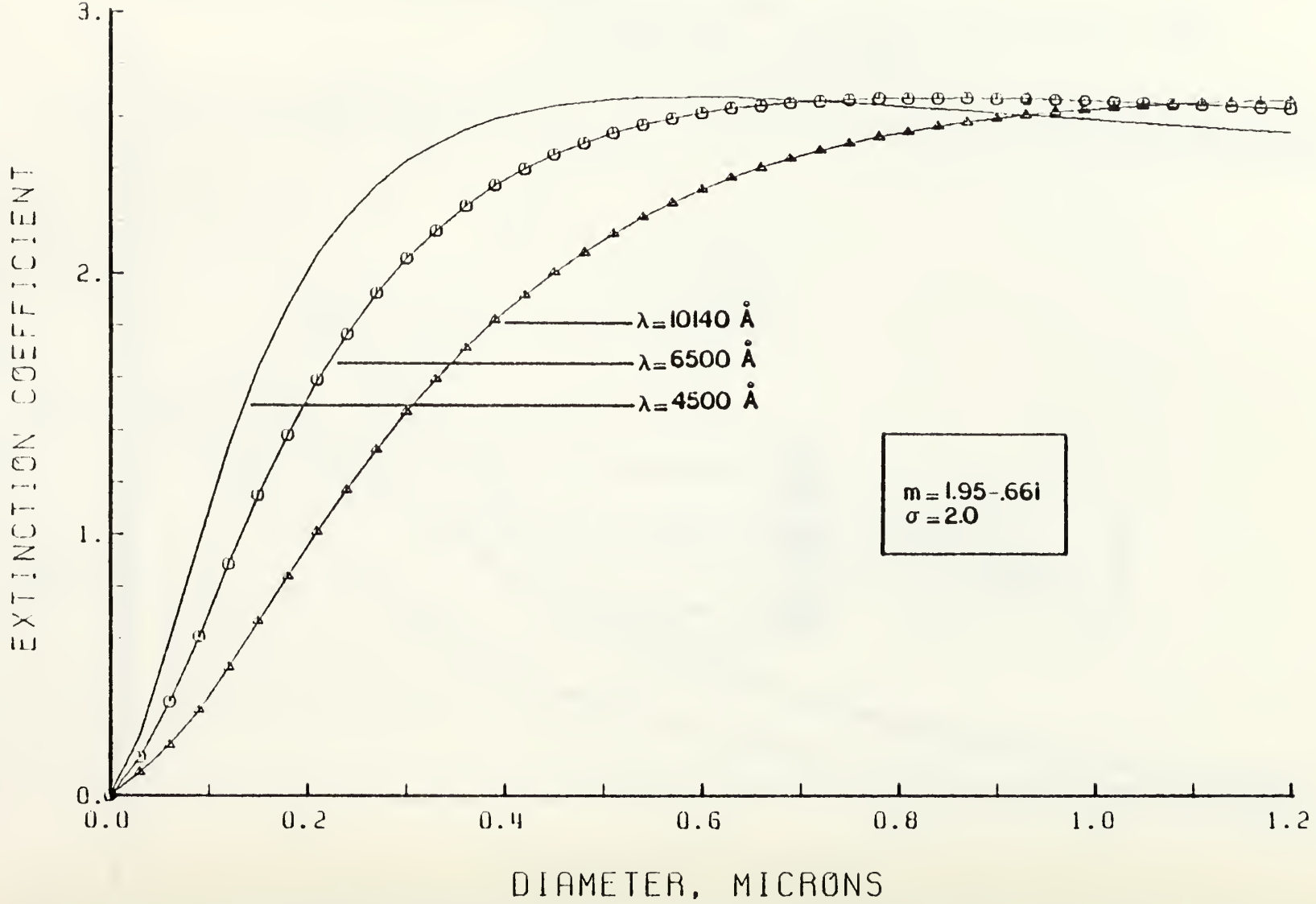

Figure 48. D_{32} vs. Extinction Coefficient (10140, 6500, 4500); m = 1.95-.66i/2.0

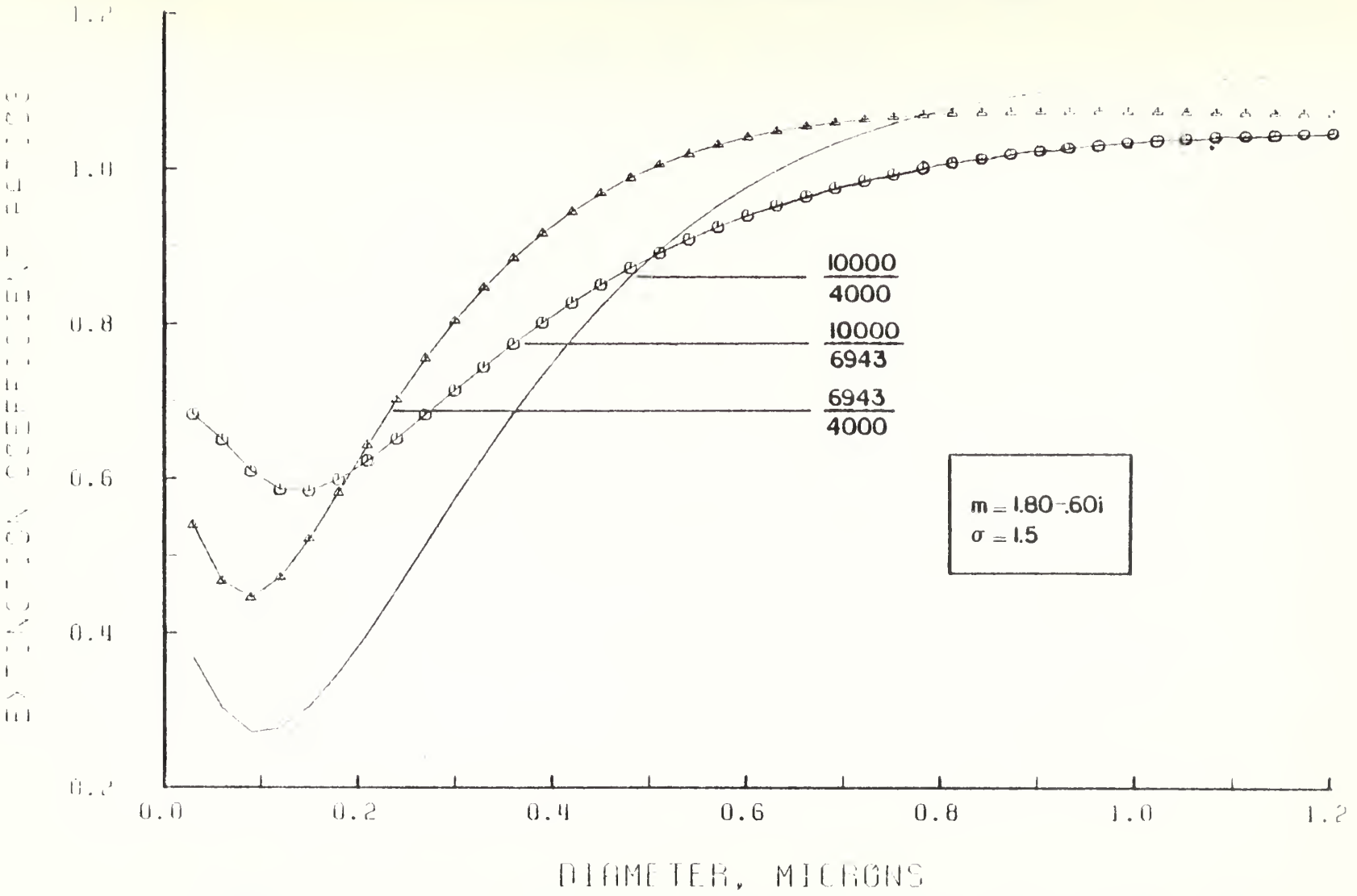

Figure 49. D_{32} vs. Extinction Coefficient Ratios (10000, 6943, 4000)
m = 1.80-.60i/1.5

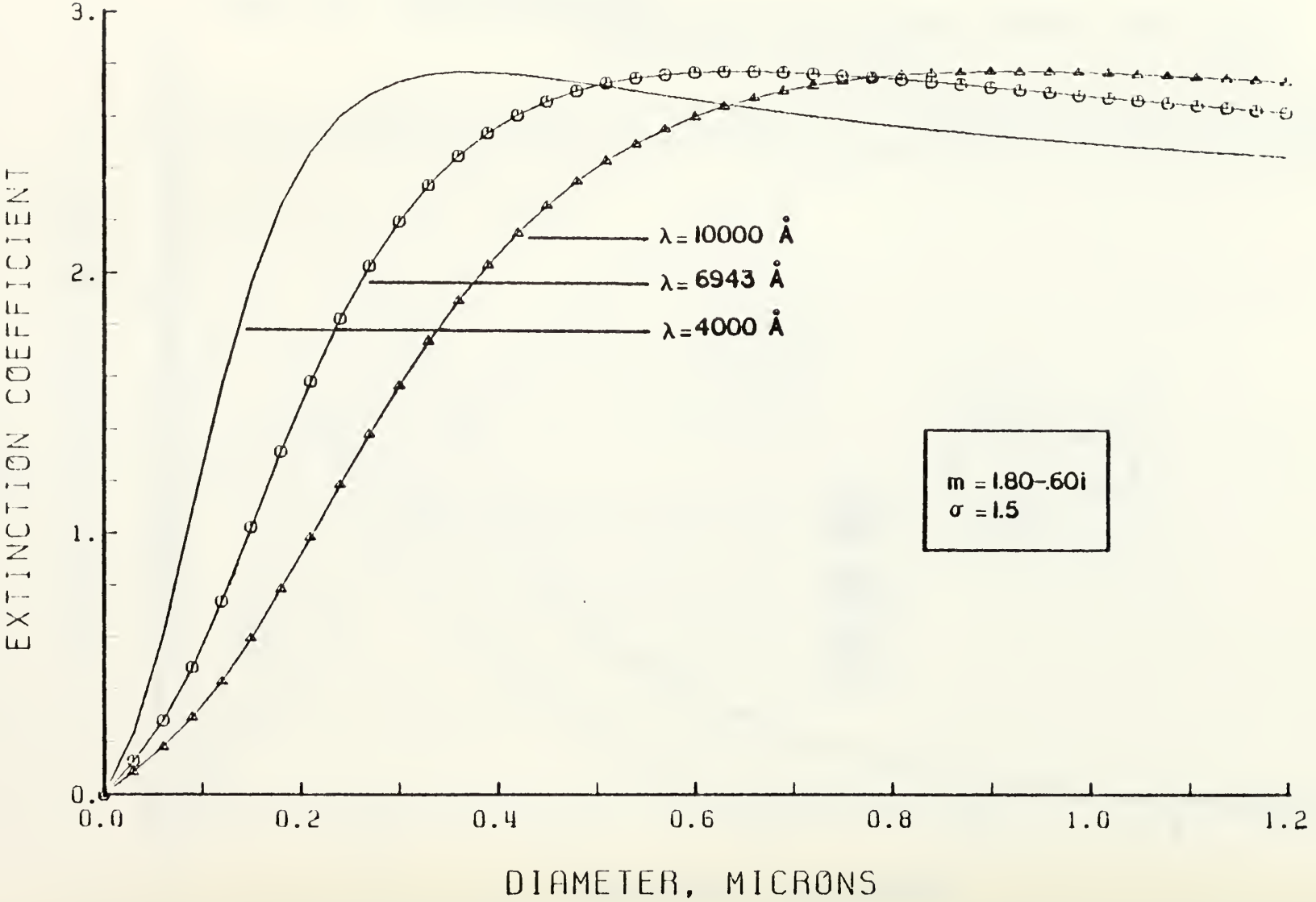

Figure 50. D_{32} vs. Extinction Coefficient (10000, 6943, 4000); m = 1.8-.60i/1.5

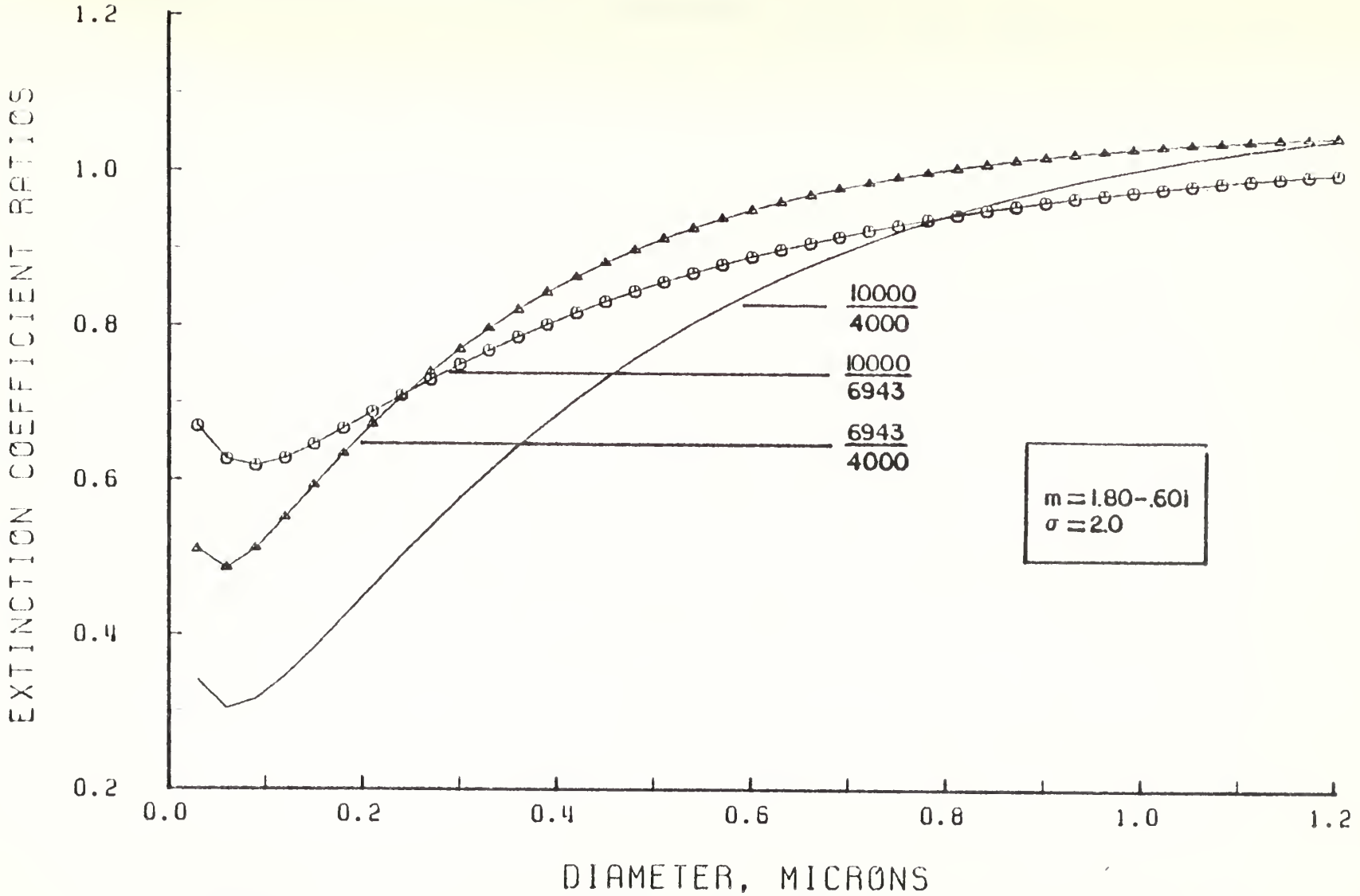

Figure 51. D_{32} vs. Extinction Coefficient Ratios (10000, 6943, 4000)
m = 1.80-.60i/2.0

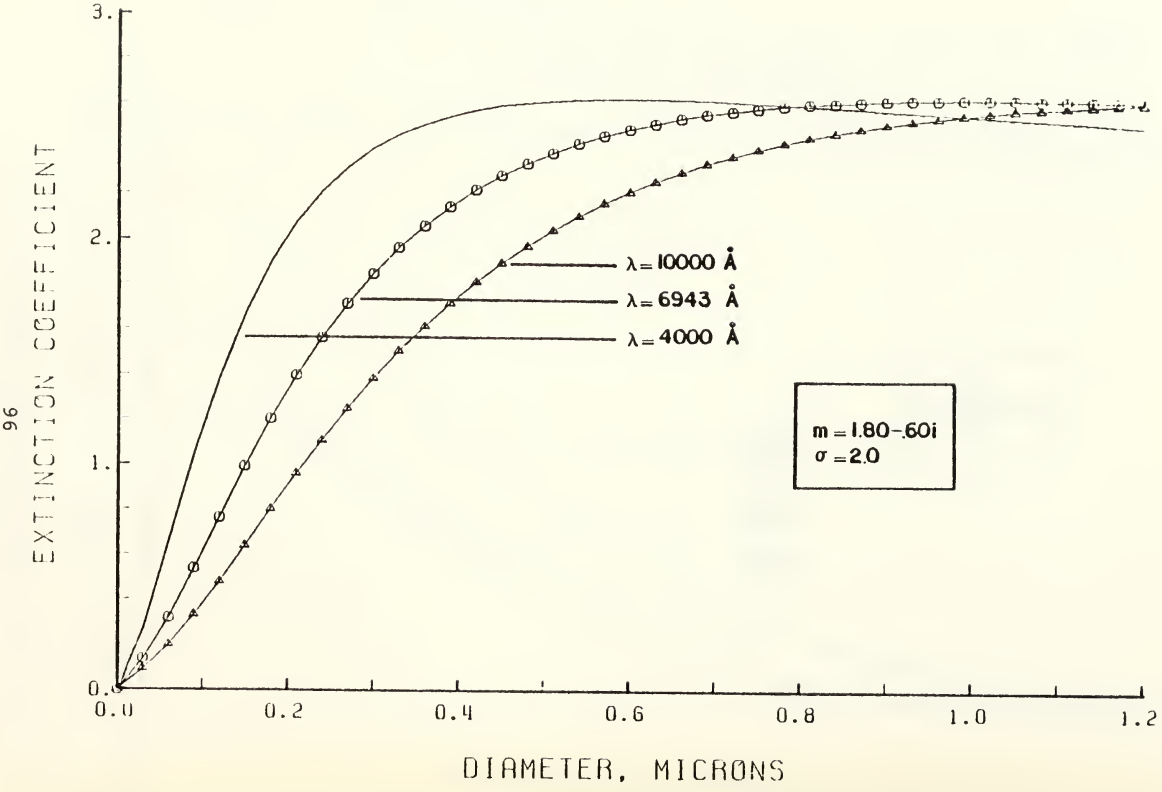

Figure 52. D_{32} vs. Extinction Coefficient (10000, 6943, 4000); m = 1.80-.60i/2.0

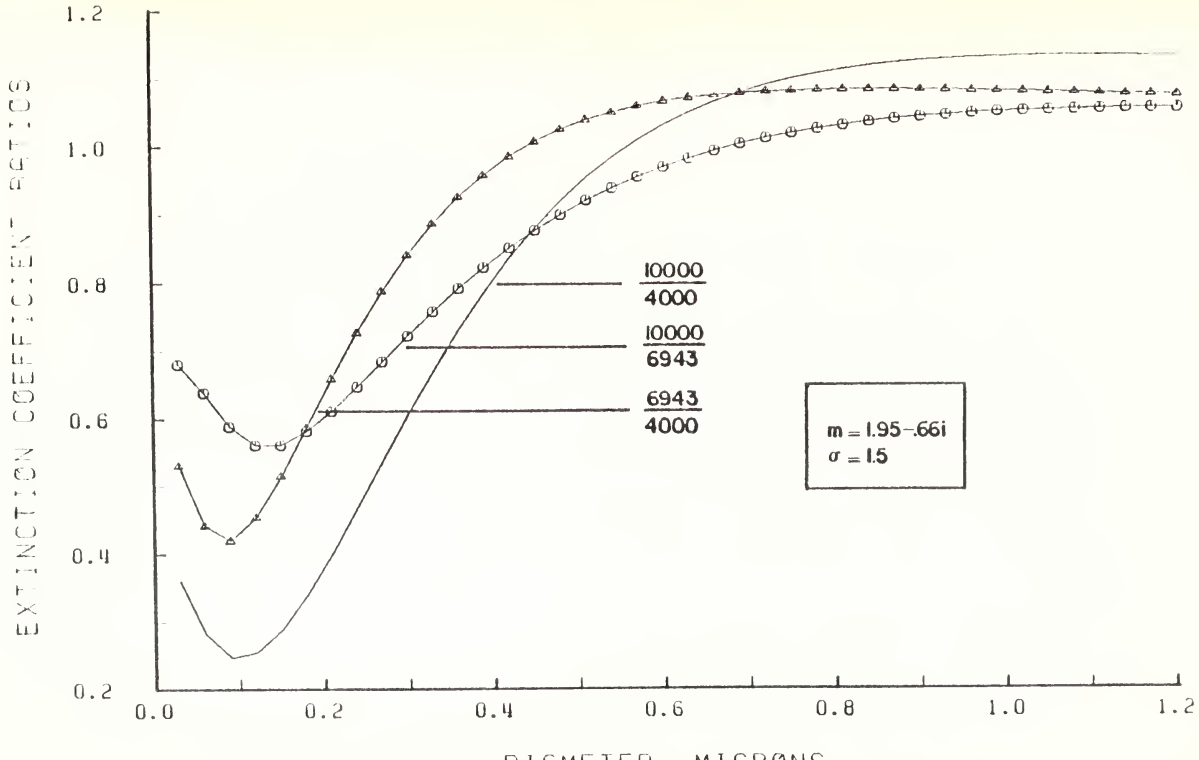

Figure 53. D_{32} vs. Extinction Coefficient Ratios (10000, 6943, 4000)
m = 1.95-.66i/1.5

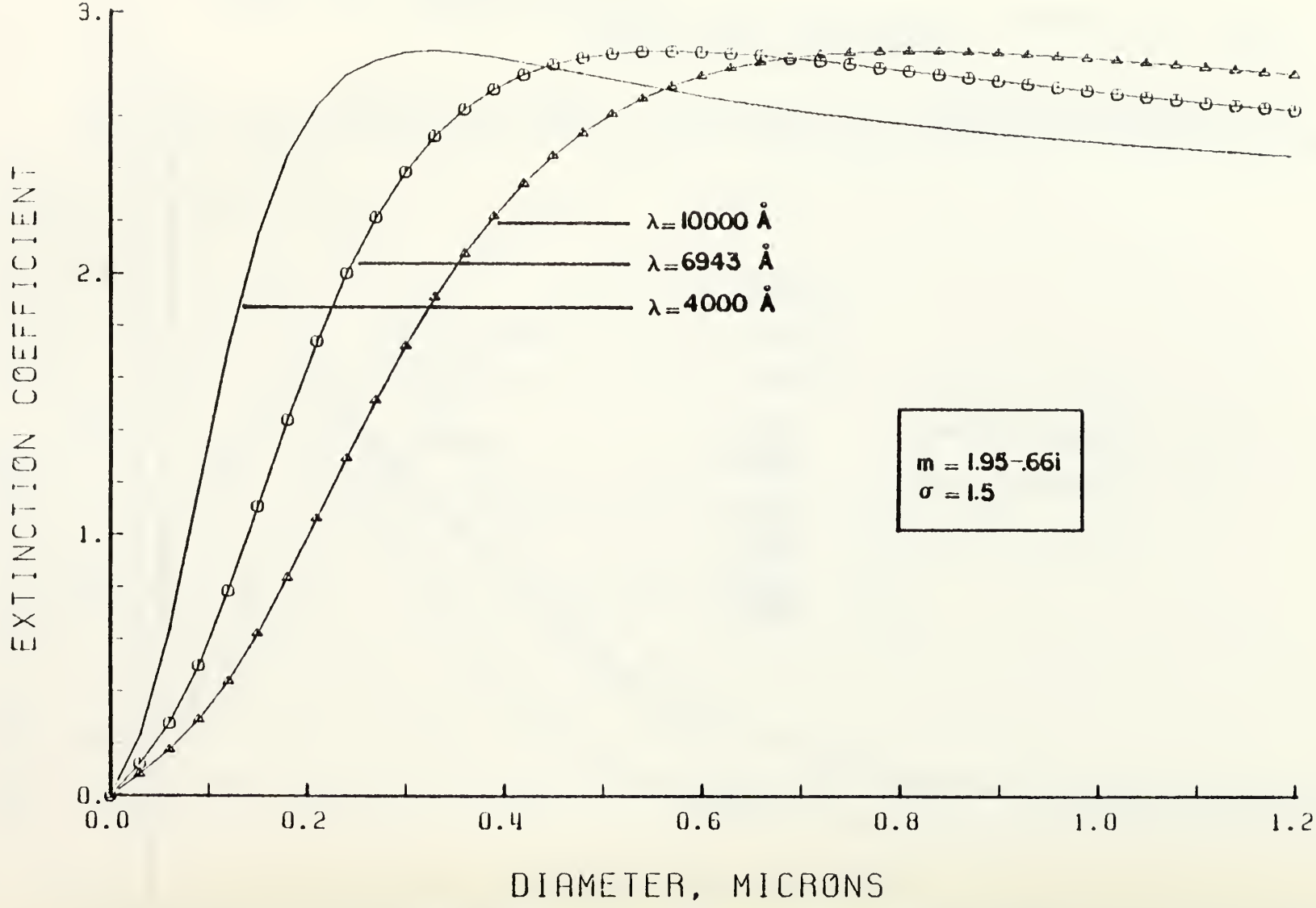

Figure 54. D_{32} vs. Extinction Coefficient (10000, 6943, 4000); m = 1.95-.66i/1.5

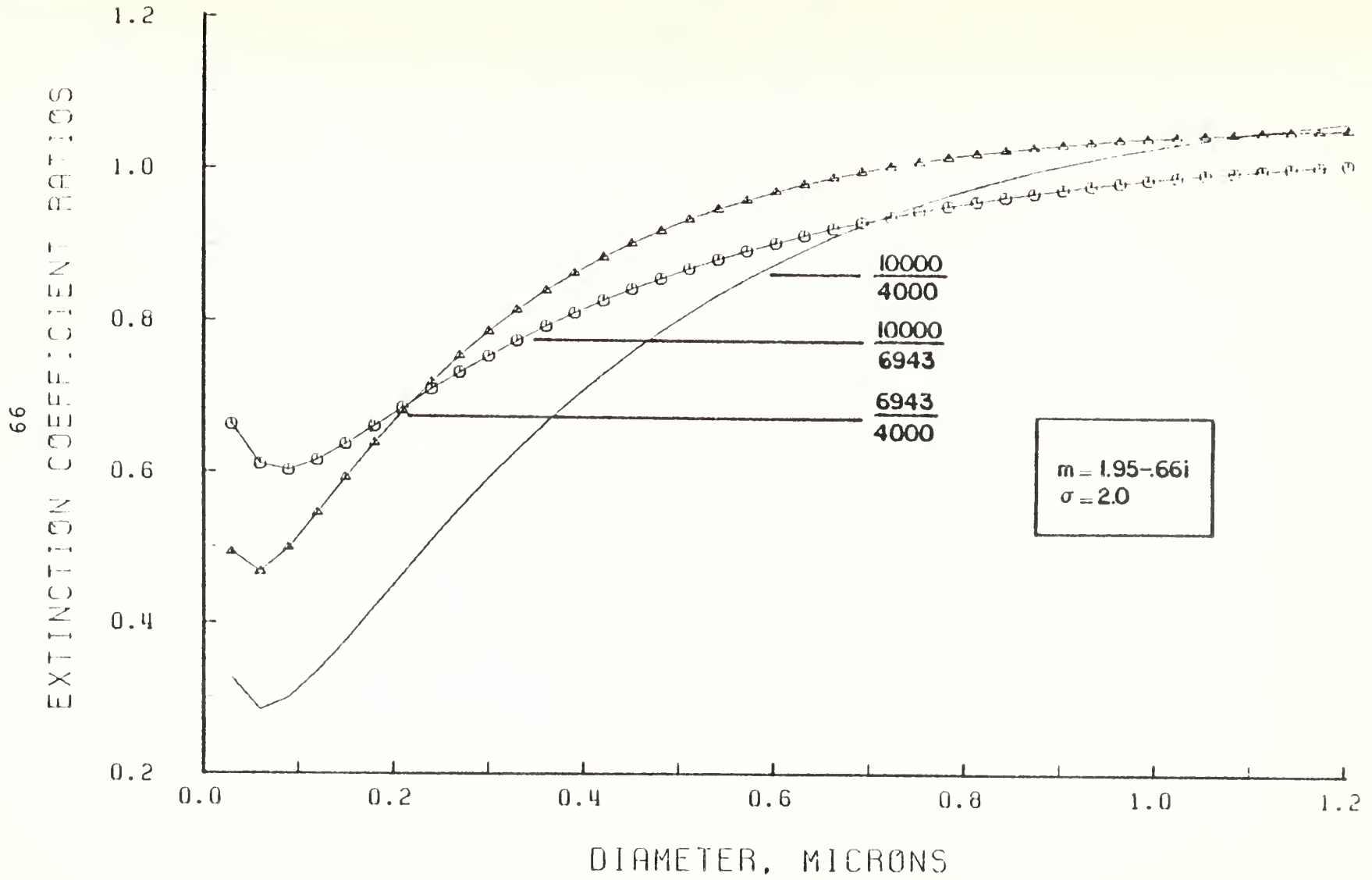

Figure 55. D_{32} vs. Extinction Coefficient Ratios (10000, 6943, 4000)
m = 1.95-.66i/2.0

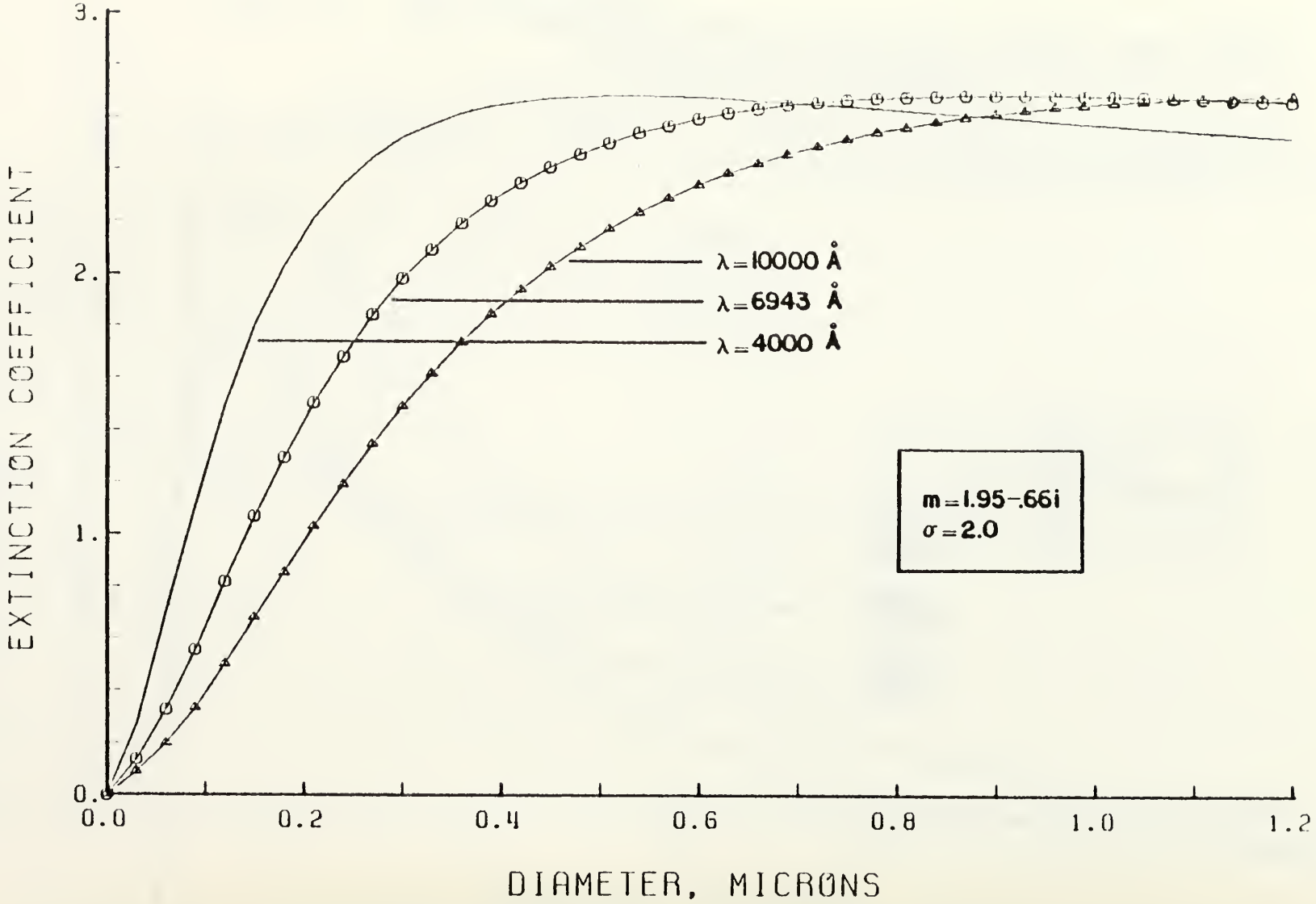

Figure 56. D_{32} vs. Extinction Coefficient (10000, 6943, 4000); m = 1.95-.66i/2.0

LIST OF REFERENCES

1. Naval Air Propulsion Center Report NAPC-LR-79-10, Application of Gaseous Emission and Smoke Reduction Technology for Selected Navy Aircraft Engines, by A. D. Bonafede and A. F. Klarman, 2 Apr 1979.

2. People of the State of California versus Department of the Navy, Civil Case No. C-76-0045 WHO, United States District Court for the Northern District of California of January 1976.

3. United Aircraft Research Laboratories, Technical Report No. AFWL-TR-73-18, Analysis of Jet Engine Test Cell Pollution Abatement Methods, by F. L. Robson, A. S. Kesten, R. D. Lessard, May 1973.

4. Naval Environmental Support Service, Report No. AESO 161.1-1-76, Field Evaluation of Instruments for the Determination of Smoke Opacity, September 1976.

5. McDonald, J. E., Visibility Reduction due to Jet-Exhaust Carbon Particles, Institute of Atmospheric Physics, the University of Arizona, Tuscon, Arizona, September 1962.

6. Naval Environmental Protection Support Service, Report No. AESO 111-72-2, Particulate Emissions from J79, J52, J57, TF30, and TF41 Engines During Test Cell Ferrocene Evaluation, February 1977.

7. Naval Air Propulsion Test Center, Evaluation of the Extended Use of Ferrocene for Test Cell Smoke Abatement; Engine and Environmental Test Results, by A. F. Klarman, October 1971.

8. University of California, Berkely, Size Distribution of Particles Emitted from a Model Combustor, Report No. TS-72-8, by P. J. Pagni and L. Hughes, October 1972.

9. Pagni, P. J., Hughes, L., and Novakov, T., "Smoke Suppressant Additive Effects on Particulate Emissions from Gas Turbine Combustors", AGARD Conference No. 125, Atomspheric Pollution by Aircraft Engines, AGARD-CP-125, 1973.

10. Air Force Engineering and Service Center, Report No. ESL-TR-79-32, Soot Control by Fuel Additives--A Review, by Howard, J. B. and Kausch, W. T., September 1979.

11. Naval Air Propulsion Test Center, Report No. NAPTC-PE-103, Evaluation of Smoke Suppressant Fuel Additives for Jet Engine Test Cell Smoke Abatement, by A. F. Klarman, February 1977.

12. Naval Postgraduate School Report 67NT-77-091, A Sub-Scale Turbojet Test Cell for Design Evaluations and Analytical Model Validation, by Hewlett, H. W., Hickey, P. J. and Netzer, D. W., September 1977.

13. Charest, J. R., Combustor Design and Operation for a Sub-Scale Turbojet Test Cell, MSAE Thesis, Naval Postgraduate School, Monterey, CA, 1978.

14. The American Society of Mechanical Engineers (ASME) PTC 19.5;4, Flow Measurement, Instruments and Apparatus, United Engineering Center, 345 East 47th, N.Y., 1959.

15. Durst, F., Principles and Practice of Laser-Doppler Anemometry, Academic Press, 1976.

16. Cashdollar, K. L., Lee, C. K., and Singer, J. M., "Three-Wavelength Light Transmission Technique to Measure Smoke Particle Size and Concentration," Applied Optics, Volume 18, Number 11, June 1979.

17. Dobbins, R. A. and Jizmagian, G. S., "Optical Scattering Cross Sections for Polydispersions of Dielectric Spheres," Journal of the Optical Society of America, Vol. 56, No. 10, October 1966, pp. 1345-1354.

18. Kleiser, T. D., Design of a Particulate Matter Collection Train, AE - 3815 Lab, Naval Postgraduate School, Monterey, California, June 1981.

19. Monitor Labs, Incorporated, Document 8440E, Instruction Manual Nitrogen Oxides Analyzer Model 8440E, 4202 Sorrento Valley Boulevard, San Diego, California, August 9, 1977.

INITIAL DISTRIBUTION LIST

		NO. OF COPIES
1.	Library Code, 0142 Naval Postgraduate School Monterey, CA 93940	2
2.	Department of Aeronautics Code 67 Naval Postgraduate School Monterey, CA 93940	
	M. F. Platzer, Chairman	1
	D. W. Netzer	10
	D. W. Thornburg	2
	T. R. Darnell	2
3.	Dean of Research Code 012 Naval Postgraduate School Monterey, CA 93940	1
4.	Defense Technical Information Center Cameron Station Alexandria, VA 22314	2
5.	Chief of Naval Operations Navy Department Washington, DC 20360 (Attn: Code OP451, OP453)	2
6.	Chief of Naval Material Navy Department Washington, DC 20360 (Attn: Codes: 08T241, 044P1)	2
7.	Commander Naval Air Systems Command Washington, DC 20361 (Codes: AIR-01B, 330D, 340[illegible], 4147A, 50184, 5341B, 53645, 536B1)	8
8.	Commanding Officer Naval Air Rework Facility Naval Air Station North Island San Diego, CA 92135 Code: 64270	1
9.	Commander Naval Facilities Engineering Command 200 Stoval Street Alexandria, VA 22332 (Codes: 104, 032B)	2

10. Naval Construction Battalion Center — 3
Port Hueneme, CA 93043
(Codes: 25, 251, 252)

11. U.S. Naval Academy — 1
Annapolis, MD 21402
(Attn: Prof. J. Williams)

12. Arnold Engineering Development Center — 1
Arnold AFS, TN 37342
(Code: DYR)

13. Air Force Aero Propulsion Laboratory — 1
Wright-Patterson AFB, OH 45433
(Code: SFF)

14. Detachment 1 — 2
(Civil & Environmental Engineering
Division Office)
HQ ADTC (AFSC)
Tyndall AFB, FL 32401
(Code: EV, EVA)

15. Army Aviation Systems Command — 1
P.O. Box 209
St. Louis, MO 63166
(Code: EQP)

16. Eustis Directorate — 1
USA AMR & DL
Ft. Eustis, VA 23604
(Code: SAVDL-EU-TAP)

17. National Aeronautics and Space Admin. — 1
Lewis Research Center
2100 Brookpark Road
Cleveland, OH 44135
(Attn: Mail Stop 60-6 (R. Rudley))

18. Federal Aviation Administration — 1
National Aviation Facility Experimental Ctr.
Atlantic City, NJ 08405

19. Naval Air Propulsion Center — 3
Trenton, NJ 08628
(Code PE 71:AFK)

20. Naval Ocean Support Center — 2
271 Catalina Boulevard
San Diego, CA 92152
(Attn: M. Lepor, M. Harris, Code 5121)

21. Naval Air Rework Facility — 1
Alameda, CA 94501
ATTN: (G. Evans, Code 642)